p66ShcA as a Prognostic and Mechanistic Biomarker for Responsiveness to PARP Inhibitor Combination Therapies in Poor Outcome Breast Cancers

By

Eduardo Cepeda Cañedo

Division of Experimental Medicine, Faculty of Medicine

McGill University

Montreal, Canada

A thesis submitted to the Faculty of Graduate Studies and Research in partial fulfilment of the requirement of the degree of Master of Science

Submitted November 2018

Abstract

Triple negative breast tumors (TNBC) lack ER, PR, and HER-2 expression and are associated with a poor prognosis. Currently, non-targeted chemotherapy remains the standard of care for these patients. PARP inhibition represented a promising approach for these women. Regrettably, clinical trials have shown limited survival benefit to date and predictive biomarkers of response are lacking. Some cytotoxic agents employed to treat TNBC, and that act in synergy with PARP inhibitors, produce reactive oxygen species (ROS) as part of their mechanism of action.

p66ShcA is a redox protein that is differentially expressed in TNBCs. Under steady state conditions, it is cytoplasmic. In response to stress stimuli, p66ShcA is phosphorylated on Ser36, which allows it to translocate to the mitochondria where it promotes the formation of ROS. I hypothesize that the expression of p66ShcA will sensitize TNBC cell lines to the combination of PARPi and chemotherapy.

To this end, p66ShcA was deleted from the genome of two TNBC cell lines by Crispr-Cas9 genomic editing. Wild-type p66ShcA or a mutant (p66ShcA-QQW), which is unable to generate ROS, were re-expressed along with the empty backbone (VC). Cell lines were subjected to cell viability assays, DNA damage assessment and oxidative damage determination upon treatment with PARPi (Niraparib), in combination with Doxorubicin, each at sub-optimal doses. p66ShcA-WT and VC breast cancer cell lines were also injected in the mammary fat pad of SCID-BEIGE mice. Animals were randomized into four groups: Niraparib alone, Doxorubicin alone, Niraparib/Doxorubicin combination therapy and vehicle control.

p66ShcA sensitized TNBC cell lines to Doxorubicin/PARPi combination therapies *in vitro* and *in vivo* as a result of an increased oxidative stress. This difference in viability is the result of the cytolytic effect of p66ShcA-induced ROS formation and is not dependent on increased induction of DNA damage.

Abrégé

Les cancers du sein de type triple négatifs (TNBC) sont dépourvus d'expression de ER, PR et HER-2 et sont associés à des pronostics défavorables. Actuellement, la chimiothérapie non-ciblée reste la norme en matière de traitement pour ces patientes. L'inhibition de PARP a représenté une approche prometteuse pour ces femmes. Malheureusement, les essais cliniques ont montré que les bénéfices en termes de hausse du taux de survie étaient limités à ce jour et que les biomarqueurs prédictifs de réponse faisaient défaut. Certains agents cytotoxiques employés pour traiter le TNBC, et qui agissent en synergie avec les inhibiteurs de la PARP, produisent des dérivés réactifs d'oxygène (DRO) dans le cadre de leur mécanisme d'action.

Le p66ShcA est une protéine rédox qui s'exprime de manière différentielle dans les TNBC. À l'état stationnaire, il est cytoplasmique. En réponse à des stimuli de stress, le p66ShcA est phosphorylé sur le Ser36, ce qui lui permet de se déplacer vers la mitochondrie où il favorise la formation de DRO. Mon hypothèse est que l'expression de p66ShcA va rendre sensibles les lignées de cellules TNBC à la combinaison de inhibiteurs de PARP et de chimiothérapie.

Pour la tester, le p66ShcA a été supprimé du génome de deux lignées de cellules TNBC par manipulation génomique Crispr-Cas9. Le p66ShcA de type naturel, ou un mutant (p66ShcA-QQW) qui est incapable de générer des ROS, a été ré-exprimé avec le plasmide (VC). Les lignées cellulaires ont été soumises à des tests de viabilité cellulaire, à une évaluation des dommages à l'ADN et à une détermination des dommages par oxydation lors d'un traitement avec PARPi (Niraparib), en association avec la doxorubicine, chacune à des doses sous-optimales. Des lignées cellulaires de cancer du sein p66ShcA-WT et VC ont également été injectées dans le tissue adipeux mammaire de souris SCID-BEIGE. Les animaux ont été randomisés en quatre groupes : Niraparib seul, Doxorubicine seule, traitement combiné de Niraparib/Doxorubicine et groupe témoin.

Le p66ShcA a rendu sensibles les lignées de cellules TNBC à la thérapie combinée de Doxorubicine/PARPi *in vitro* et *in vivo* en raison d'un stress oxydatif accru. Cette différence de viabilité résulte de l'effet cytolytique de la formation de DRO induite par le p66ShcA et ne dépend pas du déclenchement accru de dommages à l'ADN.

Table of Contents

Acknowledgements

First and foremost, I would like to sincerely thank both of my supervisors Dr. Josie Ursini-Siegel and Dr. Michael Witcher for having accepted me as a master's student. I am grateful for your advice and guidance and humbled and inspired by your passion for science, your work ethic and your determination. You gave me the opportunity to work at your labs even though I did not have a background in biology and you have inspired me to continue a career in medical research.

Thanks to the McGill Integrated Cancer and Research Training Program for providing funding for this project. Thank you to the Division of Experimental Medicine at McGill University for accepting me into your program and providing assistance and funding.

Thank you to my evaluation committee: Dr. Alex Orthwein, Dr. Luke McCaffrey and Dr. Koren Mann for your insightful advice. Thank you to Dr. Chantal Autexier and Dr. Morag Park for their collaborations in this project. Special thank you to Goldie Mansurian from the Animal Quarters of the LDI for having helped me with all my animal experiments.

Thank you to all the members of the Witcher and Ursini-Siegel labs for your helpful advice along these years. Steph, Jackie and Kyle, your scientific and personal advice have made grow during these years and I treasure your friendship.

I would like to thank my family. Thank you to my parents for allowing me to be here and for all the life lessons taught. Your influence has made me strong, perseverant and determined. To my brother. You are a big source of inspiration for me. Hermano te amo y extraño, espero hacerte sentir orgulloso de mi tal como yo me siento de ti. À JV, sans ton soutien et ton amour, je n'aurais jamais terminé ce projet.

Finally, I would like to dedicate this thesis to the memory of my beloved sister. Alejandra, te fuiste muy pronto pero tu esencia perdurará conmigo hasta mi último día. Nunca serás olvidada.

Contribution of Authors

The following is my master's thesis entitled "p66ShcA as a Prognostic and Mechanistic Biomarker for Responsiveness to PARP Inhibitor Combination Therapies in Poor Outcome Breast Cancers". It is composed of 4 chapters in accordance to the guidelines outlined by the Department of Graduate and Postdoctoral Studies. Chapter 1 (Review of Literature), Chapter 2 (Methods) and Chapter 3 (Results), and Chapter 4 (Discussion). The contributions of each author are described below.

The p66ShcA CRISPR/Cas9 Knock-out cell lines were generated by Jesse Hudson. Part of the mammary fat-pad injection were performed by Angela Ahn. Jacqueline Ha helped in the optimization of the soft-agar experiment. Stephanie Totten performed part of the drug administration to mice and tumor measurements, and kindly read and made suggestions for the editing of this thesis. Valérie Sabourin performed part of the IHC staining.

Dr. Ursini-Siegel and Dr. Witcher were in charge of the project conceptualization and project supervision. Additionally, both revised and made suggestions for the editing of this thesis.

Retro-viral transfections, cell viability assays, soft agar assay, immunoblotting, animal experiments (MFP injection, drug administration, tumor measurement, tissue collection), flow cytometry experiments, IHC staining, ELISA, immunofluorescence microscopy as well as data analysis and graphing and the preparation of all chapters of this thesis were performed by Eduardo Cepeda Cañedo.

List of Figures

List of Tables

List of Abbreviations

4-HNE	4-Hydroxynonenal
ATM	Protein Kinase Ataxia Telangiectasia Mutated
ATR	Protein Kinase Ataxia Telangiectasia Rad3-Related
BER	Base Excision Repair
BRCA	Breast Cancer, DNA repair associated
BRCT	BRCA1 C Terminus domain
CBR	Clinical Benefit Rate
Cdh1	Cadherin 1
CK	Cytokeratin
Cldn	Claudin
CR	Complete Response
DSB	Double Strand Break
EGFR	Epidermal Growth Factor Receptor
EpCAM	Epithelial Cell Adhesion Molecule
ER	Estrogen Receptor
GnRH	Gonadotropin Releasing Hormone
HBOC	Hereditary Breast and Ovarian Cancer
HER-2	Human Epithelial Growth Factor Receptor 2
HR	Homologous Recombination
IHC	Immunohistochemistry
MAPK	Mitogen-Activated Protein Kinases
MaSC	Mammary Stem Cell
MDA	Malondialdehyde
MUC1	Mucin 1, Cell Surface Associated
NAD+	Nicotinamide Adenine Dinucleotide
NHEJ	Non-Homologous End Joining
OGG1	Oxoguanine Glycosylase
ORR	Objective Response Rate
PARP	Poly (ADP-ribose) Polymerase
PARPi	PARP inhibitor
PEST	Proline- Glutamic Acid- Serine Threonine rich sequence
PI3K	Phosphoinositide 3-Kinase
PLD	PEGylated Liposomal Doxorubicin
PP2A	Protein Phosphatase 2
PR	Progesterone Receptor
PR	Partial Response
PTB	Phosphotyrosine Binding Domain
RB	Retinoblastoma protein
RING	Really Interesting New Gen (Zinc finger domain)
ROS	Reactive Oxygen Species
RTK	Receptor Tyrosine Kinase
ssDNA	Single strand DNA
TNBC	Triple Negative Breas Cancer
WGR	Tryptophan-Glycine-Arginine rich domain
XRCC1	X-Ray Repair Cross-Complementing protein 1
ZEB	Zinc Finger E-box binding Homeobox

Chapter One: Review of Literature

Breast Cancer

Morphology and Differentiation Hierarchy of the Human Mammary Gland

The morphology of normal breast is characterized by the presence of alveoli and ducts inside of an irregular connective tissue. Milk is produced in the distal part of the acini and transported to the nipple through the tubes[1]. These tubular-alveolar structures are composed principally by epithelial cells, surrounded by a basement membrane and an extracellular matrix[2]. The net of tubules is completely formed after puberty and undergoes constant cycles of proliferation and apoptosis marked by the menstrual cycle[3]. The formation and constant renewal of these type of structures is supported by a hierarchy of less differentiated and less proliferative cells: stem cells, non-committed progenitors and lineage restricted progenitors [2,4].

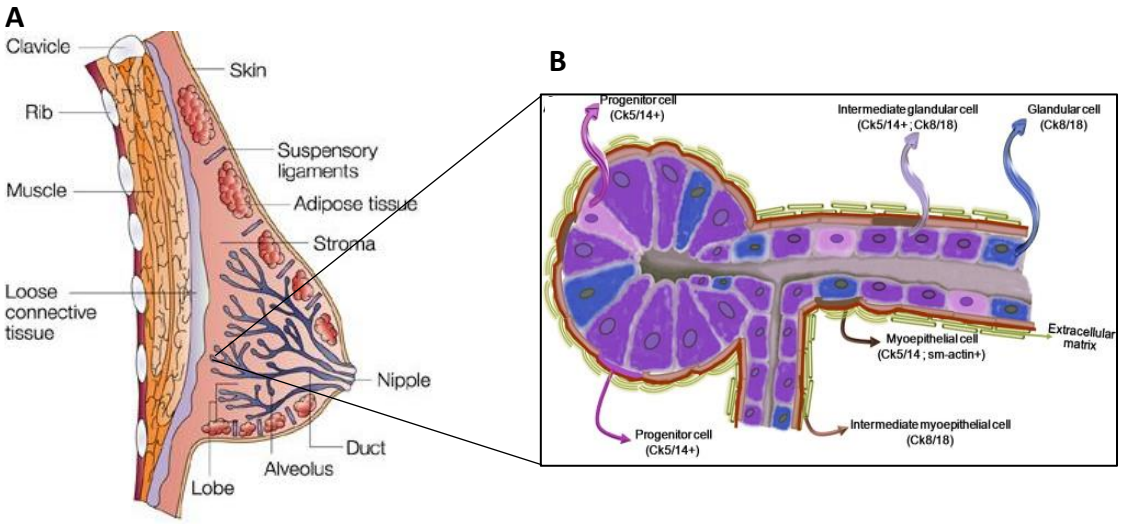

Figure 1. Schematic of the human breast anatomy. (A) The human mammary gland contains 15 to 20 lobes. Each lobe is conformed by the alveoli in the extremity of the branching net, and the ducts that bring the milk to the nipple. Adapted from Ali and Coombes[5]. (B) Representation of an alveolus and duct and the spatial distribution of the cell lineages that form the lobes. Adapted from Bosch et al[1].

On the highest point in the differentiation hierarchy are the Mammary Stem Cells (MaSC). This cell population is characterized by its Estrogen Receptor (ER), Progesterone Receptor (PR) and Human Epithelial Growth Factor Receptor 2 (HER-2) negative status and is normally located in the more distal site of the acini. Mammary stem cells give rise to the populations of progenitor cells[6]. By *in vitro* differentiating of MaSC, it has been possible to identify three types of progenitor cells in the human breast: bipotent, luminal-restricted and myoepithelial-restricted progenitors[4]. The bipotent progenitor generates a combination of cells expressing luminal markers and a subpopulation with myoepithelial characteristics. The continuous division of bipotent cells gives rise to the progenitor restricted cell populations[7].

As its name indicates, the luminal-restricted progenitors express luminal markers, including the keratins 8/18 and 19, EpCAM and MUC1[6]. On the other hand, myoepithelial cells generated from the myoepithelial-restricted progenitor, express cytokeratins (CK) such as CK 5, CK 14, and CK 17, essential proteins for the interaction between the luminal cells and the basement membrane[8]. Together luminal and myoepithelial cells form the functional net of alveoli and tubules. Luminal cells form the center of the ducts and secrete milk during pregnancy and myoepithelial cells cover the luminal layer and due to their contracting function can conduct the milk from acini to the nipple. Myoepithelial cells also maintain the integrity of the basement membrane trough the deposition of fibronectin, collagen IV, nidogen, and the bioactive laminins. This membrane is fundamental in the protection against tumorigenesis since it serves as a physical barrier preventing the invasion of transformed cells[8].

Breast Cancer, and Breast Cancer Molecular Subtypes

The understanding of the physiology and differentiation hierarchy becomes important when studying breast cancer. Breast cancer is the common name given to multiple diseases

characterized by the formation of tumors in the mammary tissue. These tumors are generally heterogeneous, making each one a different disease with different clinical characteristics and treatment response[9,10].

Histopathological examination is generally the main tool used for the determination of breast cancer subtype, treatment course, and grade. With the immunohistochemical (IHC) analysis of tumors, it is possible to identify fours main subtypes of breast cancer: Luminal A, Luminal B, HER-2+, and Triple Negative Breast Cancer (TNBC)[6,9,11–13]. The main biomarkers tested by IHC are the Estrogen, Progesterone and the Human Epidermal Growth Factor Receptors (ER, PR, HER-2), along with the proliferation marker KI-67[14]. Patients with Luminal tumors (express ER and PR) benefit from endocrine therapy (aromatase inhibitors, ER modulators, and GnRH)[10]. On the other hand, the principal drug prescribed to HER-2 driven breast cancer patients is trastuzumab, a humanized monoclonal antibody against HER-2[15]. Finally, patients with TNBC, due to the lack of targetable hormone receptors, are prescribed with unspecific systemic chemotherapies[16].

Molecular profiling has made it possible to sub-stratify breast tumors [13,17,18], leading to the identification of basal-like (TNBC), claudin-low (TNBC) and Normal-like tumor subtypes. These studies also suggest a relationship between the type of breast cancer with the characteristics of the stem and progenitor cells[6]. Further molecular profiling of TNBC has led to more detailed sub-stratification. Analysis of 587 TNBC made possible the identification of "2 basal-like, an immunomodulatory, a mesenchymal, a mesenchymal stem-like, and a luminal androgen receptor subtype"[19]. Furthermore, the classification of established breast cancer cell lines into the six TNBC subtypes made possible the identification of drug vulnerabilities by sub-type[19].

Luminal A and B tumors are presumed to be originated from fully differentiated cells or late luminal progenitors and in most cases express the estrogen receptor (ER). The differences between these two types of tumors is assessed by the analysis of expression of the PR and KI-67. Generally, tumors considered as Luminal A are ER+, KI-67 low and PR high. From newly diagnosed cases, the proportion of luminal A tumors goes from 30% up to 70%[20,21] and are generally associated with the best prognosis. On the other hand, Luminal B subtype tumors are usually ER+ and either Ki-67 high or PR low (some express HER-2)[22] and represent from 10-20% of breast tumors[1]. Compared to Luminal A, Luminal B disease is diagnosed in younger patients, these tumors tend to have higher grade and are more invasive[23,24].

HER-2 driven cancer cells normally do not express ER and are associated with highly proliferative phenotypes. The characteristics of these tumors suggest that they originate from a late luminal progenitor. They are characterized by the amplification of the HER-2 gene. This amplification results in the aberrant activation of MAPK and PI3K signaling pathways. HER2 amplification is oncogenic, in part, because it results in the overexpression of several transcription factors that increase cellular proliferation and angiogenesis, leading to the dysregulation of the cell cycle[25]. This subtype of breast cancer affects from 10 to 15% of newly diagnosed patients[23,24].

The less differentiated cellular precursors, luminal-restricted progenitor, bipotent progenitor and MaSC are believed to be the originators of TNBC tumors. It has been proposed that the embryonic MaSC gives rise to two luminal (ER+ and ER-) and one myoepithelial progenitor during puberty[26,27]. In adulthood, the ER+ unipotent progenitor gives rise to ductal cells with expression of ER. The ER- progenitor generates milk producing cells during pregnancy.

Interestingly, it has been shown that *BRCA1* mutated mammary tissues give rise to luminal progenitors with transforming potential[28,29]. Contrary to what it was previously believed, that basal-like tumors arise directly from the MaSC, these studies indicate that they actually arise from luminal unipotent progenitors[28,29]. Given that up to 80% of the *BRCA1* mutated tumors belong in the basal-like category (TNBC)[30,31], it is likely that they are originated from the ER- luminal progenitor. Furthermore, prophylactic oophorectomy reduces the risk of breast cancer development in *BRCA1* mutation carriers. This suggests the involvement ER+ luminal progenitors in the process of tumor formation in the *BRCA* mutated context[28,29].

It has been proposed that claudin-low tumors may have their origin in the MaSCs[6]. The main characteristic of this subtype (along with basal-like) is the lack of expression of any of the receptors previously mentioned (ER, PR, and HER-2). They also express basal cytokeratins (CK5/6, CK13, and CK17) and EGFR[32]. Particularly, claudin-low tumors are characterized by high expression of mesenchymal markers (Vimentin, N-Cadherin, Snail 1/2, Twist 1/2, ZEB 1/2) and low expression of luminal epithelial markers (Cdh1, Cldn 3,4,7)[18].

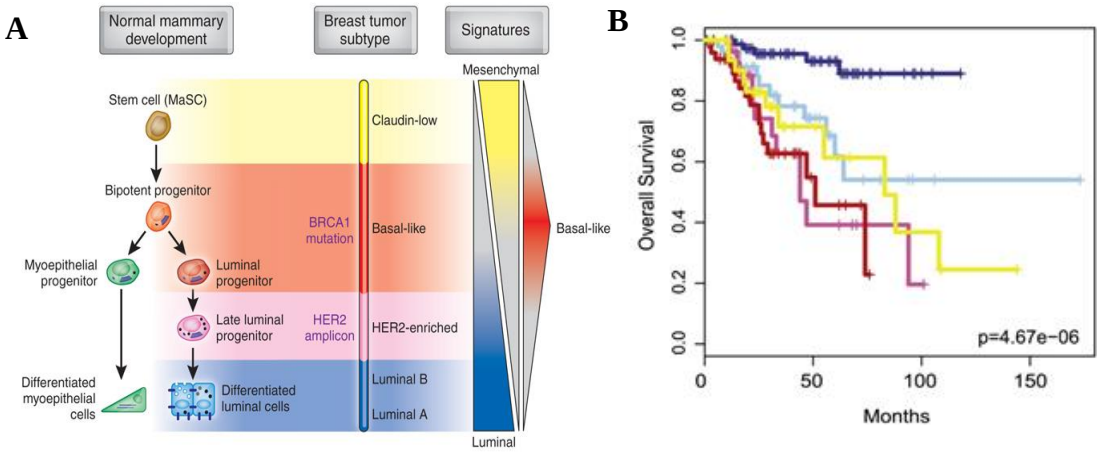

Figure 2: Potential cells of origin for the different subtypes of breast cancer. (A) Comparisons between the gene signatures of cells in the mammary differentiation hierarchy and breast tumors have allowed to related breast cancer subtypes and cells of origin. Obtained from Prat and Perou, 2009[6]. (B) Overall survival of patients stratified according the gene signatures mesenchymal/basal-like/luminal. Obtained from Prat and Perou, 2011[33]

The molecular classification of breast cancer has made it possible to identify groups of patients with similar prognosis, disease progression patterns and most importantly, therapy response[9]. Luminal A patients usually have the best prognosis while luminal B, HER-2+, basal-like and claudin-low are associated with bad outcomes[33]. One of the mains reasons for TNBC poor prognosis is the lack of targeted therapies[16].

Triple Negative Breast Cancer

TNBC is a surrogate category of breast cancer that groups all the tumors with an absence of ER, PR and HER-2[34,35]. To determine if a tumor is TNBC clinicians utilize basic morphology observation and IHC [36]. The correct identification of tumors is imperative to offer patients the best and most effective treatment options[37]. The criteria to select the best treatment course is based on expression of the receptors, mainly ER and HER-2, tumor morphology, the invasion grade and other risk factors[38]. In the end and even though TNBC tumors tend to be more aggressive[39], these patients will most likely receive taxanes and/or anthracycline based chemotherapies[16].

TNBC accounts for approximately 15-20% of all newly diagnosed breast cancer cases and is associated with poor prognosis[34–36,38]. Compared to other cancers subtypes, the average age of diagnosis for TNBC tends to be lower (less than 50 years)[35]. Premenopausal African-American and Hispanic women have been identified as the most affected by TNBC, compared to post-menopausal African-American and white women[40].

For this disease, it is highly probable to observe a relapse before the fifth year after diagnosis. This early relapse is characterized in most cases by the formation of visceral metastases. By this time, these tumors are already resistant to the most common chemotherapies used and the average life expectancy is reduced to less than 18 months[34]. In contrast, if patients

do not have a relapse during the first five years after initial diagnosis, the probability of advanced metastatic disease decreases considerably when compared to other breast cancer subtypes[34].

Genetic Characterization of TNBC

One of the primary molecular characteristic of TNBC tumors is their genomic instability, with approximately 1.7 bases mutated each Mb [41,42]. Compared to other tumors subtypes, in which several common genes are found to be mutated, in triple negative cancer the only two mutated genes found in more than 10% of the cases are *TP53* and *PIK3CA*[42].

TP53 gene is mutated in 65-80% of TNBC tumors[42–44]. Compared to ER+ breast cancers, *TP53* mutation in TNBC are more likely missense mutations[45]. It has been shown that missense mutations in the DNA binding domain of p53 have greater effects on the overall survival of patients than other types of mutations[46,47] Along with the loss of the crucial anti-cancer function of wild-type p53, missense mutations generate proteins that exert oncogenic effects (gain of function). Several studies have demonstrated that these type of mutations contribute to early tumorigenesis, tumor growth and metastasis (Reviewed by Walerych et, al.[48]) [49]. Even though non-sense mutations represent a smaller proportion than the missense-type in TNBC, they are still more common in TNBC than in any other breast tumor sub-types[45].

One of the main roles of p53, which is encoded by *TP53*, is keeping the integrity of the cellular genome through the regulation of programs like cell cycle arrest, senescence, DNA repair and apoptosis[50]. p53 is a main actor in preventing aberrant DNA mutations from giving cells any transforming advantage. The genomic instability present in TNBC may be explained by the absence of a functional p53 protein (or pathway). This genomic instability, due to the lack of a functional p53 response, has been hypothesized as one of the first and most important hits

(Knudson two hit hypothesis) or initial step in cancer formation[51]. This hypothesis becomes even more probable in the case of TNBC, due to the high prevalence of *TP53* mutations.

Recently, other roles of p53 have been studied, like the promotion of stem-like cancer phenotypes[52–55]. These studies have linked the function of wild-type p53 with cellular differentiation and its absence with the ability of cells to self-renew. With relevance to the TNBC subtype, these tumors are hypothesized to be originated from the MaSC or the bipotent progenitor which correlates with the high penetrance in *TP53* mutations and the stem-like phenotypes observed in these tumors[6].

Despite the fact that p53 has been considered to be an undruggable target, due to its crucial functions in every cell of the organism, there are studies that seek to develop drugs that specifically affect the action of mutant p53 alleles[56]. The discovery of functional drugs for the reactivation of p53 genotoxic pathways may be an important alternative to the chemotherapy given to TNBC patients.

The total mutational burden of TNBC patients is variable and its landscape is complex. There are TNBC patients with less mutations than the average for any of the other breast cancer subtypes. There are also TNBC patients with a higher mutational burden[41]. The fact that studies have only identified two main common DNA alterations for TNBC tell us that most of the remaining DNA aberrations are likely passenger mutations or could imply a significant heterogeneity of the driver mutations that cooperate with *TP53* in the formation of TNBC. The second most common mutation found in TNBC tumors corresponds to the *PIK3CA* gene (around 10% of the patients)[42]

TNBC and BRCA

Of special interest among the less common mutations found in TNBC are the genes *BRCA 1* and *2*. Mutations in *BRCA1* or *BRCA2* are related to the Hereditary Breast and Ovarian Cancer Syndrome (HBOC). Depending on the country in which the study was done, or on the race of the patients included, there are some studies suggesting that the frequency of mutations in *BRCA1* and *BRCA2* are as high as 20% across all TNBC cases [30,57–62]. Conversely, up to 80% of *BRCA* mutated tumors exhibit TNBC gene signatures (most likely basal-like)[30,31].

BRCA1 and *BRCA2* are tumor suppressor genes involved in DNA repair through homologous recombination (HR). While highly homologous, the functional relationship between the two proteins is not completely understood. The fact that the loss of one their alleles (either *BRCA1* or *BRCA2* independently) is enough to cause Hereditary Breast and Ovarian Cancer (HBOC) has led scientists to hypothesize that they have non- overlapping functions. Nevertheless, similar phenotypes are caused by their independent mutations[63].

BRCA1

Women carrying a *BRCA1* mutation have an 80% increased risk of developing breast cancer[64]. From all the domains of *BRCA1* only three of them carry the mutations that are considered clinically important: the RING domain, the region encoded by exons 11-13 and the BRCT domain. The RING domain works as a E3 ubiquitin ligase while BCRT and exon 11-13 function as protein-protein interaction domains.

- RING domain

Seen from a broad perspective, the process of ubiquitination consists of three main steps. First, an E1 enzyme is activated by the ubiquitin (Ub) molecule. Second, the Ub molecule is transferred to and E2 enzyme. Finally the E3 protein brings the substrate or the protein to be

degraded close to E2-Ub, in order for it to be marked for degradation[65]. The most common targets of ubiquitination mediated by BRCA1 include the estrogen and progesterone receptors, CtIP and the histone H2A[66–68]. It can be noted that proteins like CtIP and histone H2A are involved in the repair of double strand breaks and in the condensation of DNA[69,70]. The activity of the RING domain of BRCA1 protein is inhibited by platinum alkylating agents. BRCA1 suffers conformational changes due to platinum based molecules[71].

- Exon 11-13

Exon 11-13 constitutes 65% of the encoded protein. This region of the protein binds RB, MYC, Rad50 and Rad51[72]. All these proteins have important roles in DNA repair pathways and cell cycle progression and their dysregulation has been associated with cellular transformation[73–76]. For the specific case of MYC, it has been shown that the ability MYC/Ras expression (transfection) to transform cells, is reduced with the co-expression of *BRCA1*[77]. For this reason, the region encoded by exon 11-13 is considered a fundamental part of the tumor suppressor functionality of the BRCA1 protein. Another important function in the exon 11-13 region of *BRCA1* has to do with its cellular localization. This region contains two nuclear localization sequences that are compatible with the importin machinery localized in the nuclear membrane[78].

- BRCT domain

The main characteristic of the BRCT domain is its ability to identify and bind phospho-proteins. Specifically, the BRCT domain in BRCA1 is capable of recognizing phospho-serine residues[79]. In response to DNA double strand breaks, proteins like abraxas, ctIP and BACH1 get phosphorylated and are able to interact with BRCA1 through their pSer-X-X-Phe motif[80,81]. All of these proteins are involved in DSB repair, mainly by homologous recombination, and are

common phosphorylation targets of ATM/ATR kinases[82]. Although its function is not completely understood, BRCA1 has been shown to interact directly with the site of DNA damage and mediate non phospho-protein interactions[83].

BRCA2

The incidence of breast cancer in women carrying a *BRCA2* germline mutation goes up to 80%[84]. The primary anti-tumor activity of the BRCA2 protein appears to be related to the repair of DNA DSB through the HR pathway[85]. The structural characterization for BRCA2 is less understood than that of the BRCA1 protein. Nevertheless, it is known that BRCA2 plays a key role in the recruitment of RAD51 recombinase to the ssDNA overhangs generated during the process of DNA repair[86]. It has also been shown that BRCA2-deficient cells are sensitive to strand linking agents like platinum based chemotherapies[87,88].

Homologous Recombination DNA Repair

Here I will present a description of the homologous recombination repair pathway and the role of BRCA proteins within this process.

It is well accepted that the first step in the repair of DSB by HR is the 5' end resection of DNA to generate single-stranded DNA in the site of the break. The MRN complex, formed by Mre11, Rad50 and Nbs1 proteins, recognizes and binds the DSB site [89]. Through studies in budding yeast, it has been shown that Mre11 is the enzyme with exonuclease activity, Rad50 is involved in the immobilization of the DNA and Nbs1is the activator of ATM[90,91]. Phosphorylated proteins, as mentioned before, can interact with BRCA1 through its BRCT domain. It is possible that ATM kinases are brought to the site of damage due to their interactions with BRCA1[82,92]. The histone γH2AX (phospho serine 139 of H2AX), is also modified by ATM and colocalizes with the MRN complex through its interaction with the

BRCA1 BRCT domain[93]. CtIP (after activation by ATM), in cooperation with the MRN complex, carries out 5' end resection thereby generating ssDNA[89,94–96].

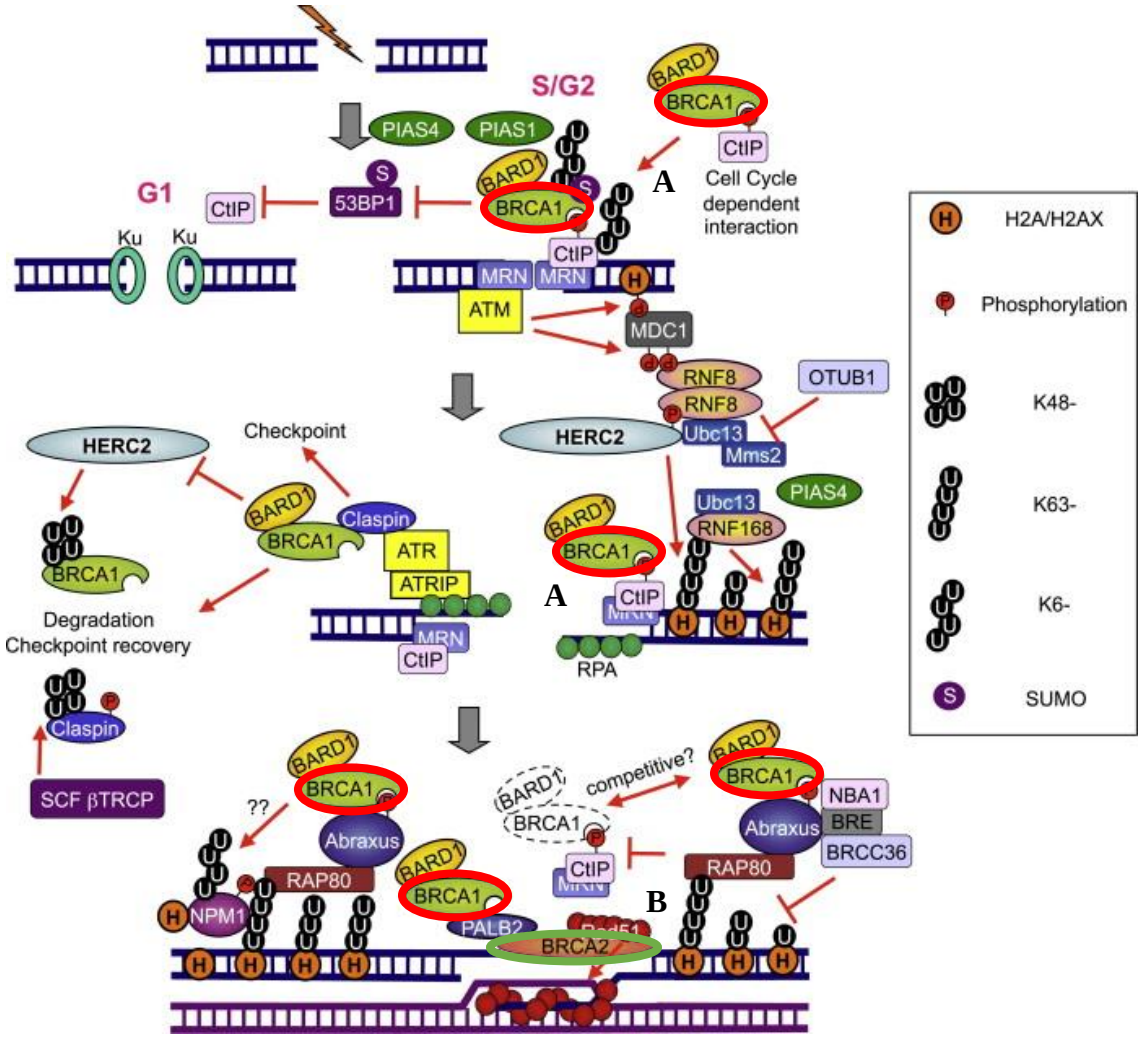

Figure 3 : Presence of BRCA1/2 in HR. (A) BRCA1 plays a crucial role in the recruitment of HR proteins (mainly CtIP) that execute the 5' end DNA resection at the place of DSB. (B) BRCA2 is implicated in the accession of the recombinase Rad51 to promote DNA strand invasion into the sister chromatid and homologous DNA synthesis. Adapted from Ohta et. al, 2011[97]

It has been shown that HR is mostly active during the S/G2 phases of the cell cycle[98], partially due to the availability of sister chromatids. NHEJ remains active thorough the cell cycle, but it appears to be more important during the G1 phase[99]. The decision of DNA repair pathways depends on CDK activity and on the active competition between HR related proteins and NHEJ complexes[94]. The resection of DNA, as previously described, is the main criteria in the decision of the DNA repair pathway that is engaged. Once the resection has occurred, classical NHEJ is no longer an option but HR may compete with alternative-NHEJ[100]. If the HR pathway is favored, Rad51 is recruited to the ssDNA. Both BRCA1 and BRCA2 proteins have the ability to interact with Rad51, but BRCA2 is fundamental for its positioning in the ssDNA[101,102].

Rad 51 is fundamental for the invasion of ssDNA into the complementary DNA templates (pair chromosomes). One of the ssDNA strands localizes to, and invades, the complementary strand by nucleotide pairing in the already dissociated DNA template. The complementary nucleotides to the ssDNA, now contained within a "D-loop" (Figure 3B), are then synthesized through the activity of polymerase delta, and probably additional polymerases. The new ssDNA strand dissociates from the template and is ligated back to its original place in the chromosome. Finally, this newly synthesized DNA strand will be the template for the synthesis of the final double-strand DNA[94].

In conclusion, mutations in *BRCA1* (specifically the BRCT domain) may impair HR by the disruption of the MRN complex or the interruption of the recruitment of CtIP, affecting the resection of the 5' DNA ends. In the case of *BRCA2* mutations, they are more likely to impair the invasion of ssDNA produced during the first stage of HR.

Although *BRCA* mutations are not present in most cases of TNBC, the majority of TNBC tumors are considered to have defects in other HR repair pathways and are thus referred to as BRCA-like[31,49,103,104].

TNBC Treatment

Currently, the treatment for TNBC patients is decided by taking into consideration the patient characteristics and the toxicity profile of the chemotherapies. With this strategy, half of the patients with TNBC stage I-III have a relapse and nearly 40% of them die during the next five years after diagnosis[105]. The prognosis for metastatic TNBC is worse, with a progression free survival of around three to four months[106]

To date, it is not clear whether a difference in the chemotherapy modality, adjuvant vs neoadjuvant, has any benefit in the progression free survival or overall survival of TNBC patients[107–109]. The decision of the chemotherapy regime seems to be based on the surgical approach since neoadjuvant chemotherapy treatment improves lumpectomy and breast conservation[110]. For both neoadjuvant and adjuvant treatments, the chemotherapies utilized are anthracyclines in combination with taxanes.

Although platinum derived drugs were intensively used in the past to treat advanced breast cancer, they never became the standard of treatment[111]. The main reason for this was the superior efficacy of other agents like anthracyclines and taxanes. Another reason is their low efficacy when given as a secondary treatment, inefficiency to treat metastasis and their high toxicity levels[111].

The superiority of the treatment efficacy of anthracyclines for ER negative cancer patients has been demonstrated in different clinical trials[112,113]. Nevertheless, the evidence in

these studies can be confounding due to the lack of patient stratification between HER2 positive and TNBC. Additionally, it was demonstrated that ER negative cancer patients benefited the most from polychemotherapy that may or may not include anthracyclines (5-fluoracil and cyclophosphamides)[114] and dose-dense treatment regimes[115]. Another study showed that epirubicin in combination with cyclophosphamide have improved the Event Free Survival and Overall Survival of TNBC[116].

Doxorubicin is the most commonly employed anthracycline clinically, yet the exact mechanism of action remains uncertain. Various studies on anthracyclines have pointed out five possible pathways: topoisomerase II poisoning, DNA adduct formation, reactive oxygen species (ROS) production, ceramide overproduction[117] and histone eviction[118]. It is possible that the cytotoxicity exerted by doxorubicin is a result of the combination of the mentioned mechanisms.

Of interest to this project is the fact that a major component in the cytotoxicity of doxorubicin is ROS. Once in the cell, doxorubicin is oxidized into a semiquinone form. This unstable molecule constantly transitions between its oxidized and reduced form in a process that produces ROS. It has been shown that the cytotoxic effect of the doxorubicin analog, 5-iminodaunorubicin , which is not transformed into a semiquinone (not oxidised), is not reversed by ROS scavengers, like in the case of doxorubicin [119].

One of the main drawbacks of doxorubicin is its cardiotoxicity. This side effect is also related with the induction of iron mediated ROS and mitochondrial damage[120]. Interestingly, it has been reported that the cytotoxic mechanism of doxorubicin between non-cancer and cancer cells (p53 wild-type tumors) may not be the same. While the apoptosis induced in normal cells seems to be primarily governed by the production of ROS by the anthracycline, in cancer cells apoptosis relies to a major extent on the activity of p53[121].

PARP inhibition as a Targeted Therapy for TNBC

Poly (ADP-ribose) polymerase, or PARP, is the general name for a family of 18 proteins that catalyze a posttranslational modification, called poly (ADP-ribosylation), or PARylation. While PARP1, 2 and 5a/b (tankyrases 1/2) synthesize chains of poly(ADP-ribose) using NAD+ as a building block, the rest of the enzymes in the family have only been shown to add one PAR unit (a process called MARylation)[122,123124]. PARylation occurs within seconds of the production of DNA damage and promotes the recruitment of DNA repair complexes[125].

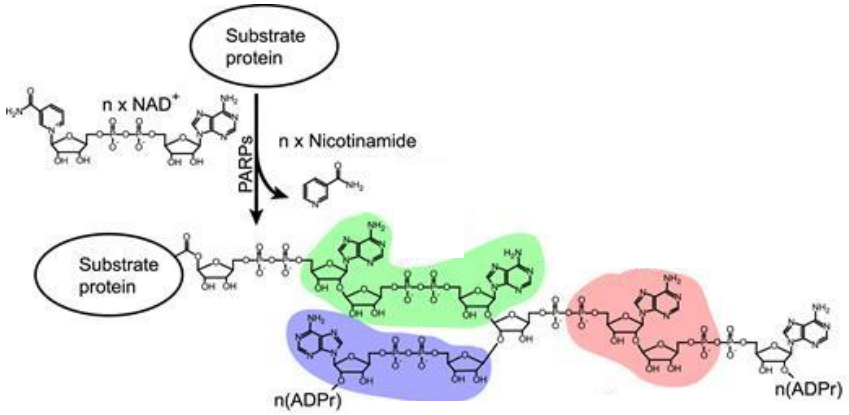

Figure 4: PARylation Schematic. PARPs hydrolyze NAD+ into the nicotinamide part and the ADP-ribose moiety. This last molecule is covalently attached to the substrate protein generating linear or branched PAR chains. Obtained from Liu et al. 2017[125].

PARP1 protein domains

PARP1 contains seven identified domains: three zinc-finger domains, a BRCT domain, a tryptophan-glycine -arginine rich domain (WGR), a PARP regulatory domain and a catalytic PARP domain. The N-terminal region of PARP1 contains two of the homologous zinc fingers domains and a nuclear localization sequence. The presence of the zinc fingers is essential for the

localization and binding to the site of DNA damage[126]. The third zinc finger is not directly related with the DNA damage binding capacity of PARP1, but it is essential for its catalytic activation[127]. The BRCT domain promotes the interaction of PARP1 with DNA repair proteins (e.g. BRCA1, BRCA2) by its autoparylation[128].

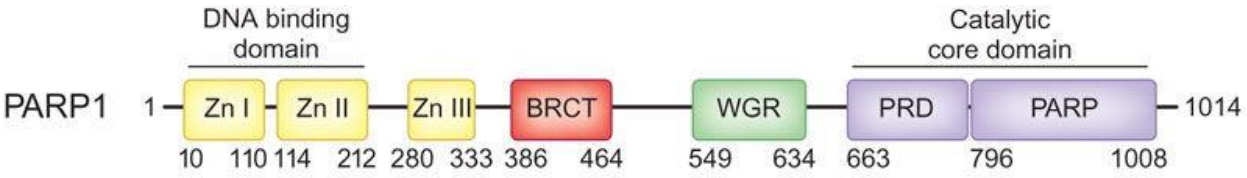

Figure 5: Domain Architecture of PARP1. PARP1 contains seven identified domains: three zinc-finger domains, a BRCT domain, a tryptophan-glycine -arginine rich domain (WGR), a PARP regulatory domain (PRD) and a catalytic PARP domain. Obtained from Till et al., 2008[129].

The WGR domain in PARP1 has been reported to be involved in the activation of the catalytic subunit of the enzyme after the interaction with DNA damage mediated by the third zinc finger[123]. It was recently shown that the function of the WGR may be involved in the activation of PARP1 under conditions of oxidative stress. This study demonstrated that the interaction of salidroside, an antioxidant extracted from the plant *Rhodiola rosea*, with the WGR domain of PARP1 promotes PARP1 activation and cell survival under oxidative stress in hematopoietic stem cells[130]. Lastly, the catalytic c-terminal domain in PARP1 utilizes the substrate NAD^+ to synthesize the PAR chains on itself (11 PARylation sites), on histones and various proteins involved in the repair of DNA.

PARP inhibition in HR deficient cancer

The classical vision of PARP inhibition as an effective therapy necessitates a synthetic lethality[131]. PARP1/2 recognize the site of DNA damage and initiate a response to mediate it. PARP synthesizes poly(ADP-ribose) chains on proteins implicated in the DNA damage response

(PARylation)[132]. Base Excision Repair (BER) is one of the pathways whose activation depends largely on PARylation. This pathway is implicated in the repair of ssDNA breaks, as well as damaged bases and abasic sites[133,134]. The classical view of synthetic lethality proposes that the inhibition of BER promotes the accumulation of ssDNA breaks that eventually progress into DSBs[135]. Normal cells would be unaffected by the action of PARP inhibitors, since the DSB generated would be repaired by HR. In the case of *BRCA1/2* mutated tumors or HR defective TNBC, the inhibition of BER implicates the dysfunction of two DNA repair mechanisms. These dysfunctions, along with the high genomic instability present in TNBC, would cause accumulation of toxic DSB, G2/M cell cycle arrest and ultimately apoptosis[131,135,136].

It has been shown that PARP not only mediates BER (reparation of ssDNA breaks) but is also implicated in HR. These observations have made it possible to hypothesize that the consequences of PARP inhibition are more complicated than the model of synthetic lethality previously described[137]. Herein, I present a description of the various activities of PARP in different pathways.

PARP in ssDNA repair

BER is a repair pathway highly utilized for ssDNA breaks. These type of breaks are, to a great extent, the direct result of oxidative stress (oxidation of the DNA phosphate backbone), methylation and carboxylation of nucleotides[138]. ssDNA breaks are also produced by the action of APE1 or by bifunctional glycosylases that target oxidized bases (OGG1, NTH1, NEIL1, NEIL2). Oxidative purine lesions are removed primarily by OGG1, whereas oxidative pyrimidine lesions are removed primarily by NTH1, NEIL1, or NEIL2. These enzymes have both glycosylase and AP/lyase activity that generate single-strand nick 3' to the AP site via beta (OGG1, NTH1) or beta-delta (NEIL1, NEIL2) elimination (reviewed in [139–141]).

OGG1 is the main enzyme involved in the processing of oxidized purines (e.g. 8-oxodG). It has been shown that under oxidative stress conditions, this enzyme stimulates the activation of PARP1, due to the ssDNA breaks produced by its glycosylase activity. Cells with deficiency in OGG1 have less activation of PARP1 leading to more genetic instability. As with many other enzymes involved in DNA repair pathways, OGG1 interacts with PARP1 via the BRCT domain. The activation of PARP1 leads to a decrease in the activity of OGG1[142].

PARP1 recognizes the SSBs that are mainly generated by ROS[143,144]. Upon recognizing and binding the SSB produced by BER, PARP1 is activated[145]. PARP1 recognizes the site of the DNA break through its N-terminal region containing two zinc fingers[126]. After the ssDNA (or DSB) is localized, PARP undergoes conformational modifications of an autoinhibitory region in the catalytic domain (helical subdomain), initiating the catalysis of PAR chains[146].

The process of PARylation starts with PARP (auto-PARylation) and histones as substrates. PARylation of PARP and histones is necessary to create space for the DNA repair complexes to access the site of damage. The negative charge of the PAR chains loaded onto the histones may produce the opening of the tightly packed nucleosomes[147,148].

With space to access the site of damage, the complexes of reparation of DNA translocate from all parts around the nucleus to the specific site of damage[149]. One of the most important proteins to translocate into the PARylated-PARP sites is XRCC1. The BRCT domain in XRCC1 is necessary for the recognition of PARylated proteins. Furthermore, the interaction between PARP1 and XRCC1 is mediated by the shared BRCT domain[150]. XRCC1 is an important scaffold for the recruitment of DNA repair enzymes such as DNA ligase III[151] and DNA polymerase β[152].

Ultimately, XRCC1 also acts as an inhibitor of PARP1 activity. The negative charge of PARylated PARP1 reduces its binding affinity to DNA (the negative charge of DNA repels negatively charged PARP) and contributes along with PARG to the enzyme and PAR chain recycling[153].

PARP in DSB repair

It has been shown that PARP activity is important for most types of DSB repair. NHEJ, initiates with the recruitment of DNA-PKcs by Ku70 and Ku80 proteins to the DSB. It has been shown that the activity of this enzymes is promoted by PARylation[154]. PARP activity is similarly important for alt-NHEJ, a repair process that occurs in the absence of the Ku proteins[155]. Studies attribute PARylation to the recognition of DNA damage sites and the formation of stable complexes of the DNA repair machinery[156,157]. It has been shown that the inhibition of PARP with Olaparib in HR defective cell lines promotes NHEJ. This type of DNA damage repair is error prone and promotes genomic instability subsequently leading to apoptosis[158].

In the case of HR, the involvement of specifically PARP1 has proved to be dispensable and the effect of PARylation seems to be regulatory. The absence of PARP1 during HR processes induces a hyper-recombination phenotype but is not directly related to the execution of the pathway[159]. However, it has been shown that PARP does accumulate at the sites of DSB and is an important contributor in the repair of stalled replication forks through the localization of MRE11/Rad5/NBS1 complex[160,161]. Furthermore, PARP1 knock-out studies in mice did not show early tumor onset, defects in fertility or viability defects. Nevertheless, cells isolated from those mice showed increased activation of HR. In this case, the accumulation of SSB due to the lack of PARP1 causes the stalling of replication forks, defect that is fixed by HR[162]. Moreover,

PARP1/PARP2 mouse models showed embryonic lethality[163]. This indicates an indispensable function that overlaps between both proteins.

PARP trapping vs Synthetic Lethality

Studies involving the comparison of cytotoxicity between PARP inhibition and PARP knock-down in HR deficient cells showed a greater effect with the inhibitors[164,165]. The synthetic lethality (achieved by a PARP knock-down) is not the only mechanism of action of PARP inhibitors. The mechanism of action of PARP inhibitors is not only related to the inhibition of its catalytic domain, but also related to the trapping of the enzyme at the DNA break site[164,165].

PARP inhibitors were designed with the primary intent of impairing the catalytic activity of PARP. All the PARP inhibitors used nowadays in the clinic hold this ability. The PARP inhibitors olaparib, veliparib and niraparib have in their structures a nicotinamide moiety. In this way, the inhibitors compete directly with the substrate of the PARylation reaction, NAD^{+}[165]. The inability to initiate the DNA repair, due to the lack of PARylation, promotes the accumulation of ssDNA breaks. ssDNA lesions are responsible for the generation of replication stress through DNA replication slowing or stalled replication forks[166]. The cellular response to fix this type of error is catalyzed by ATM/ATR kinases with protein complexes that include BRCA1/2, working through the HR pathway[165].

The other mechanism of toxicity exerted by PARP inhibitors is PARP poisoning. This mechanism may explain why although all the PARP inhibitors used in clinic have similar catalytic inhibitory activity, their cyto-toxicities are quite different. PARP poisoning, also called PARP trapping, is defined as immobilizing PARP1/2 on chromatin in its current position such that it cannot dissociate. Similar to inhibition of PARylation, PARP trapping leads to the

collapsing of replication forks. The reparation of collapsed replication forks caused by PARP trapping requires the activation of a PARP-independent response. Along with the classical ATM kinase activation, the Fanconi pathway, template switching and FEN1 are also required to mediate repair[165]. The different PARP trapping activities of the most used PARP inhibitors has been evaluated. Niraparib has the highest trapping capacity when compared to olaparib and veliparib[165].

PARP inhibition in TNBC

Most of the PARP inhibitors currently used in the clinic are potent inhibitors of the catalytic activity of PARP1 and 2, with the exception of olaparib that also inhibits the activity of PARP3[167]. The utilization of these drugs has been explored in several clinical trials. As monotherapies, the administration of the drug has been mainly limited to those patients with a proven abnormality in HR. The most common criteria to determine the HR deficiency is the sequencing of *BRCA1/2*, and consideration of the family clinical history (HBOC).

Olaparib

The first stage I clinical trial for Olaparib was performed for patients mainly with advanced ovarian, prostate and breast cancer[168]. The only patients that benefitted to some extent from the drug had confirmed mutation in *BRCA* or had a history of familial cancer. This clinical trial confirmed for the first time that *BRCA* deficiency sensitizes tumors to PARP inhibition in clinic. The patient responses to the drug, in *BRCA* mutated cancers, were varied. There were patients that had a short slowing down in the growth of tumors and those who benefited from the therapeutic response for up to 76 weeks. There were also patients with mutations in *BRCA* that did not benefit from the PARP inhibitor. It is surmised that the variable response is due to genetic resistance predispositions. However, olaparib was given as a second-line therapy post-

chemotherapy and there is evidence that chemotherapy may deplete PARP-1 expression, thereby generating a resistance mechanism[169].

The secondary effects reports after PARP inhibitor exposure were nausea, vomiting, fatigue and anorexia, with each of the symptoms presented in less than one third of the patients enrolled in the trial. None of the secondary effects were as drastic as those presented after chemotherapy administration. The absorption of the drug was rapid, with a maximum peak of bioavailability at one to three hours. The half-life of the drug in the system was determined to be from five to seven hours. For these reasons the drug was deemed safe to use and was recommended to be administered specifically in patients with germline *BRCA1/2* mutations.

A phase II non-randomized clinical trial for advanced poorly differentiated ovarian cancer and TNBC was performed[170]. 69 ovarian cancer patients and 26 TNBC were administered with 400mg daily dose of Olaparib. Patients were stratified according to their *BRCA1/2* status and the endpoints were response rate and progression-free survival. The trial shows a clear division between TNBC with *BRCA* mutations and non-*BRCA* tumors. Only *BRCA* mutant carriers benefited to some extent from the therapeutic action of Olaparib (consideration: the cohort of TNBC was composed by only 26 patients). For the ovarian cancer cohort, the results were different. Patients from both groups *BRCA* and non-*BRCA* mutation carriers had a positive response to the monotherapy. The progression-free survival for TNBC patients was improved in greater extent when comparing *BRCA* and non-*BRCA* in comparison with ovarian cancer cases.

Although the results from the stage I and II clinical trials seemed promising for TNBC *BRCA* mutant cases, the stage III clinical trial OlympiAD, showed no additional benefit when compared to standard care. The trial tested the effect of the administration of Olaparib as monotherapy (daily administration) in advanced breast cancer/*BRCAmut* patients compared to

the standard of care (capecitabine, vinorelbine, eribulin in 21-day cycles) [171]. The median progression-free survival was delayed by three months with the use of Olaparib. Nevertheless, Olaparib failed to improve overall survival of patients. Both treatment options had an average overall survival of 19 months after trial started.

Veliparib

A phase I 3+3 dose scalation clinical trial was performed to determine the optimal dosage for the phase II trial[172]. Serous ovarian and basal-like cancer patients were included in the study. Toxicity analysis indicated as the most serious secondary effects grade two vomiting and seizures at a 500mg dose (optimal dose was fixed at 400mg). The half life of the inhibitor was 5.2 hours on average. The response to the drug was determined by stratifying patients according to their *BRCA* status. The parameters compared were ORR (CR+PR) and the clinical benefit rate (CBR=CR+PR+ stable disease). In the *BRCA* deficient cohort, the ORR was 23% and CBR 58%. Only 4% of the patients with wild-type alleles of *BRCA* achieved a complete or partial response (ORR) and the CBR was 38%.

The results obtained by this first stage clinical trial made clear the necessity to limit the use of Veliparib to *BRCA* mutated carriers. The negative results obtained in the Olaparib stage III clinical trial OlympiAD, questioned the clinical benefit of prescribing PARP inhibitors in breast cancer. Clinical trials like the Veliparib Phase III in NSCLC and TNBC focused on the utilization of PARP inhibitors as potentiators of chemotherapy instead of monotherapy[173]. This double-blind multicenter phase III randomized trial had as principal objective comparing the effect of veliparib, paclitaxel and carboplatin together against placebo, paclitaxel and carboplatin in early stage disease. Unfortunately, the research team behind the trial communicated that

Veliparib failed to meet the primary endpoint, stating that there is not evidence that the drug in combination with chemotherapy potentiates the therapeutic response.

Niraparib

The toxicity for Niraparib was evaluated mainly in ovarian cancer patients[174]. As with the Olaparib and Veliparib phase I trials, the results were analyzed by stratifying the patient response according to *BRCA* status. Once again it was confirmed that *BRCA* mutations sensitize tumors to PARP inhibition. In general, Niraparib yielded similar activity as Olaparib. An ongoing phase III clinical trial for advanced metastatic breast cancer (BRAVO), is comparing the use of Niraparib against four different chemotherapies (physician choice). In this trial, only women with confirmed *BRCA* mutation were admitted[175].

BRCA mutations are until now the major marker for response to PARP inhibition. These mutations represent up to 20% of the newly diagnosed cases of TNBC[62,176]. Whether PARP inhibitors are potential therapeutics for TNBC *BRCA wild-type* patients is still in question. Newly designed PARP inhibitors like Rucaparib and Talazoparib, with more potent trapping activity are currently under phase I/II trial for TNBC patients as monotherapies[177]. The three more studied PARP inhibitors, Olaparib, Veliparib and Niraparib have progressed into exploring the benefits of combination therapies for *BRCA*-null and *BRCA* wild-type patients (Refer to Table 1). The mixed results obtained in clinical trials suggest the necessity for identification of therapeutic response biomarkers.

The Redox Protein p66ShcA as a Possible Biomarker for PARP Inhibition Response

p66ShcA Structure and Function

The Src Homology 2 Domain-Containing gene *ShcA*, encodes by alternative translational initiation the isoforms p46ShcA and p52ShcA. With the use of a different promoter, it encodes the third isoform p66ShcA[178]. The first two isoforms act as docking proteins for the transmission of signals downstream of activated Receptor Tyrosine Kinases (RTK)[179]. The signals transmitted through MAPK and PI3K/AKT/mTOR pathways, in the context of cancer cells promote proliferation, survival, invasion and angiogenesis[179]. *ShcA* deletion has been shown to be embryonic lethal, demonstrating its essential role as a signaling node during development[180].

Mitogenic signaling is not a function shared by the third isoform, p66. The deletion of this isoform in MEFs contributes to increased cellular survival and resistance to oxidative stress. More importantly, *in vivo* experiments with p66 knock-out mice showed a similar effect. The ablation of this isoform contributed to their resistance to oxidative stress and a 30% increase in lifespan[181]. Along with its role in oxidative stress, p66 has been shown to act as an antagonist of signaling downstream of RTKs by binding and sequestering Grb2 away from the p46 and p52ShcA isoforms. The CH2 domain of p66, rich in prolines, changes the interaction of the scaffold protein with Grb2 producing a decrease in the binding with SOS1[182]. In concordance with this, it has been shown that cells that are p66-deficient have higher signaling through the MAPK pathway[178,183,184].

The three ShcA isoforms share the SH2 domain, a central proline-rich collagen homology domain (CH1) and a phospho-tyrosine binding domain (PTB). After ligand binding, the three isoforms interact with phosphorylated RTKs, mostly through the PTB domain[185]. There, three

tyrosine residues located in the CH1 domain (239/240 and 317 from the human p52 isoform) get phosphorylated. While p52/46 transmit the mitogenic signaling previously mentioned, p66 due to the additional CH2 N-terminal domain[186] disrupts the complex interactions and cannot transmit signaling through RAS or AKT pathways[183,187], making p66 an inhibitor by competition.

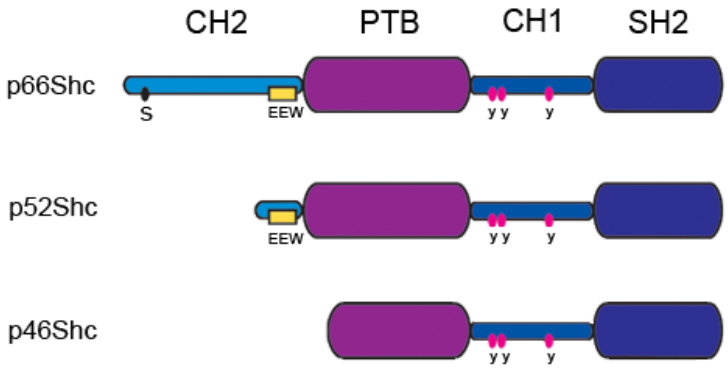

Figure 6: Domain Architecture of the ShcA proteins. The three isoforms encoded by Shc1 share similar structures. They contain two phosphotyrosine binding domains, the namely Phosphotyrsosine Binding Domain (PTB) in the N-terminal region and the Src Homology 2 domain (SH2) in the C-terminal region, separated by a Collagen Homology domain 1 (CH1). The longest isoform, p66, contains another glycine/proline-rich domain (CH2) [188].

p66ShcA Expression

While p52/46 are ubiquitously expressed[189], p66 expression is restricted. Hematopoietic, peripheral blood and brain cells express the protein in minimum quantities[189,189–191]. On the other hand, it has been reported that certain highly metastatic breast tumors upregulate the expression of this *ShcA* isoform[192]. The expression of p66 is mainly regulated at the transcription level. The promoter used for the transcription of p66 is the target of DNA methylation and there is a negative correlation between p66ShcA protein levels and the methylation status of its promoter[190].

p66 protein level has also been shown to be controlled by post-translational modifications[193]. One study identified two PEST sequences in two different domains of p66,

namely the CH2 domain (amino acid 14 to 64) and CH1 domain (328 to 327). As they describe, PEST sequences can act as a permanent signal for proteasome degradation or as a conditional signal. The phosphorylation of these serine/threonine residues is most likely performed by JNK and p38MAPK proteins in a Rac1 dependent manner[193]. The phosphorylation of p66 increased the half life of p66 by a 70% (from 4.5 to 8 hours), possibly by hiding the signal of the PEST sequences.

p66ShcA, Mechanism of Action and production of ROS

As mentioned above, p66 knock-out mice and their derived cell lines have an increased resistance to oxidative stress, when compared to p66-Wild-type controls. This p66 ablation also contributes to a prolonged lifespan in those mice[181]. The most likely mechanism by which p66 regulates this phenotype is the direct production of ROS.

There are two main states of p66ShcA. Under basal conditions, overexpression of p66ShcA does not cause apoptosis. It is only with a stress stimulus that this protein will cause the disruption of the mitochondrial membrane potential[194]. It has also been shown that a fraction of the cytoplasmic p66ShcA exists in the mitochondria. In steady-state conditions, p66ShcA forms a complex with Hsp70. This complex obstructs the oxidative activity of p66ShcA[194].

Upon a stress stimuli that may be caused by an oxidant like H_2O_2, UV radiation, ligands from RTKs (EGF)[181,183] or chemotherapies like Taxol[195] the serine 36 (S36) residue in the CH2 domain of p66ShcA is phosphorylated. Diverse studies show that this phosphorylation is performed by p38MAPK, JNK or members of the PKC protein family[196–198]. After the phosphorylation at S36, p66ShcA becomes a target of PIN1. This enzyme recognizes prolines followed by phospho-serine residues. After PIN1-mediated isomerization, p66 is dephosphorylated by PP2A and translocated into the mitochondria[199]. The mitochondrial fraction

of p66ShcA is released from the Hsp70 complex, possibly as an effect of the accumulation of cytoplasmic p66ShcA after its translocation[186,194].

Studies in the redox capacity of p66ShcA provided evidence of the oxidation of cytochrome c (cyt c). In this reaction, there is a transfer of electrons from cyt c to p66ShcA, onto oxygen as the final electron acceptor, leading to the production of ROS. To map the redox center of p66ShcA, the interaction of cyt c with different sections of p66ShcA was assessed through protein pull-down studies. It was discovered that a sequence of 52 amino acids in the N-terminal region of the PTB domain was the site of interaction with cyt c (cyt c binding sequence, CB)[186]. From the CB, the sequence E125, E132, E133, W134 and W148 is essential for the binding to cyt c[200].

A similar amino acid sequence was identified among p66ShcA proteins of different invertebrates. The change of two amino acids (EEW to QQW) abrogated the ability of p66ShcA to bind cyt c[186]. It has also been shown that the oxidative activity of p66ShcA may be promoted by its ability to downregulate *FKHRL1* (forkhead transcription factor) and ultimately downregulate expression of catalase[201]. Furthermore, the inhibitory interaction of p66ShcA with RTKs, has as consequence in the displacement of the SOS from Grb2 complexes and the interruption of RAS signaling. The free SOS protein promotes the activation of the GTPase Rac1 and this leads to the activation of membrane bound NADPH-oxidases, causing the production of cytoplasmic ROS[202].

The function of p66ShcA in a p53 wild-type context has been linked to the apoptotic p53 mediated program[181,203]. It has been shown that the activity of p66ShcA is dependent on the presence of p53, possibly by protein stabilization (studies performed in MEFs). The increased levels of ROS disrupts the mitochondrial membrane potential, leading to the formation of the

permeability transition pore, release of cyt c and activation of the apoptosome[203]. Although most of its oxidative activity has been linked to p53, p66ShcA is also able to induce oxidative stress in p53-deficient cancer cell lines in response to chemicals[204].

Oxidative Stress and Anti-Tumor Effect

The three main oxidants, superoxide anion, hydrogen peroxide and hydroxyl radical along with their derivatives can cause oxidative stress. This condition takes place when the production of ROS surpasses the capacity of the antioxidant machinery. Oxidative stress manifest in cells as direct damage in the macromolecules like proteins, lipids and DNA.

Aerobic respiration is the major source of cellular ROS. Approximately two percent of the oxygen used in aerobic respiration is converted into reactive oxygen species as a by-product of the electron transport chain[205]. This reaction produces superoxide anion. Part of the superoxide is released into the matrix where it is neutralized by Mn-superoxide dismutase (SOD2) [206].

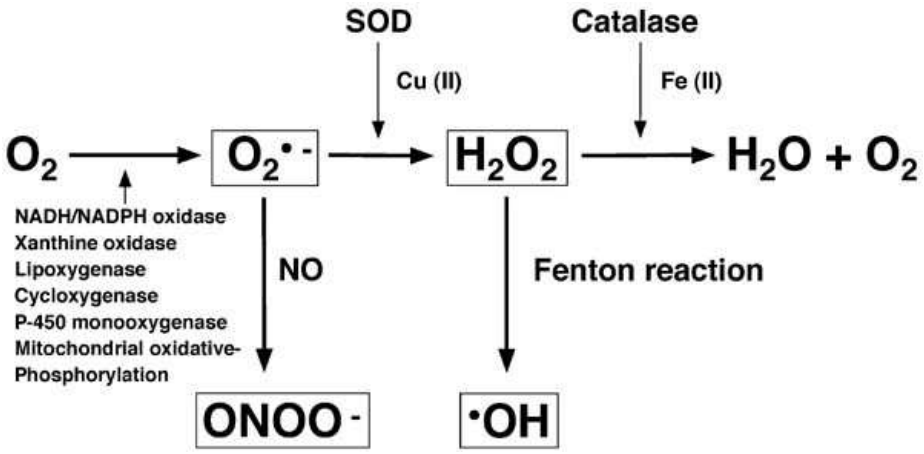

Figure 7: Reactive Oxygen Species Generation. Multiple cellular processes cause the production of mitochondrial ROS. The addition of an unpair electron into the oxygen molecule created superoxide anion. Superoxide anion produced in the matrix of the mitochondria is neutralized mainly by SOD2 in a reaction that generates hydrogen peroxide. H_2O_2 diffuses trough the organelle membranes and can be neutralized by catalase into oxygen and water. The reaction of hydrogen peroxide with Fe (II) initiated the self preserved Fenton Reaction and production of hydroxyl radicals. Adapted from Al-Dalaen et al.2014[207].

The neutralization of superoxide anion released into the mitochondrial intermembrane space is performed by Zn/Cu-superoxide dismutase (SOD 1)[208,209]. It is important to consider that the spatial localization of cyt c, the principal target of p66ShcA, resides in the intermembrane space of the mitochondria[210].

Superoxide anions are transformed into hydrogen peroxide and water by SOD2/SOD1. Hydrogen peroxide can cross mitochondrial membranes to the cytoplasm by diffusion. Although it does not have high reactivity, the interaction with ferrous cations Fe (II) will lead to the formation of hydroxyl radical (Fenton Reaction) and the oxidation of iron to Fe (III)[211]. The Fenton reaction is reversed with the reduction Fe (III) back to Fe (II) by the action of superoxide anion (Haber-Weiss reaction)[212]. A cell with constant production of superoxide anion may saturate its antioxidant capacity perpetuating the Fenton/Haber-Weiss reaction with constant production of hydroxyl radical. This radical has the biggest oxidative activity from all the ROS[213].

Oxidation of proteins can happen as a direct reaction with ROS or through the formation of an adduct with a product of lipid peroxidation (e.g. 4-HNE, MDA). The most common types of protein oxidation are the formation of disulfide bonds, methionine sulfoxide formation, destruction of Fe-S clusters (all reversible) or the oxidation of the alcohol groups in amino acids to form carbonyl groups (irreversible)[214].

Carbonylation is a type of oxidation that takes place in proteins specifically on the side chains of lysine, arginine, threonine and proline. It is characterized by the formation of ketones and aldehydes. More importantly, the identification of carbonyl functional groups in proteins has been directly linked with protein dysfunction and disease[215–218]. Mildly carbonylated proteins are

active targets of the proteasome, but under severe oxidative stress, the activity of the proteasome can be compromised and contributes to the accumulation of highly oxidized proteins. Toxic and highly carbonylated protein aggregates are formed, causing growth arrest and ultimately apoptosis[219].

One of the products of oxidation of DNA is 8-oxodG[220]. As previously mentioned, oxidation-related DNA lesions lead to the generation of ssDNA breaks by the action of glycosylases. The enzyme OGG1 excises the damaged base from the DNA chain generating the break[142]. Under conditions of oxidative stress, the generation of this type of lesion increases, leading to a hyper-activation of PARP1/2. Both enzymes are implicated in the recognition of DNA lesions and are necessary for the recruitment of the DNA repair machinery. The enzymatic activity of PARP depends on the substrate NAD+. It has been shown that increased PARP activity leads to depletion of the NAD+ pools, causing cell death due to lack of NADH and pyruvate[221].

Finally, lipids are damaged by the peroxidation of unsaturated chains mainly by hydrogen peroxide and hydroxyl radical. An important characteristic of lipid peroxidation is its self propagation. Once lipids are peroxidised they are unstable molecules that contribute to the distribution of damage mainly in the cellular and organelles membranes[222]. Among the principal products of lipid peroxidation are the lipid hydroperoxides (LOOH), which are the cause of the propagation of oxidative cellular damage. Alongside hydroperoxides, several types of aldehydes are formed. One example is 4-hydroxynonenal (4-HNE), which besides being the most toxic product of lipid peroxidation is used as a biomarker for oxidative stress[223]. The toxicity of lipid peroxidation is caused by the high reactivity of aldehydes with amino-acids producing

carbonylation[224], and the membrane rigidity caused by hydroperoxides[225]. This leads to cell dysfunction and death.

Rationale and Objectives

Although basal/triple negative breast tumors lacking ER, PR and HER2 expression are associated with a poor prognosis, non-targeted chemotherapy remains the standard of care for these patients[16]. The advent of PARP inhibitors represented a promising class of compounds for these women. Regrettably, clinical trials have shown limited survival benefit afforded to many TNBC patients treated with PARP inhibitors. However, cohorts of TNBC patients do show response to PARP inhibition, but predictive biomarkers of response are lacking. Of significance to this proposal, many cytotoxic agents employed to treat TNBC, and that act in synergy with PARP inhibitors, rely on the production of reactive oxygen species (ROS) to elicit a DNA damage response and induce apoptosis. Previous research from this lab has shown that p66ShcA is expressed in all subtypes of breast cancer but selectively in tumors with increased expression of mesenchymal markers[226].

Hypothesis

The increased ROS generated by p66ShcA in response to ROS-producing chemotherapies will generate DNA damage that needs to be repaired for survival. PARP activity will be required for this repair. As such, heightened p66ShcA expression may actually serve as a biomarker to predict responsiveness to PARP inhibition.

Aim 1: To determine whether p66ShcA regulates the cytotoxic activity of PARP inhibitors in vitro and in vivo.

In vitro studies: p66ShcA was deleted from the genome of two mesenchymal, TNBC breast cancer cell lines (MDA-MB-231 and Hs578T) using Crisper/CAS9 technology. These p66ShcA null cells were engineered to re-express wild-type p66ShcA or a p66ShcA mutant (QQW) that can no longer induce ROS. The cytotoxicity of control and p66ShcA null breast cancer cell lines to a pharmacological PARP inhibitor (Niraparib) was examined. This PARP inhibitor was combined with doxorubicin (chemotherapy that induces oxidative stress) at IC20 concentrations. Given that p66ShcA is a key mediator of stress–induced apoptosis, it was expected that p66ShcA-null cells would show decreased sensitivity to Dox alone, or in combination with PARP inhibitors. It was also expected that the re-expression of wild-type p66ShcA, but not the p66ShcA-QQW mutant would restore sensitivity to these combination therapies. The effects of the combination therapy were analyzed by performing cell viability assays, cell cycle analysis and Annexin V staining. Furthermore, DNA damage was assessed through the quantification of γH2AX foci, which marks double stranded DNA breaks, by immunofluorescent microscopy and distinct oxidative stress markers were measured.

In vivo studies: Control, p66ShcA-null and p66ShcA re-expressing Hs578T cells (1 x 10^6) were injected into the mammary fat pads of SCID-Beige mice. Once tumors reached 100mm3, the animals were randomized into four groups: (1) 25 mg/kg Niraparib daily by oral gavage, (2) 2.5 mg/kg Doxorubicin intraperitoneally every three days, (3) combination of Niraparib and Doxorubicin and (4) vehicle control. Tumor growth was monitored every two days by caliper measurements. When control tumors reached 750 mm3, the animals were sacrificed, and tissue harvested for IHC analysis using Ki67 and cleaved-caspase-3 specific antibodies to

measure the degree of cell proliferation and apoptosis, respectively. DNA damage (γH2AX) and oxidative stress (8-oxodG) were also assessed in these tumors.

Aim 2: To compare the effects of the combination of PARPi/Doxorubicin with PARPi/Carboplatin.

Given that clinical trials and current research in PARP inhibition in TNBC is leaning towards understanding the mechanisms behind PARPi in combination with platinum-based drugs (Table 1), here I compared the efficacy of the PARPi/Dox versus PARPi/Carboplatin combination therapies in reducing the growth potential of TNBC tumors, based on relative p66ShcA levels.

In vitro studies: p66ShcA-wild-type and null cells were exposed to the combination of Niraparib with doxorubicin or carboplatin. The effects of the combination therapy were analyzed by performing cell viability assays.

In vivo studies: Control, p66ShcA-null and p66ShcA re-expressing Hs578T cells (1 x 10^6) were injected into the mammary fat pads of nude mice. Once tumors reached 100mm3, the animals were randomized into six groups: (1) 25 mg/kg Niraparib daily by oral gavage, (2) 2.5 mg/kg Doxorubicin intraperitoneally every three days, (3) 15mg/Kg carboplatin every three days (4) combination of Niraparib and Doxorubicin and (5) combination of Niraparib and Carboplatin and (6) vehicle control. Tumor growth was monitored every two days by caliper measurements. When control tumors reached 750 mm3, the animals were sacrificed.

Chapter 2: Methods

Cell culture

Cell lines Hs578T and MDA-MB-231 were obtained from ATCC and cultured in 10% FBS (Wisent Bio Products catalog no. 080-150) DMEM (Wisent Bio Products catalog no. 319-005-CL).

Cell line generation

p66ShcA was deleted from the genome of Hs578T and MDA-MB-231 cell lines. The standard protocol of Fugene reagent (Promega catalogue no. E2311) was used to transfect both cell lines with 2µg of guide plasmid (targeting the ShcA CH2 domain), 2µg of hCas9, and 1µg of pQCXIB (lacking insert or GFP) to confer blasticidin resistance. Resistant cells were then selected using 10µg/mL blasticidin and clonal cell lines were established. Individual clonal lines were examined for expression of p66ShcA by immunoblot and five that completely lacked p66ShcA expression were pooled into a single cell population.

C-terminal flag-tagged p66ShcA-Wild-Type and p66ShcA-QQWmut[186] were cloned into the pMSCV (Clonetech) backbone (XhoI and EcoRI restriction sites). Phoenix (293T) cells were then transfected with p66ShcA expression vectors (Wild-Type and mutant) along with the backbone (VC) using the Effectene reagent (Qiagen catalogue no. 301425) following manufacturer's protocol. Centrifuged viral supernatants were used to infect Hs578T and MDA-MB-231 p66ShcA-KO cell lines. Expresser cells were selected by adding 2ug/mL of puromycin. All cell lines were routinely screened for mycoplasma contamination using a Mycoprobe Mycoplasma Detection Kit (R&D Systems, catalog no. CUL001B), at least once per month or one day prior to any mammary fat pad injection.

Cell Viability Assays

Hs578T and MDA-MB-231, p66ShcA-WT, p66ShcA-QQWmut and VC cells were cultured in 24 well plates with 3000 cells as an initial inoculum. The next day, cell lines were treated with doxorubicin (1nM, Sigma-Aldrich catalogue no. D1515), PARPi MK-4827 (300nM, APExBIO catalogue no. A3617) alone or in combination (Dox/PARPi) or DMSO (BioShop catalog no. DMS666) every two days. Cell counts were performed during the third and fifth day of treatment and the viability was evaluated by Trypan blue exclusion.

For the ROS scavenger growth curves, mitoTEMPO (10μM Sigma-Aldrich, catalogue no. SML0737) or pH 7.4 buffered N-acetyl cysteine (5mM, Sigma-Aldrich, catalogue no. A9165) were added from the day of seeding everyday during the course experiments. Media was only replaced when the chemotherapy and PARPi was added every two days.

Soft Agar Assay

A total of 20,000 cells (Hs578T) were plated into 1.5 mL of 20% FBS DMEM 0.4% Agar (Bioshop catalog no. AGR001.500) over a layer of 2 mL 20% FBS DMEM 0.6% Agar in 6-well plates. The day after seeding, cells were treated with 10% FBS containing drugs (Doxorubicin, PARPi, Dox/PARPi or DMSO). The concentration of drugs was calculated considering the agar volume (3.5 mL) and the media added (200uL) (1nM Dox, 300nM PARPi). Both drugs were added every 3 days and cells were kept in culture for 10 days.

Mammary fat pad injection

A total of $1x10^6$ cells (Hs578T p66ShcA and VC) were injected into the fourth mammary fat pad of 10-12 weeks-old SCID-BEIGE female mice. Upon first palpation, tumor growth was monitored using caliper measurements using the calculation as described by Ahn, et al., 2013[227]. When tumors reached $150mm^3$, mice were randomized into four groups: Doxorubicin alone,

PARPi alone, Dox/PARPi combination and vehicle control. Doxorubicin (2.5mg/Kg) was administered via Intraperitoneal Injection (IP) every three days and the PARPi (25mg/Kg) and vehicle via gavage daily. The volume of the tumors was monitored every two days until the vehicle control group reached an approximate volume of 750mm^3 (10 days). Breast tumors were fixed in 10% buffered formalin, or frozen in liquid nitrogen. All animal studies were approved by the Animal Resources Council at McGill University and comply with guidelines set by the Canadian Council of Animal Care.

Immunoblot Analysis

Cells were lysed with Whole Cell Lysis buffer (20mM Tris pH 7.5, 420 mM NaCl, 2mM MgCl2, 1mM EDTA, 10% glycerol, 0.5% NP40, 0.5% Triton) supplemented with 5mM NaF, protease and phosphatase inhibitor cocktail (PIN: 1 µg/ml Chymostatin, 2 µg/ml Antipain, 2 µg/ml Leupeptin, 1 µg/ml Pepstatin, 2 µg/ml Aprotinin) and 5mM $NaVO_4$. 2 volumes of lysis buffer (relative to cell pellet) was added to the collected cells and left on ice for 25 min. Lysates were centrifuged at 16,000 g, 4ºC during 20 min. Supernatant was collected into a new tube. Protein concentration was measured by Pierce BCA Protein assay (Thermo Fisher, catalogue no. 23227). 10ug of protein were loaded into 8% acrylamide gels and transferred into PDVF membrane at 80V for 2h. Membranes were blocked with 5% milk TBST (Tris base 20mM, NaCl 137mM, 0.05% Tween 20) and incubated in primary antibody (Millipore ShcA, 1:5000, catalogue no. 06-203, Sigma-Aldrich α-Tubulin, 1:5000 catalogue no. T5168). Secondary IgG antibodies coupled to horseradish peroxidase and ECL (Thermo Fisher, catalogue no. 32106) were used for protein detection.

Co-Immunoprecipitation

High density cell cultures (400,000 cells/6cm dish) were exposed to drugs (Dox 10nM, PARPi 300nM alone or in combination) for 48h. Cells were collected and lysed as described above. Protein concentration was determined by Pierce BCA Assay. A total of 1mg of protein was diluted in PLCγ lysis buffer (cytoplasmic buffer) supplemented with PIN, NaF and $NaVO_4$ (up to 300uL of total volume). FLAG antibody (Sigma-Aldrich, catalogue no. F3165) was added to the lysates (1:250 proportion). Lysates with FLAG antibody were nutated during 4h at 4ºC. Protein G sepharose beads were equilibrated in PLCγ lysis buffer without inhibitors and added into the lysates/antibody mixture (30uL bead volume) and left mixing overnight. Beads were washed with PLCγ lysis buffer three times (3000xg, 2min, 4ºC centrifugations). Proteins were eluted by adding cytoplasmic lysis buffer (with DTT) and incubating them at 95ºC for 5 min with a final centrifugation of 2 min at 5000xg at RT. After the collection of the supernatant, loading buffer was added and the eluted proteins were loaded into 8% acrylamide gels. Western blot was performed as described above with Anti-Shc phospho S36 (1:1000) (abcam, catalogue no. ab54518) and anti-Shc (1:5000) (Millipore, catalogue no. 06-203).

Immunohistochemistry

Immunohistochemical analyses were performed on paraffin-embedded sections (5 μm). The primary antibodies along with its respective antigen retrieval conditions are listed in Table 2. Rabbit antibodies, KI-67 (proliferation marker) and cleaved caspase 3 (apoptosis marker) IHC procedure was performed as follows. Tumor sections were permeabilized with three 5-minute washes with TBST (0.05% Tween 20 in 1mM Tris, pH 8, 15mM NaCl). Slides were incubated for 10 min at RT with unconjugated avidin, followed by 5-minute TBST wash and 10 min incubation with unconjugated biotin. Slides were washed with TBST for 5-minute and blocked

with 10% bovine serum albumin (BSA) in TBS. After blocking, slides were incubated in primary antibody (conditions found in Table 2) at 4º overnight. The tissues were then subjected to three 5 min washes with TBST. The slides were then incubated in avidin/biotinylated complex (ABC) for 30 min, followed by three 5-minute washes. Finally, the staining was developed using diaminobenzidine (DAB) substrate. The reaction was stopped before background staining was visible by adding water. Tissues were counter-stained with 20% hematoxylin for 1 minute and submerged in water for 5 min. Staining with monoclonal antibodies (8-oxodG and γH2AX) was performed with the Mouse on Mouse Polymer IHC Kit (abcam, catalogue no. ab127055) according to manufacturer instructions. Slides were scanned using a ScanScope XT Digital Slide Scanner (Aperio) and data were analysed using Image Scope software.

Immunofluorescence

Immunofluorescence was carried out similarly as described previously[228]. 6,000 cells were seeded on coverslips (24 well plate). After attachment, cells were treated with doxorubicin (1nM) alone, PARPi (300nM) alone, the combination of drugs and DMSO. After 48h of drugs exposure, cells were fixed in freshly prepared paraformaldehyde for 15 min. After fixation, cells were incubated for 10 min in 0,3% Triton X-100, 1% BSA and 2% normal goat serum. The primary antibody was added (Millipore catalogue no. JBW301, 1:1000) in PBS 1%BSA, overnight at 4ºC. After three five-minute washes (PBS 1%BSA), the secondary antibody was added (Mouse Alexa 488 nm, Invitrogen catalogue no. A11029, 1: 2000) for 1h at room temperature. Cells were washed as described before and stained with DAPI (1 μg/ml) and subjected to a final wash. The coverslips were mounted onto glass slides using ProLong gold antifade reagent (Thermo Fisher, catalogue no. P36930). Images were acquired using a Leica Widefield DM LB2 microscope.

Cell cycle analysis and apoptosis analysis

Cell cycle analysis was carried out as described previously[229]. Cells were cultured at low confluency (40,000 cells/ 6cm dish) in 10% FBS DMEM and treated with doxorubicin (1nM) alone, PARPi (300nM) alone, the combination of drugs and DMSO. After 48h of drug exposure cells were trypsinized and washed in 1X PBS with 3%FBS and spun down for 5 min at 500xg. Cells were fixed in 75% ethanol (PBS) and stored at 4°C. Cells were centrifuged and washed in PBS with 3%FBS followed by overnight staining with PI (25μg/mL PI, 500ug/mL RNAse, 3.6mM Na citrate). Before flow cytometry, cells were resuspended in 300μL of fresh propidium iodide (25 μg/mL). For apoptosis analysis, Annexin V (BD Bioscience, catalogue no. 556547) staining protocol was followed as per the manufacturer's instructions. Flow cytometry was performed in a BD LSR Fortessa (BD Bioscience) cell analyzer. The analysis of the data was carried out with the software FlowJo.

ROS production quantification

Cells were cultured at low confluency (40,000 cells/ 6cm dish) in 10% FBS DMEM and treated with doxorubicin (1nM) alone, PARPi (300nM) alone, the combination of drugs and DMSO. After 48h of drug exposure cells were washed with prewarmed 1x PBS. The probe H_2DCFDA (Thermo Fisher, catalogue no. D399) was added directly to the wells at a concentration of 5μM. Cells were incubated for 30 min at 37ºC. The cells were washed with 1xPBS, trypsinized and collected in a tube for a final wash. A final centrifugation at 500xg for 5 min was performed and cells and resuspended in 100 μL PI (5 μg/mL in 1xPBS). Cells were analyzed by flow cytometry in a BD LSR Fortessa (BD Bioscience) cell analyzer. The analysis of the data was carried out with the software FlowJo.

Protein Carbonylation ELISA

Cell cultures in the similar conditions described above (low confluency and drug exposure) were lysed by sonication (3 pulses of 10s at 20 kHz) in Tris-HCl (pH 7.5) buffer in ice. Cell lysates were centrifuged for 10 min at 16,000g, 4ºC and supernatant was collected. Protein carbonylation ELISA was performed according to manufacturer instructions (OxiSelect™ Protein Carbonyl ELISA Kit, Cell Biolabs Inc. catalogue no. STA-310).

Statistical Analysis

The statistical analysis and graphing were done with the software Prism-Graphpad 7. Data from viability assays, cell cycle staining, annexin V staining and protein carbonylation ELISA were analyzed with a two-way ANOVA (Tukey's multiple comparisons test). Soft agar, γH2AX immunofluorescence, and pS36-p66ShcA densitometry were analyzed with one-way ANOVA (multiple t-test). Finally, tumor growth curves, H_2DCFDA staining and IHC positivity were analyzed with two-tail, non-paired t-tests.

Chapter 3: Results

p66ShcA sensitizes TNBC cell lines to Doxorubicin/PARPi combination therapies *in vitro* and *in vivo*

To investigate whether p66ShcA sensitizes TNBC to the combination of chemotherapy/PARPi, we generated isogenic TNBC systems. p66ShcA was deleted from the TNBC cell lines Hs578T and MDA-MB-231 by CRISPR-Cas9 genomic editing. Both cell lines are *BRCA1/2* wild-type and express p66ShcA[226]. We re-expressed wild-type p66ShcA and the corresponding vector control (VC) (Figure 8A).

Cell lines were subjected to cell viability assays, as assessed by trypan blue exclusion, upon treatment with PARPi (Niraparib), or Doxorubicin, alone or in combination, each at sub-optimal doses (1nM Doxorubicin, 300nM Niraparib). Both cell lines showed similar reduction in viability at two timepoints (Figure 8B). The effect of both drugs as monotherapies was approximately 10-25% for Doxorubicin and 10-20% for Niraparib in viability reduction relative to DMSO. The viability reduction caused by the monotherapies was independent of the expression of p66ShcA. The combination of both drugs reduced the viability of cells lacking p66ShcA to approximately 30% on the third day of treatment and 40% after the fifth day. In contrast, p66ShcA expressors showed significantly reduced cell viability to a Doxorubicin/Niraparib combination therapy: 50-60% and 70% reduction in cell number after 3 or 5 days respectively, following drug treatments. This highlights a 40% difference in cell viability between VC and p66ShcA cell lines.

Similar results were obtained when testing the drugs as monotherapies and in combination in an anchorage independent growth assay (Figure 8C). p66ShcA-expressing cells

experienced a significative reduction in the formation of foci in all the treatment options (monotherapy or combination). Nevertheless, the reduction in foci formation exerted by the combination Dox/PARPi is 50% compared to the 25-30% reduction caused by the monotherapies in p66ShcA-carrying cells. Compared to p66ShcA cells, the transforming potential of VC cell lines remained unaffected by all the treatment options.

The growth potential of the foci was also analyzed with the soft agar experiment. By measuring the area of the foci formed after cells were exposed to DMSO, doxorubicin and PARPi alone or in combination, it was determined that p66ShcA drastically decreases the growth potential of TNBC anchorage-independent foci, specifically in the presence of the drug combination. In contrast, VC cells were able to grow without significant effect in the presence of the monotherapies or the combination of drugs. Together these data provided important insight about the feasibility of an *in vivo* experiment.

To test this, we injected VC or p66ShcA-expressing Hs578T cells into the mammary fat pads of immunodeficient mice (Figure 8D). At 150 mm^3, mice were treated with control (vehicle), doxorubicin (2.5 mg/kg every 3 days), PARPi (25 mg/kg daily) or doxorubicin + PARPi. Consistent with the *in vitro* studies, tumors were relatively insensitive to the tumoricidal properties of Dox and PARPi as monotherapies. Combination treatment administered to VC tumors marginally reduced tumor growth (<30%) compared to vehicle tumors at endpoint. Indeed, VC tumors exhibited progressive growth in the face of Dox/PARPi combination therapy (Figure 8D). In contrast, p66ShcA tumors displayed a ~ 5-fold reduction in tumor volumes following combined drug treatment, resembling stable disease (Figure 8D). These data suggest that p66ShcA sensitizes TNBCs to Dox/PARPi combination therapy in a synergistic manner.

p66ShcA Increases Apoptosis Induced by Doxorubicin/PARPi in TNBC

To gain mechanistic insight into this observed synergy, we examined how p66ShcA controls cell cycle progression and/or apoptosis in TNBCs in response to Dox/PARPi. Cell cycle analysis was carried out 48 hours post-treatment by PI staining followed by flow cytometry. In both p66ShcA expressing, or null cells, modest changes in cell cycle distribution were observed upon exposure to Dox/PARPi. (Figure 9A). Along with this observation, the Ki-67 IHC analysis of the Hs578T xenografts revealed the same levels of proliferation among p66ShcA-expressing and -deficient cells (Figure 9B). Together, these experiments suggest that the reduction of viability observed *in vitro* and the decreased tumor growth of p66ShcA carrying cells in the presence of the combination of drugs is not appreciably related to a cell cycle arrest.

Ruling out cell cycle arrest as the primary cause of reduced proliferation led me to focus on cellular death as a potential cause of the observed viability and tumor growth differences. Cells were exposed to the drugs alone and in combination for 48h. We compared the apoptotic profiles of VC and p66ShcA carrying cells by Annexin V/flow cytometry. p66ShcA expression resulted in a > 2-fold increase in the apoptotic rate in response to Dox/PARPi therapy (Figure 9C). As mentioned before, the decrease in viability (compared to DMSO control) for the VC cell lines during the third day of exposure to Dox/PARPi was approximately 30% and 60% for p66ShcA carrying cell lines (Figure 8B). These proportions correspond to the Annexin V positivity observed.

Comparable results were observed after the assessment of cleaved Caspase 3 by IHC in tumors collected at endpoint. p66ShcA-expressing tumors exposed to Dox/PARPi had a 2-fold increase in the number of apoptotic cells compared to vehicle control treated tumors (DMSO).

On the other hand, VC tumors showed no significant increase in cleaved caspase 3 positivity upon exposure to Dox/PARPi (Figure 9D). These data suggest that the reduced viability of p66ShcA-TNBCs to Dox/PARPi therapy results from an apoptotic response.

To observe the dynamics of cellular proliferation and death along the duration of the xenograft experiments, we also performed an early timepoint tumor necropsy (five-day treatment) (Figure 10 A, B). This timepoint was based on the results obtained in first animal experiment (Figure 8D). At this timepoint it is possible to observe a significative difference in tumor volume between VC and p66ShcA in Dox/PARPi group. While the levels of proliferation among VC and p66ShcA are comparable across treatments (around 50% of Ki-67 positivity), the apoptosis assessment revealed a slight increase in apoptosis caused by p66ShcA expression. Nevertheless, no significant differences among treatments were observed. This could suggest that the tumors were extracted before the p66ShcA-induced stress was fully activated by the drugs.

p66ShcA does not impact DNA damage in response to Doxorubicin/PARPi combination therapy

Given the crucial role of PARP1 in the reparation of DNA damage[230], as well as the mechanism of action of Doxorubicin[117], we aimed to determine if p66ShcA potentiates DNA damage caused by the drug combination. Ultimately, we sought to determine if DNA damage accumulation was the cause of the increased apoptosis observed.

We performed γH2AX immunofluorescent staining of vehicle and drug-treated VC and p66ShcA expressing TNBCs. The formation of phosphorylated γH2AX foci is indicative of double strand DNA breaks (DSB)[93]. As expected, the combination of drugs produced an obvious increase of DSBs, but this increase was independent of p66ShcA expression (Figure 11A). The proportion of nuclei with more than 10 foci after the Dox/PARPi exposure was approximately 65% for VC and p66ShcA cell lines.

Additionally, DNA damage was assessed by γH2AX staining by IHC for the Hs578T xenografts. Similar levels of DNA damage were observed between tumors and treatments after 10 days of exposure to drugs (Figure 11B). Together *in vitro* and *in vivo* data suggest that p66ShcA does not quantifiably impact DNA damage in response to a Dox/PARPi therapy.

Molecular Features of p66ShcA and their Role in the Production of Reactive Oxygen Species.

As it has been previously shown, p66ShcA related induction of apoptosis is dependant on Ser36 phosphorylation[186]. This posttranslational modification is induced by stress-kinases (e.g. p38MAPK[193], JNK[197], PKCs[198]) and allows p66ShcA to translocate to the mitochondria, where it catalyzes the formation of ROS[181,186]. We observed that the phosphorylation of p66ShcA with drugs as monotherapies is marginally increased, but the exposure induces a significant increase in p66ShcA S36 phosphorylation (Figure 12A). This level of protein activation may explain the reduction in viability observed in the p66ShcA-carrying cells and potentially narrows the molecular mechanism of the observed synergy to the activity of p66ShcA inside the mitochondria.

We sought to investigate if the impaired *in vitro* growth potential of p66ShcA-expressing cells to PARPi/Dox treatment was related to the ability of p66ShcA to produce ROS. To this end, we compared the viability growth curves of VC, p66ShcA-Wt and p66ShcA-QQmut[186] (Figure 12B). This mutant (amino-acids E132, E133 change to QQ) version of p66ShcA can be imported into the mitochondria but lacks the critical amino acids that mediate its interaction with cytochrome c[186], thus preventing the formation of ROS. As previously described, the drugs as monotherapies had marginal effects on the viability of p66ShcA-Wt cells while the combination, drastically reduced the number of cells. Furthermore, the growth curves obtained from the p66ShcA-QQmut cell lines phenocopied the growth observed in the VC cells (Figure 12C). The data suggests that the observed reduction in viability exerted by p66ShcA in the presence of the drug combination is dependent on its ability to interact with cytochrome c. This ultimately points

to the formation of ROS as the underlying mechanism of the phenotype observed, which was subsequently experimentally tested.

p66ShcA Induces an Oxidative Stress Response in Breast Cancer Cells in Response to Doxorubicin/PARPi

To investigate whether p66ShcA-expressing Hs578T cells had an increase in ROS production upon exposure to Dox/PARPi therapy we used the H_2DCFDA probe. This probe diffuses passively into the cells, where it is deacetylated by intracellular enzymes and ultimately oxidized by ROS. Its oxidized form cannot exit the cell and has an Excitation/Emission wavelength of ~492–495/517–527 nm respectively. The intensity of the fluorescence is proportional to the amount of intracellular ROS.

After 48h of exposure to the drugs, p66ShcA and VC cells were stained with the probe and fluorescence intensity was analyzed by flow cytometry. The histograms show a comparison between VC and p66ShcA cell lines in the treatments (Doxorubicin and PARPi alone or in combination) normalized to basal (DMSO) levels of ROS (Figure 13A). While the levels of ROS remained close to baseline for the cells treated either with doxorubicin or PARPi (slight increase), the cells exposed to the combination therapy showed a more pronounced ROS increase. VC cells showed a 75% increase in ROS whereas p66ShcA cells had a 150% increase. This suggests that the drugs by themselves can generate ROS, but that p66ShcA stimulates a further 2-fold increase in ROS production.

Finally, we sought to determine if the observed increase in intracellular ROS caused oxidative damage in the cells. Using an ELISA colorimetric assay, we quantified protein carbonylation in whole cell lysates from VC and p66ShcA cells exposed to the drugs. The results

are expressed as the fold increase in protein carbonylation relative to control (DMSO). Here, we show that Doxorubicin by itself induces a 2-fold increase in protein carbonylation in p66ShcA cells (Figure 13B). Most importantly, p66ShcA cells had a 7-fold increase in protein carbonylation treated with the combination of drugs. This experiment suggests that the viability difference between VC against p66ShcA-Wt may be due to oxidative protein damage. Additionally, we show IHC analysis of tumors stained for 8-oxodG (oxidative stress marker) at endpoint (Figure 13C) and early timepoint (Figure 10C). Although, there is a modest increase in oxidized DNA in p66ShcA-carrying tumors exposed to the Dox/PARPi combination compared to vehicle group, at basal levels VC tumors seem to have more damage than p66ShcA (approximately 15% for p66ShcA and 30% for VC) (Figure 13C). Even though VC tumors have higher baseline levels of oxidative damage, the combination Dox/PARPi does not induce further 8-oxoG accumulation. The damage observed in tumors extracted at an early timepoint (5 days of treatment) showed similar levels of oxidative damage among treatments. Nevertheless, it is possible to observe increased basal DNA oxidation in the p66ShcA group compared to VC (Figure 13C). At both timepoints, the levels of DNA oxidative damage do not explain the phenotype observed *in vivo* possibly due to a kinetic issue. Together these data suggest that the combination of Dox/PARPi activates the molecular mechanism of p66ShcA leading to ROS production and oxidative damage.

ROS scavengers reverse p66ShcA-induced sensitivity of TNBCs to Doxorubicin/PARPi combination therapy

Finally, cell viability assays were carried out to investigate if ROS scavengers could reverse the observed phenotypes. mitoTEMPO, a mitochondrial superoxide anion scavenger and

N-acetyl-cysteine (NAC), a precursor in the synthesis of glutathione (molecule involved in the neutralization of ROS) were administered to the cells a day before the chemotherapy and PARPi treatment and then replenished daily. Both scavengers were able to rescue the viability of p66ShcA-expressing cells to 3 and 5 days of PARPi/Dox treatment to the levels of drug-treated VC cells (Figure 14A, B). Overall, these data strongly support the hypothesis that p66ShcA generates mitochondrial ROS to sensitize TNBCs to a Dox/PARPi combination therapy.

p66ShcA sensitizes TNBC cell lines to Doxorubicin/PARPi but not to Carboplatin/PARPi combination

To investigate whether there is a difference in sensitivity depending on the chemotherapy utilized in the combination therapy, cell viability assays were performed (Figure 15A). Cells were collected and counted at the fifth day of treatment. As expected, PARPi showed a marginal reduction in viability independent of p66ShcA status. A similar phenotype was observed after the exposure to carboplatin as monotherapy. In contrast, p66ShcA sensitized Hs578T to doxorubicin (approximately 20% difference in viability between VC and p66ShcA) and doxorubicin plus PARPi (40% difference in viability between VC and p66ShcA).

Interestingly the combination of carboplatin and PARPi decreased the viability of Hs578T cells to 60% independently of p66ShcA status. This result may indicate that the molecular mechanism of action of the combination of carbo/PARPi may be different to the one from the dox/PARPi combination. MDA-MB-231 VC cells showed more resistance to the combination of carboplatin and PARPi (80% viability) compared to p66ShcA carrying cells (60% viability). Nevertheless, there is a difference of nearly 40% of viability between Dox/PARPi and Carbo/PARPi combinations in p66ShcA expressing cells. This shows that although the mechanism of action of p66ShcA may be also activated by carboplatin in combination with PARPi, doxorubicin is superior in its ability to synergize with PARPi, specifically in p66ShcA-expressing cells.

Next, we sought to determine the effects of the combination of both chemotherapies with PARPi *in vivo.* As observed previously, p66ShcA expression had minor effects on the growth of tumors treated with drugs as monotherapies (Figure 15B). However, the combination

Dox/PARPi exacerbated the death of p66ShcA expressing tumors in comparison to VC. In contrast, p66ShcA had no effect on the sensitivity of Hs578T tumors to the carbo/PARPi combination treatment. The *in vivo* data recapitulates the observations made *in vitro* and together these data suggest that doxorubicin may be a better chemotherapy to combine with PARPi for tumors with high expression of p66ShcA.

Figure 8

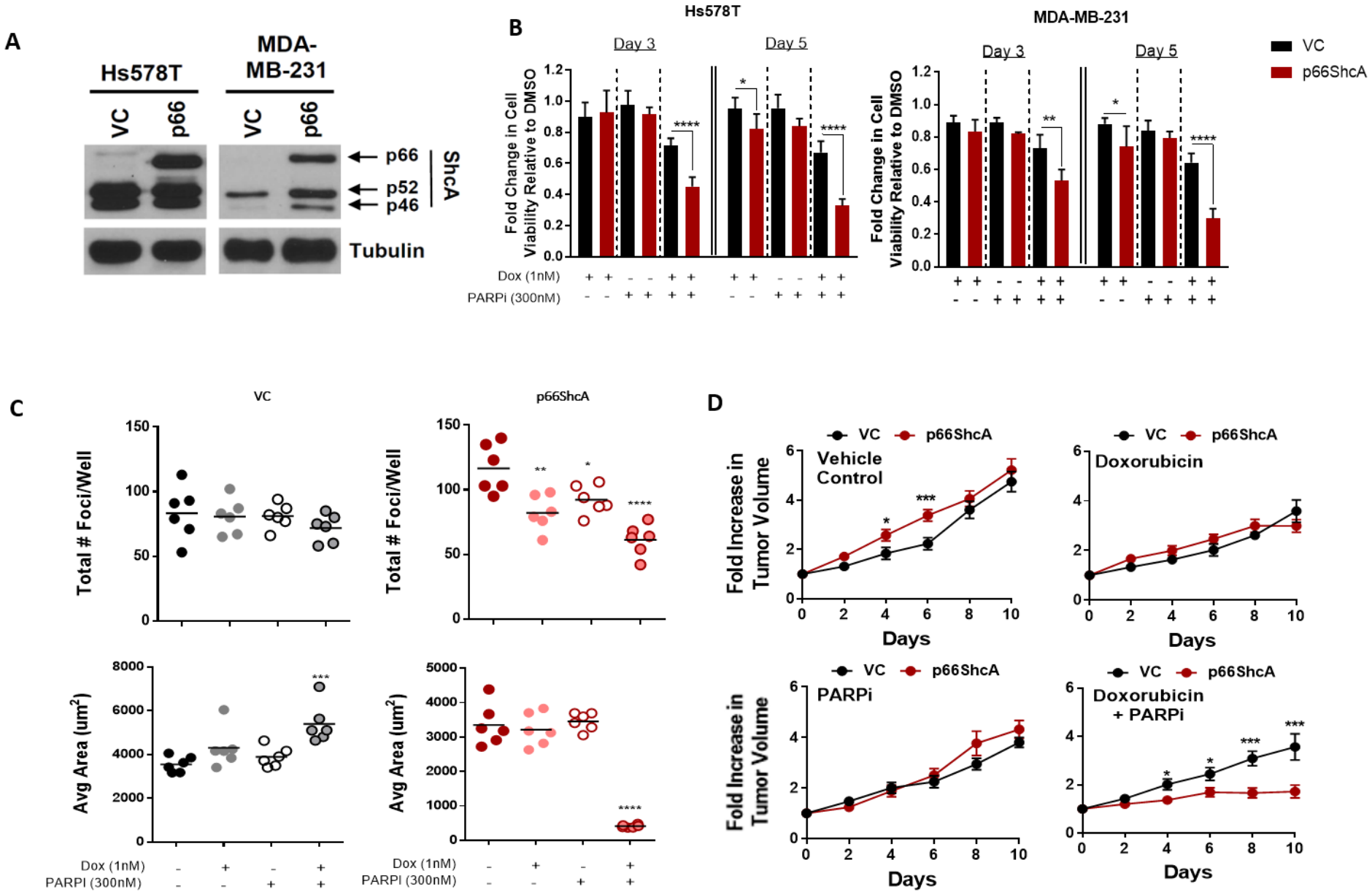
A
Hs578T
MDA-MB-231
VC
p66
p66
p52
p46
ShcA
Tubulin
B
Hs578T
MDA-MB-231
Day 3
Day 5
Fold Change in Cell Viability Relative to DMSO
Dox (1nM)
PARPi (300nM)
VC
p66ShcA
C
VC
p66ShcA
Total # Foci/Well
Avg Area (um²)
Dox (1nM)
PARPI (300nM)
D
Vehicle Control
Doxorubicin
PARPi
Doxorubicin + PARPi
Fold Increase in Tumor Volume
Days

Figure 8: p66ShcA sensitizes TNBC cell lines to Doxorubicin/PARPi combination therapies in vitro and in vivo. (A) p66ShcA was deleted from Hs578T and MDA-MB-231 cells by Crispr/Cas9 editing. These cells were infected with an empty vector (VC) or p66ShcA-expressing vector (p66). (B) Cells were cultured either in DMSO, doxorubicin (1 nM), PARPi (Niraparib) (300 nM), alone or combined for 3 or 5 days. Viable cells were quantified by trypan blue exclusion. Data is shown as fold change in the number of viable cells relative to DMSO ± SEM (n=3 biological replicates, 4-6 wells each condition): *, $P<0.05$; **, $P < 0.01$; ****, $P < 0.0001$. (C) Soft agar assay to assess the tumorigenic potential of Hs578T-VC and –p66ShcA expressing cells cultured in response to continuous culture in the presence of vehicle control (DMSO), Doxorubicin (1 nM), PARPi (300 nM), alone or in combination over a 10-day period. The total # foci per cell and average area of each foci was quantitated (n=6 wells each): *, $P<0.05$ **, $P < 0.01$; ***, $P < 0.001$; ****, $P < 0.0001$. (D) VC or p66ShcA-expressing Hs578T cells were injected into the mammary fat pads of SCID-Beige mice. At 150mm^3, mice were randomized into four treatment groups: (1) DMSO, (2) doxorubicin; 2.5 mg/kg, (3) PARPi; 25 mg/kg or (4) doxorubicin + PARPi combination therapy. The data is shown as fold increase in tumor volume relative to the start of treatment (Day 0) ± SEM (n= 20-22 mice per group): *, $P<0.05$; ***, $P < 0.001$.

Figure 9

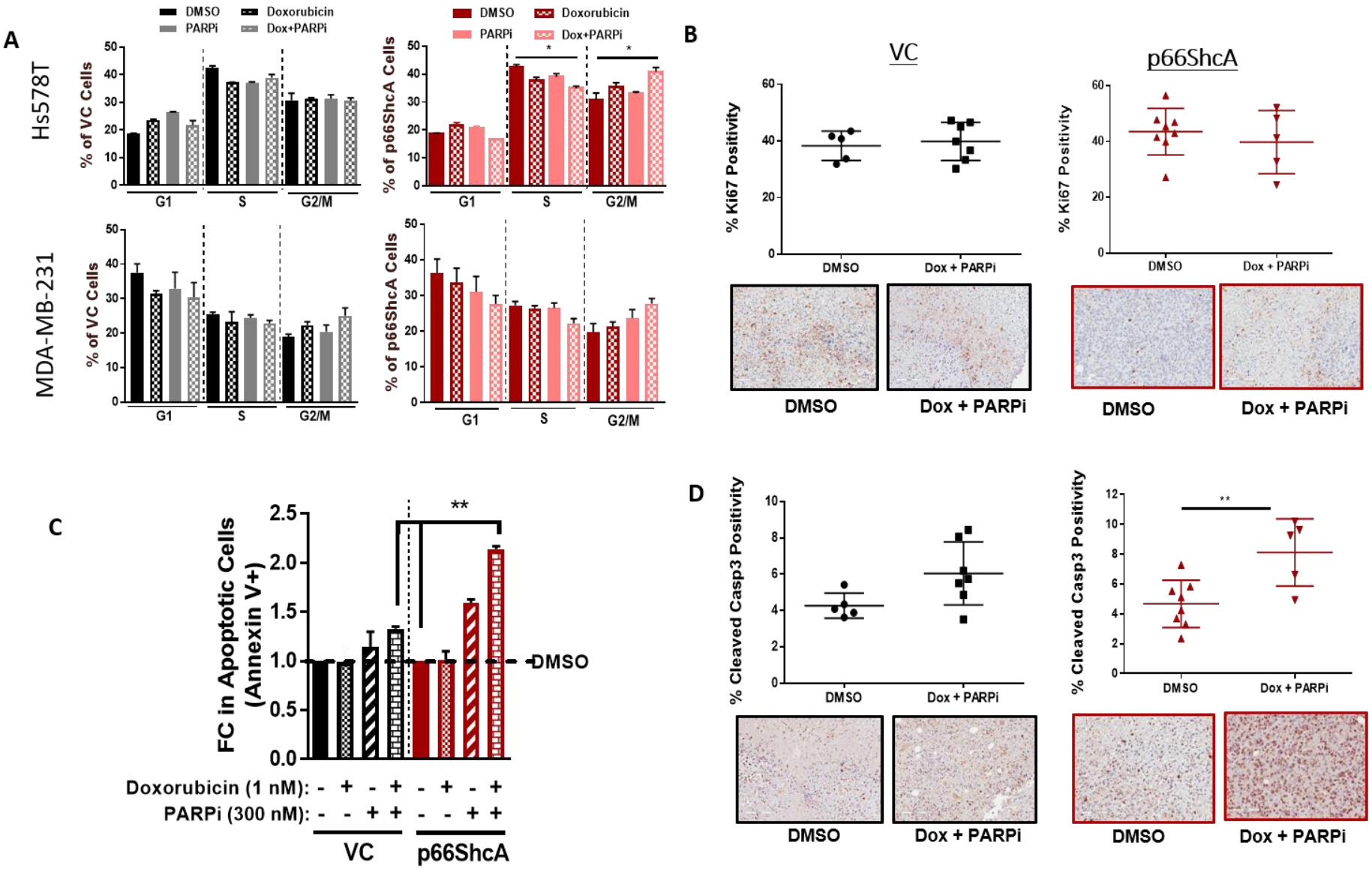
A
Hs578T
MDA-MB-231
DMSO
PARPi
Doxorubicin
Dox+PARPi
% of VC Cells
% of p66ShcA Cells
G1
S
G2/M
B
VC
p66ShcA
% Ki67 Positivity
DMSO
Dox + PARPi
C
FC in Apoptotic Cells (Annexin V+)
**
Doxorubicin (1 nM): - + - + - + - +
PARPi (300 nM): - - + + - - + +
VC
p66ShcA
D
% Cleaved Casp3 Positivity

Figure 9: p66ShcA Increases Apoptosis Induced by Doxorubicin/PARPi in TNBC. (A) VC or p66ShcA-expressing Hs578T cells were treated with Doxorubicin (1 nM), PARPi (300 nM), alone or in combination. PI staining/flow cytometry was performed to measure DNA content and determine cell cycle distribution. The data is shown as % cells in G1, S or G2/M phase of the cell cycle ± SEM (n=3 biological replicates): *, $P<0.05$. (B) VC and p66-ShcA expressing Hs578T tumors were treated with doxorubicin (2.5 mg/kg) and PARPi (25 mg/kg) or vehicle control. The proliferative rate was determined by Ki67 immunohistochemical staining. The data is depicted as % average of positive Ki-67 nuclei (n=6-8 tumors per group) Representative images of the IHC staining illustrating Ki-67 are shown (C) VC or p66ShcA-expressing Hs578T cells were treated with Doxorubicin (1 nM) and PARPi (300 nM), alone or in combination. The % of apoptotic cells was determined by Annexin V staining/flow cytometry. Results are presented as "fold change" in % of Annexin V positive cells relative to DMSO (control) (n=2 biological replicates): **, $P < 0.01$. (D) VC and p66-ShcA expressing Hs578T tumors were analyzed by cleaved caspase 3 IHC staining (n=6-8 tumors each): **, $P < 0.01$. Representative images IHC staining illustrating cleaved caspase 3 positivity are shown.

Figure 10

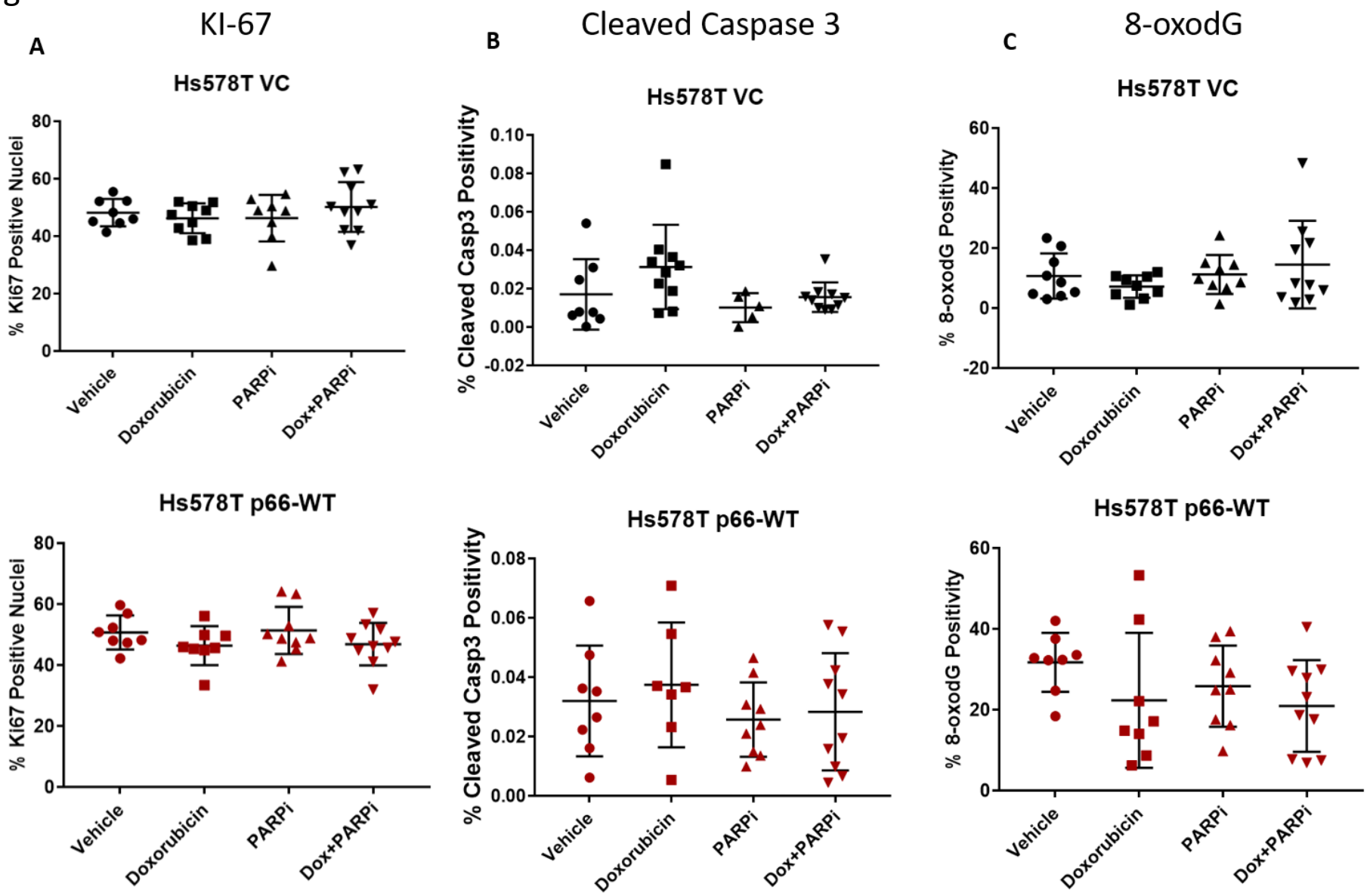
KI-67
A
Hs578T VC
% KI67 Positive Nuclei
0
20
40
60
80
Vehicle
Doxorubicin
PARPi
Dox+PARPi
Hs578T p66-WT
% KI67 Positive Nuclei
0
20
40
60
80
Vehicle
Doxorubicin
PARPi
Dox+PARPi
Cleaved Caspase 3
B
Hs578T VC
% Cleaved Casp3 Positivity
-0.02
0.00
0.02
0.04
0.06
0.08
0.10
Vehicle
Doxorubicin
PARPi
Dox+PARPi
Hs578T p66-WT
% Cleaved Casp3 Positivity
0.00
0.02
0.04
0.06
0.08
Vehicle
Doxorubicin
PARPi
Dox+PARPi
8-oxodG
C
Hs578T VC
% 8-oxodG Positivity
-20
0
20
40
60
Vehicle
Doxorubicin
PARPi
Dox+PARPi
Hs578T p66-WT
% 8-oxodG Positivity
0
20
40
60
Vehicle
Doxorubicin
PARPi
Dox+PARPi

Figure 10: IHC Analysis of Early Timepoint *In Vivo* Experiment. Hs578T VC and p66ShcA cells were injected in the mammary fat-pad of SCID-Beige mice. Upon tumor growth of 150mm^3 animals were randomized into four groups (1) vehicle control (2) doxorubicin (2.5mg/Kg every three days) (3) PARPi (15mg/Kg daily) and (4) combination Doxorubicin/PARPi. Tumors were extracted after 5 days of treatment and tissue was analyzed by IHC. (A) The proliferative rate was determined by Ki67 immunohistochemical staining. The data is depicted as % average of positive Ki-67 nuclei (n=10 tumors per group). (B) VC and p66-ShcA expressing Hs578T tumors were analyzed by cleaved caspase 3 IHC staining (n=10 tumors each). (C) Oxidative stress marker 8-oxodG was analyzed by IHC staining in VC and p66-ShcA expressing Hs578T tumors. The data is depicted as average % of 8-oxodG positivity (n=10 tumors each).

Figure 11

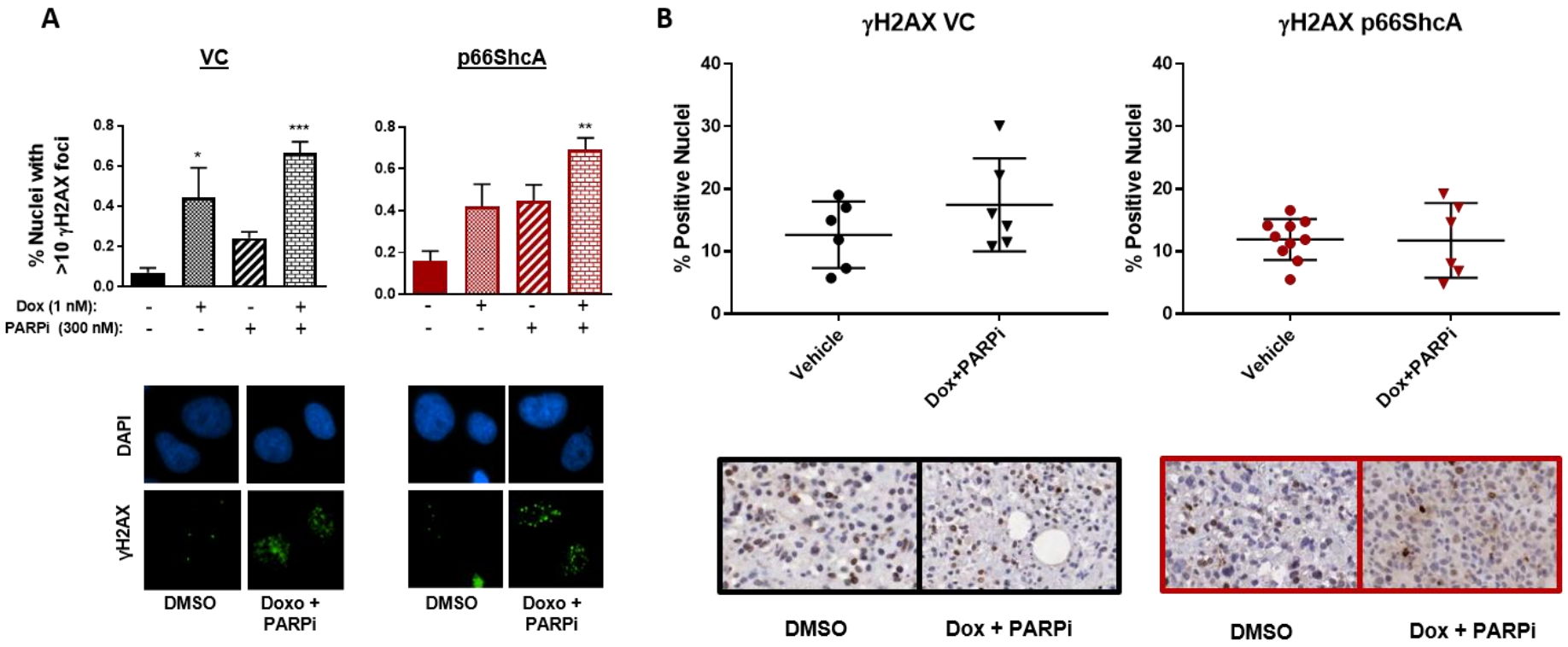
A
VC
p66ShcA
% Nuclei with >10 γH2AX foci
0.8
0.6
0.4
0.2
0.0
*
***
**
Dox (1 nM):
PARPi (300 nM):
DAPI
γH2AX
DMSO
Doxo + PARPi
B
γH2AX VC
γH2AX p66ShcA
% Positive Nuclei
40
30
20
10
0
Vehicle
Dox+PARPi
DMSO
Dox + PARPi

Figure 11: p66ShcA does not impact DNA damage in response to Doxorubicin/PARPi combination therapy.

(A)VC or p66ShcA-expressing Hs578T cells were treated with Doxorubicin (1 nM) and PARPi (300 nM), alone or in combination for two days. Double stranded DNA breaks were assessed by pγH2AX immunofluorescent staining. % nuclei with >10 γH2AX foci was quantified ± SEM (n=3 biological replicates). Representative images of the fluorescent staining illustrating γH2AX foci are shown. (B) VC and p66-ShcA expressing Hs578T tumors were treated with doxorubicin (2.5 mg/kg) and PARPi (25 mg/kg) or vehicle control. DNA damage levels were determined by pγH2AX immunohistochemical staining. The data is depicted as average % of positive pγH2AX nuclei (n=6-8 tumors per group). Representative images IHC staining illustrating pγH2AX positive nuclei are shown.

Figure 12

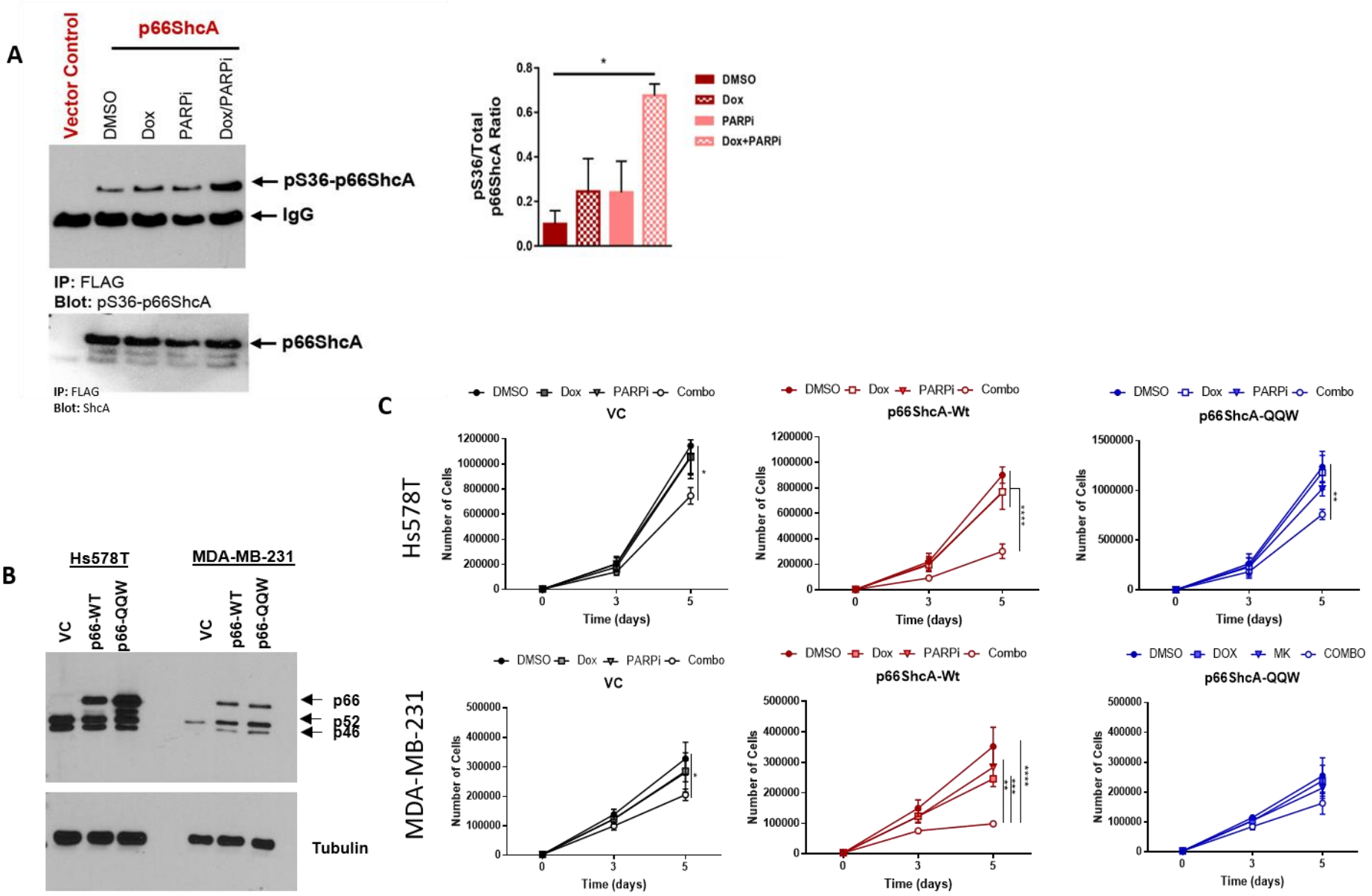
A
Vector Control
p66ShcA
DMSO
Dox
PARPi
Dox/PARPi
pS36-p66ShcA
IgG
IP: FLAG
Blot: pS36-p66ShcA
p66ShcA
IP: FLAG
Blot: ShcA
pS36/Total p66ShcA Ratio
DMSO
Dox
PARPi
Dox+PARPi
B
Hs578T
MDA-MB-231
VC
p66-WT
p66-QQW
p66
p52
p46
Tubulin
C
Hs578T
MDA-MB-231
DMSO Dox PARPi Combo
DMSO DOX MK COMBO
VC
p66ShcA-Wt
p66ShcA-QQW
Number of Cells
Time (days)

Figure 12: Molecular Features of p66ShcA and their Role in the Production of Reactive Oxygen Species. (A) Hs578T cells were cultured in the absence (DMSO) or presence of Doxorubicin (1 nM), PARPi (300 nM) alone or combined for 48 hours. (A) FLAG immuno-precipitates were blotted with pS36-p66ShcA or Shc antibodies. (B) Quantification from 3 experiments: *, $P<0.05$. (B) Immunoblot showing relative expression levels of wild-type p66ShcA or the p66-QQ mutant (cannot induce ROS formation) in Hs578T and MDA-MB-231 cells. (C) VC, wild-type p66ShcA- or p66ShcA-QQmut expressing Hs578T and MDA-MB-231 cells were treated with Doxorubicin (1 nM) and PARPi (300 nM), alone or in combination. The number of viable cells was determined by trypan blue exclusion on days 3 and 5 post treatment. The graphs show the average number of cells at each timepoint ± SEM (n=3 biological replicates): *, $P<0.05$ **, $P < 0.01$; ***, $P < 0.001$; ****, $P < 0.0001$.

Figure 13

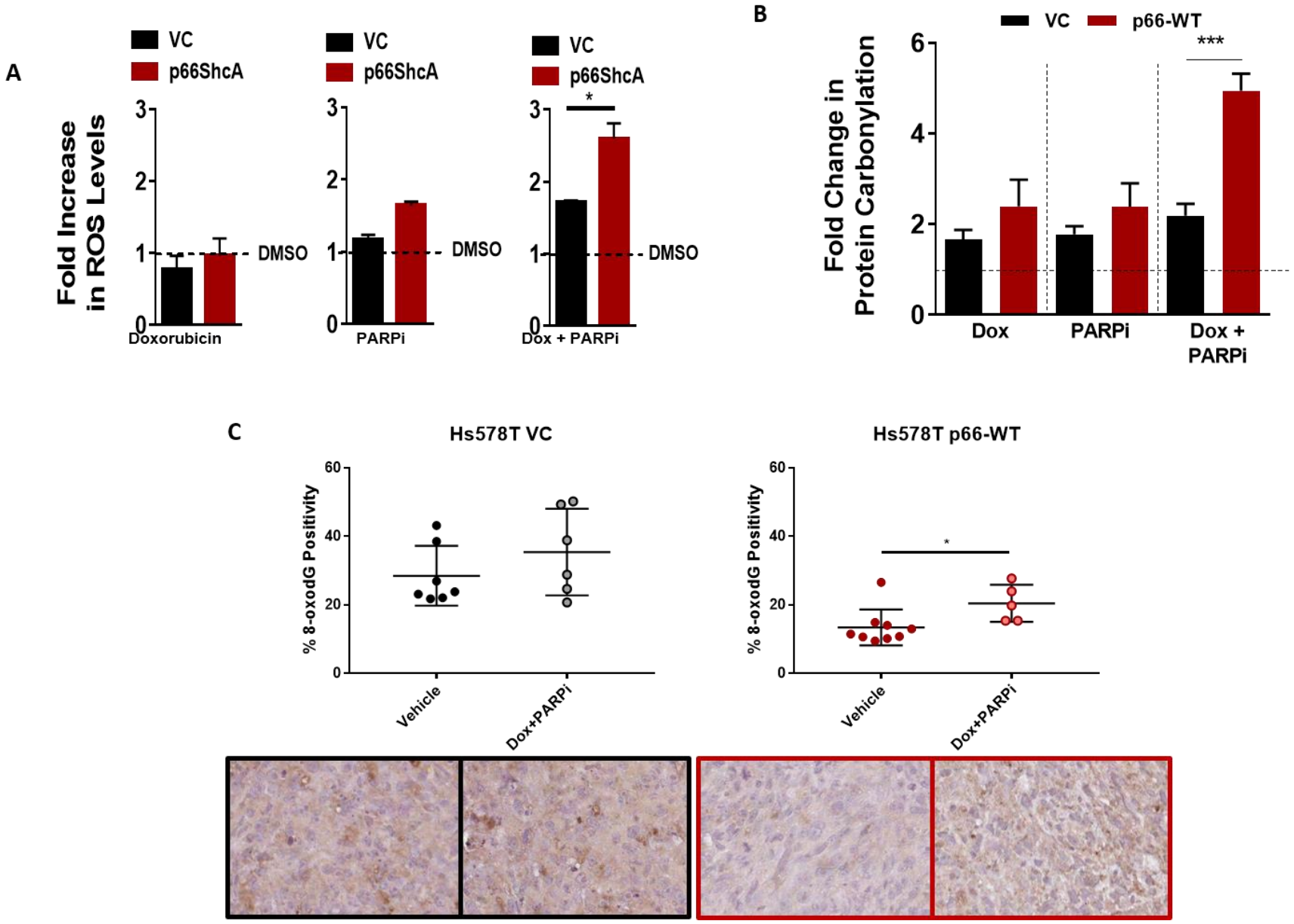
A
VC
p66ShcA
Fold Increase in ROS Levels
DMSO
Doxorubicin
PARPi
Dox + PARPi
*
B
VC
p66-WT
***
Fold Change in Protein Carbonylation
Dox
PARPi
Dox + PARPi
C
Hs578T VC
Hs578T p66-WT
% 8-oxodG Positivity
Vehicle
Dox+PARPi

Figure 13: p66ShcA Induces an Oxidative Stress Response in Breast Cancer Cells in Response to Doxorubicin/PARPi. (A) VC or p66ShcA-expressing Hs578T cells were treated with Doxorubicin (1 nM) and PARPi (300 nM), alone or in combination for two days. ROS levels were determined by H_2DCFDA staining and measured by flow cytometry. The data is shown as fold increase in H_2DCFDA mean fluorescence intensity compared to control (DMSO) treated cells (n=2). (B) VC, p66ShcA-WT or p66ShcA-QQmut Hs578T cells were treated with Doxorubicin and PARPi for three days. Protein carbonylation was measured by ELISA. The data is shown as average fold change compared to control (DMSO) ± SD (n=3): ***, $P < 0.001$. (C) Oxidative stress marker 8-oxodG was analyzed by IHC staining in VC and p66-ShcA expressing Hs578T tumors. The data is depicted as average % of 8-oxodG positivity (n=6-8 tumors each): *, $P < 0.05$. Representative images of the IHC staining illustrating 8-oxodG positivity are shown.

Figure 14

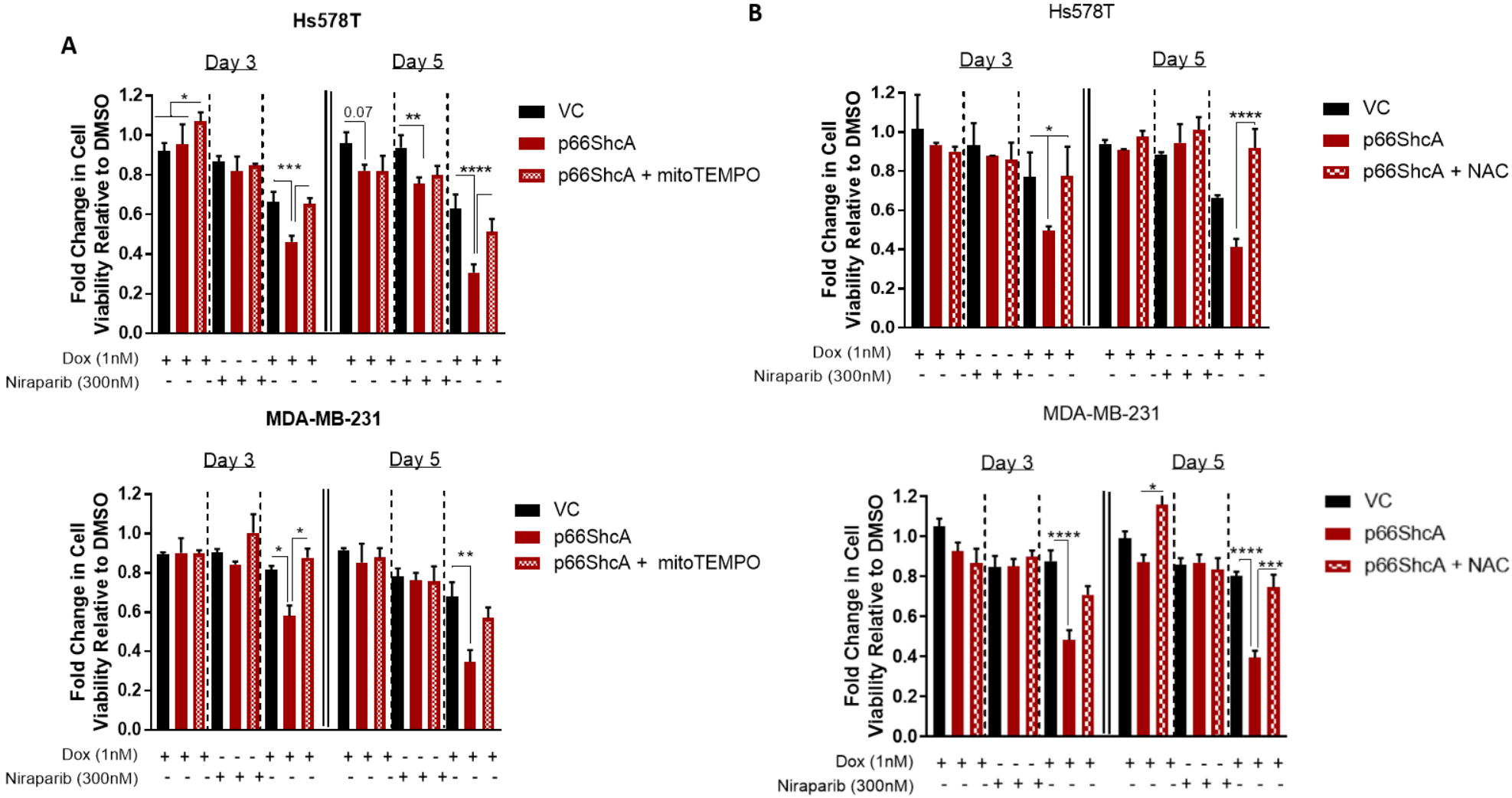
A
Hs578T
Day 3
Day 5
Fold Change in Cell Viability Relative to DMSO
0.07
VC
p66ShcA
p66ShcA + mitoTEMPO
Dox (1nM)
Niraparib (300nM)
MDA-MB-231
B
Hs578T
p66ShcA + NAC
MDA-MB-231

Figure 14: ROS scavengers reverse p66ShcA-induced sensitivity of TNBCs to Doxorubicin/PARPi combination therapy. VC and wild-type p66ShcA-expressing Hs578T and MDA-MB-231 cells were treated with Doxorubicin (1nM) and PARPi (300 nM), alone or in combination in presence or absence of MitoTEMPO (10μM) or NAC (5mM). Cell viability was determined by trypan blue exclusion. Results are depicted as average fold change in cell viability relative to DMSO ± SD: *, $P<0.05$ **, $P < 0.01$; ***, $P < 0.001$; ****, $P < 0.0001$.

Figure 15

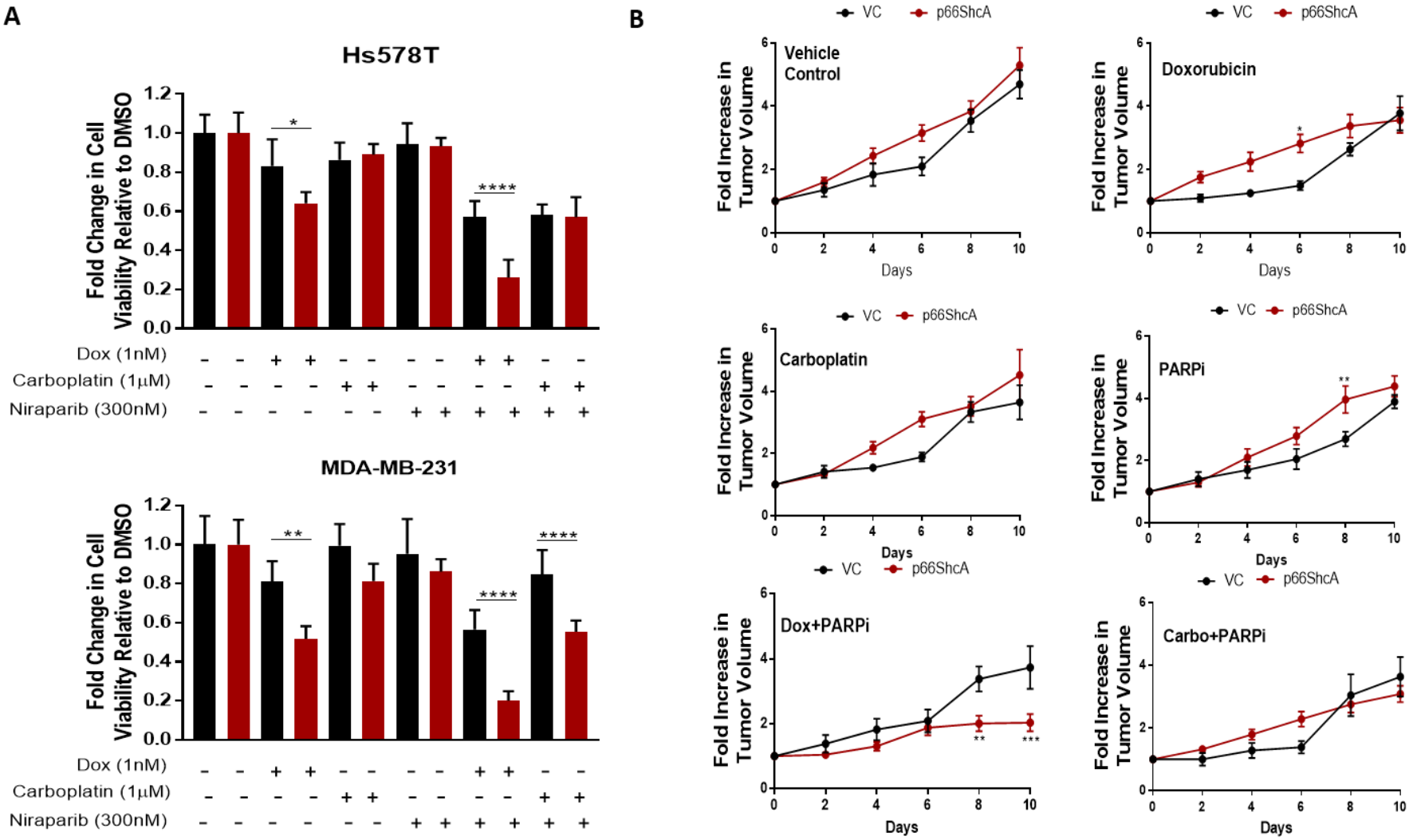
A
Hs578T
Fold Change in Cell Viability Relative to DMSO
1.2
1.0
0.8
0.6
0.4
0.2
0.0
*
****
Dox (1nM) - - + + - - - - + + - -
Carboplatin (1μM) - - - - + + - - - - + +
Niraparib (300nM) - - - - - - + + + + + +
MDA-MB-231
Fold Change in Cell Viability Relative to DMSO
**
****
****
Dox (1nM) - - + + - - - - + + - -
Carboplatin (1μM) - - - - + + - - - - + +
Niraparib (300nM) - - - - - - + + + + + +
B
VC
p66ShcA
Vehicle Control
Doxorubicin
Carboplatin
PARPi
Dox+PARPi
Carbo+PARPi
Fold Increase in Tumor Volume
Days
0
2
4
6
8
10
*
**
***

Figure 15: p66ShcA sensitizes TNBC cell lines to Doxorubicin/PARPi but not to Carboplatin/PARPi combination. (A) Cells were cultured either in DMSO, doxorubicin (1 nM), carboplatin (1μM) PARPi (Niraparib) (300 nM), alone or combined for 5 days. Viable cells were quantified by trypan blue exclusion. Data is shown as fold change in the number of viable cells relative to DMSO ± SD (n=6 wells each condition): *, P<0.05; **, P < 0.01; ****, P < 0.0001. (B) VC or p66ShcA-expressing Hs578T cells were injected into the mammary fat pads of SCID-Beige mice. At 150mm3, mice were randomized into four treatment groups: (1) DMSO, (2) doxorubicin; 2.5 mg/kg, (3) carboplatin; 15mg/kg, (4) PARPi; 25 mg/kg, (5) doxorubicin + PARPi or (6) carboplatin + PARPi combination therapy. The data is shown as fold increase in tumor volume relative to the start of treatment (Day 0) ± SEM (n= 8-14 mice per group): *, P<0.05; **, P< 0.01; ***, P < 0.001.

Chapter 4: Discussion

In this project we aimed to determine whether p66ShcA could be used as a predictive biomarker for TNBC cells exposed to the combination of PARPi and chemotherapy. As mentioned before, phase III clinical trials have shown that the administration of PARPi as monotherapy does not represent a clinical advantage on the overall survival of patients. The rationale behind the utilization of PARP inhibitors in TNBC patients was that even though only 15-20% of TNBC tumors have mutations in any of the *BRCA* genes, most TNBC tumors have some sort of dysregulation in the HR DNA damage repair pathway[31,231]. Nevertheless, *BRCA1/2* mutation carrier tumors have been shown to be the most responsive to PARPi (compared to non-*BRCA* mutations carriers) and even for those patients, the clinical trials are now exploring combinations with chemotherapies like cisplatin or carboplatin (Table 1).

The heterogenous response to PARPi in TNBC has prompted the necessity of identifying prognostic biomarkers. The research in the area of predictive biomarkers for PARP inhibition has been focusing in DNA repair proteins, specifically in those mutations or deficiencies that impair HR. Experimental models have shown that the chemical inactivation of the kinases ATM and CHK2 confers the cell with a *BRCA*-like phenotype[232]. Further genetic screens identified CDK12, RAD51B, and RAD51C as other contributors for the *BRCA*-like phenotype[233]. These studies suggest that the predictive biomarkers for PARPi response are likely to be found in the DNA repair pathways of cells. Although p66ShcA expression does not appreciably alter sensitivity to PARPi as a monotherapy, our data suggests that p66ShcA is a predictive biomarker of increased responsiveness of TNBCs to PARPi/Doxorubicin combination therapy, through increased oxidative stress.

We investigated if the ability of p66ShcA to sensitize TNBCs to this combination therapy was due to DNA damage accumulation. The mechanism of action of doxorubicin (main chemotherapy used in this project) is also implicated the generation of DSB through the poisoning of topoisomerase II. Although there is an accumulation in DSB in cells after the exposure to the combination Dox/PARPi (Figure 11A), this DNA damage is independent of the presence of p66ShcA. This evidence rules out DSB as the cause of the differential in cell death between VC and p66ShcA-carrying cells after exposure to Dox/PARPi.

The DNA damage quantification (Figure 11A) results are further supported by the cell cycle analysis (Figure 9A). In the context of Hs578T and MDA-MB-231 cell lines, characterized for their deficiency in p53 checkpoint, after the formation of multiple DSBs an accumulation of cells in G2/M phase would be expected to take place ultimately leading to cell death[234]. As it can be observed in the histograms representing the proportions of cells trough the cell cycle phases, there is not a drastic accumulation of cells in any of them. Together, these data suggest that the levels of DSB are not enough to kill the TNBC models chosen for this project and that the reduction in viability mediated by p66ShcA (Figure 8) is not DNA damage dependent.

Recent studies have shown a new possible mechanism for the cytotoxicity exerted by PARPi in cancer cells: ROS production[235–237]. This novel mechanism of action opens the door for the identification of new biomarkers in cellular pathways that go beyond DNA damage repair. The sensitivity of cancer cells to ROS production seems to be determined by p53 (a key regulator of ROS). Of importance for this project is the fact that about 80% of TNBC tumors have mutations in *TP53*[43]. Furthermore, it has been shown that TNBC cell lines have a lower tolerance to the exposure to H_2O_2 [238]. According to this study, the sensitivity to ROS is comparable between *BRCA* mutant and non-mutant TNBC cell lines. These data support the

observation made in this thesis that the mechanism of action of PARPi triggering cell death of TNBC cell lines could be the oxidative injury rather than defects in HR and nuclear DNA damage accumulation.

A study performed in Head and Neck Squamous Cell Carcinoma (HNSC), a type of cancer that shares some genetic features with TNBC (70-85% of the tumors are mutated in *TP53*), showed that the cytotoxic activity of the PARP inhibitor 6(5H)-phenanthridinone is mediated by the accumulation of ROS through the inactivation of TrxR1[239].

Another study showed that the cytotoxic activity of the PARP inhibitor PJ-34 in multiple ovarian cell lines correlated with mitochondrial ROS increase and increase in phosphorylation of p38MAPK. This process was mediated through the upregulation of NOX1 and NOX4[240]. The mechanism showed by this publication has several commonalities with the p66ShcA mediated mechanism described in this project. The activation of the oxidative function of p66ShcA has been shown to be mediated by stress kinases like p38MAPK[193]. Furthermore, it was shown that the mitochondrial oxidant, superoxide anion, was formed after the exposure to PJ-34 (PARPi). In this project, we showed that the mitochondrial superoxide anion scavenger (mitoTEMPO) was sufficient to reverse the phenotype caused by the combination of Dox/PARPi (Figure 14A).

PJ-34 belongs to a second generation of PARP inhibitors with higher potency compared to Olaparib/Niraparib/Veliparib[241]. This, along with the high concentration of PJ-34 (order of 10μM) used in the study may explain why, by itself, it induced apoptosis by the increase in the activity of the stress kinase (p38) and ROS accumulation. Furthermore, it has been shown that the phosphorylation of p66ShcA and interaction with RTKs, disrupts the complex Grb2-SOS1[202]. This event promotes the interaction of p66ShcA with RAC1 and subsequent production of ROS

by NOX1. The findings form this publication, and the previous research in p66ShcA interactions may suggest that p66ShcA could be a potentiator of a PARPi mediated ROS increase.

A recent study that examined the effects of PARPi in bladder cancer cell lines showed that the co-treatment of cells with NAC rescued cell viability, linking the mechanistic effect of Olaparib to the production of ROS. Furthermore, they show that the sensitization to radiation by Olaparib is increased in *TP53* mutated cell lines. Among those cell lines (*TP53* mutated), the ones carrying a further anomaly in the HR pathway (e.g. ATM, *BRCA*-like phenotype) had increased production of ROS[242]. These data may suggest that key regulators of HR pathway could also be implicated in redox signaling and ROS production.

The studies previously described showed the importance of ROS production in the cytotoxic activity of PARP inhibitors. We aimed to determine if the exposure of TNBC cell lines to sub-optimal doses of doxorubicin and PARPi (both ROS generators) would activate the mechanism of action of p66ShcA and ultimately lead to the overproduction of ROS and oxidative stress.

Together the results obtained suggest that indeed, an overexpression of p66ShcA confers susceptibility to the PARPi combination treatment (Figure 8A). By observing the growth rate of the p66ShcAQQ mutant (Figure 12C), a variant of this protein that cannot produce ROS, we can affirm that the effect in viability observed trough the experiments is attributed to the capacity of p66ShcA to produce ROS. *In vivo* experiments recapitulate some of the observations made *in vitro* (Figure 8D). When treated with PARPi and Dox, VC tumors show a reduction of volume of approximately 40% at endpoint. The effect on the combination treatment on p66ShcA carrying tumors is a reduction of approximately 80% of the volume by the same day. Most importantly,

the growth curve of VC tumors exposed to Dox/PARPi shows a progressive increase in tumor volume while p66ShcA-tumors resemble stable disease.

The apoptotic effect of PARP inhibitors in combination with doxorubicin in *TP53* mutated breast cancer cell lines has been previously shown. In this article the mechanism of cell death was linked to the loss mitochondrial membrane potential and cyt c release[243]. It has been widely documented that the loss of mitochondrial membrane potential can be caused by ROS production (Reviewed by Turrens, 2003[244]). It is likely that the production of ROS by p66ShcA after the exposure to Dox/PARPi is causing a similar phenotype, where the functionality of the mitochondria is compromised. Nevertheless, the *in vivo* 8-oxodG quantification (Figure 13C) shows lower levels of oxidative stress for the p66ShcA expressors compared to VC. A possible explanation for this observation is that the cells with high oxidative injuries died, leaving only the cells with low levels of oxidative stress.

ROS production was measured (Figure 13A). There is a 2-fold increase in ROS accumulation in p66ShcA-carrying cells (compared to VC) when exposed to the combination of Dox/PARPi. Although there is not statistical difference in ROS production between VC and p66ShcA, the administration of the PARPi alone increased oxidant accumulation compared to DMSO (Figure 13A). Contrary to what was expected, Doxorubicin by itself did not increase ROS production, possibly due to the low dose employed (1nM). Nevertheless, the administration of the drugs as monotherapies minimally impacted phosphorylation of p66ShcA, and it is only the Dox/PARPi combination that allows high phosphorylation levels of p66ShcA (S36) and possibly higher amount of protein translocated into the mitochondria. (Figure 12A).

The production of mitochondrial ROS as the molecular mechanism of cellular death is further supported by the cell growth of the p66ShcAQQ mutant (Figure 12C). This mutation

disrupts the ability of p66ShcA to engage cyt c and prevents the production of ROS. The effect in viability observed can be attributed to the capacity of p66ShcA to interact with cyt c and produce ROS. Additionally, the phenotype rescues with mitoTEMPO and NAC confirm the dependency of the phenotype in the production of ROS.

The cytotoxic effect of the combination of PARP inhibitors and chemotherapies is likely produced by several factors. The chemotherapies that exert the highest synergies with PARP inhibitors are Topoisomerase 1 inhibitors (e.g. camptothecin, topotecan) and cross-linking agents (like temozolomide), due to an increase in DNA damage and the generation of poisoning complexes[245–247].

Clinical data on the combination of doxorubicin with PARPi in TNBC is scarce. The utilization of doxorubicin as one of the first lines of treatment in TNBC[112,113] limits the use of this anthracycline in combination with PARPi in advanced disease due to the resistance acquired. This may be the reason why there is an increasing interest in exploring the combination of platinum-based salts and PARPi. As mentioned before, drugs like cisplatin or carboplatin did not become standard of care for TNBC due to their lower anti-cancer activity and high toxicity[111]. The combination of platinum-based salts with PARP inhibitors could exert higher cytotoxic activity mediated by the accumulation of DNA damage in doxorubicin resistance tumors.

There are few clinical trials principally in ovarian metastatic disease that utilized doxorubicin and PARPi. In a phase II clinical trial by Kaye et al. 2012[248], it was shown that PLD (PEGylated Liposomal Doxorubicin) had superior activity than Olaparib as monotherapy. Interestingly, patients that received PLD and then changed to the PARPi treatment showed sustained benefit from the inhibitor. In a Phase I trial (solid tumors) of Olaparib with PLD, 33% of the patients observed antitumor activity (13 out of 14 responders had ovarian cancer)[249].

As the final part of this project, the effect of p66ShcA on the combinations Dox/PARPi and Carboplatin/PARPi was explored. The phenotypes observed by cell viability assays and tumor growth *in vivo*, indicate that p66ShcA promotes a sensitization to Dox/PARPi but not to the Carboplatin/PARPi combination (Figure 15 A, B). The reason for the different response between Dox and Carboplatin in combination with PARPi may be explained by the molecular mechanisms of actions of the chemotherapies. Production of ROS by oxidation/reduction cycles of doxorubicin is a main component of the cytotoxicity observed in cancer cells[117,119]. On the other hand, the main mechanism of action of carboplatin is the cross-linking of DNA and the formation of adducts[250]. Interestingly, it has been determined that the reason why cisplatin is more toxic than carboplatin is the higher capacity of the former to produce mitochondrial ROS[251]. In conclusion, the oxidation stimulus from the combination carboplatin/PARPi may not be enough to activate the mechanism of p66ShcA (induce S36 phosphorylation).

The utilization of PARPi and doxorubicin to treat advanced TNBC may not be a possibility due to the resistance acquired by the cancer cells as a result of the first line of treatment after diagnosis. Nevertheless, Dox/PARPi combination could be administered as part of the adjuvant or neoadjuvant regime for patients with high expression of p66ShcA. The evidence provided suggests that for patients with high expression of p66ShcA, the dose of doxorubicin could be lowered. This may ameliorate the severe side effects of the anthracycline while conserving anti-tumor activity. Furthermore, there is pre-clinical evidence of cardiomyocyte protection upon administration of PARP inhibitors[252–254]. Heart failure due to cardiomyocyte induced apoptosis is one of the most severe side effects of doxorubicin. Although the data suggest that Dox/PARPi combination increases ROS in TNBC, this effect may be different in normal cells (cardiomyocytes).

Higher levels of ROS/RNS are found in cancer cells compared to normal tissues[255–257]. This phenomenon may be explained by the highly inflammatory microenvironment and the propitiated pro-oxidant signaling (NF-κB, cFOS/JUN). An increase in inflammatory signalling as well as general oxidative levels is a common event in the process of carcinogenesis. This increase in ROS production leads to a rewiring of the antioxidant response to cope with oxidative stress and maintain cell functionality. This rewiring causes the dependency of cancer to certain antioxidant molecules or signaling pathways. Ultimately, the adaptations give them an advantage to continue dividing and sometimes allows them to be resistant to chemotherapy. Examples of the dependency of cancer cells to antioxidant networks are the Nrf2-mediated resistance to chemotherapy of lung, breast and brain tumors [258] and the mesenchymal types of cancer and their reliance in glutathione synthesis[259,260]

While the rewiring of cancer cells gives them a proliferative advantage, it also exposes their vulnerabilities and opens a window for clinical targets. Recent studies aim to take advantage of those vulnerabilities in order to produce high amounts of ROS that will ultimately kill cancer cells[261,262]. These clinical strategies are based on the fact that, compared to normal cells, cancer cells have a lower resistance to ROS production due to their unbalanced antioxidant response. In this project, we presented a novel mechanism for the anti-cancer activity of PARP inhibitors in combination with doxorubicin. This mechanism is based on the activation of the oxidoreductase p66ShcA and the generation of ROS.

Future work for this project should center on the corroboration of the translocation of p66ShcA into the mitochondria after combination of Dox/PARPi stimulus. It is also necessary to investigate if the ROS produced by p66ShcA is affecting mitochondrial integrity since it has

been previously shown the combination Dox/PARPi in p53 null breast cancer cell lines, affects mitochondrial membrane potential and induces cyt c release[243].

Furthermore, it is worthwhile to explore the efficacy of this combination therapy in metastatic models of ovarian cancer (where clinical trials show more promising results) and investigate if p66ShcA plays the same role in the cytotoxic response. For metastatic TNBC disease, future work could explore if p66ShcA sensitizes tumors to a combination of PARPi and cisplatin (a more potent ROS generator than carboplatin). Along with these studies, the cardiomyocyte protection exerted by PARP inhibition should be tested in combination with either doxorubicin or cisplatin.

Finally, for those tumors that have low expression of p66ShcA, the administration of epigenetic drugs could be an alternative strategy as p66ShcA expression is regulated by methylation of its promoter. Interestingly, a recent study showed that the combination of the PARPi talazoparib and the hypomethylating agent guadecitabine had a synergistic cytotoxic effect in ovarian and breast cancer cell lines irrespective of *BRCA* status. This anti-cancer activity was reversed with the administration of NAC, linking this phenotype to the production of ROS[263]. It would be interesting to study to which extent the upregulation of expression of p66ShcA by the hypomethylating agent contributed to the formation of ROS in the combination with PARPi.

Conclusions

Altogether, we present a novel prognostic and mechanistic biomarker for the utilization of PARPi combination therapy in poor prognosis breast cancer. p66ShcA sensitizes TNBCs to Doxorubicin/PARPi combination therapies *in vitro* and *in vivo*. This sensitization depends on the activation of the molecular mechanism of p66ShcA (phosphorylation) that leads to the production of ROS and increased oxidative stress. The p66ShcA-related increase of ROS production cytolytic effects are not dependent on increased induction of a DNA damage.

Table 1: Main Ongoing PARP inhibitor Clinical Trials in TNBC

PARP inhibitor	Clinical trial	Description	Patients
Olaparib	Phase III (PARTNER)	Olaparib + platinum base chemotherapy vs placebo +platinum-based chemotherapy (Neoadjuvant regime)	TNBC or *BRCA* associated breast cancer
Veliparib	Phase II	Veliparib+ cisplatin vs placebo+ cisplatin	TNBC or *BRCA* associated stage IV breast cancer
	Phase III (BROCADE-3)	Veliparib+ carboplatin and paclitaxel vs placebo+ carboplatin and paclitaxel	*BRCA* associated metastatic or locally advanced breast cancer.
Niraparib	Phase III (BRAVO)	Niraparib vs physician choice	*BRCA* associated breast cancer (HER-2 neg)
	Phase I/II (TOPACIO)	Niraparib+ Pembrolizumab	TNBC or ovarian cancer.
Rucaparib	Phase II (RUBY)	Monotherapy	*BRCA*ness genomic signature breast cancer
Talazoparib	Phase III (EMBRACA)	Talazoparib vs physician choice chemotherapy.	*BRCA* associated advanced metastatic breast cancer
	Phase II (TBB)	Monotherapy	Advanced metastatic TNBC *BRCA* Wild-type

Table 2: Antibodies used for immunohistochemistry

Epitope	Catalogue Number	Company	Dilution	Tissue	Antigen Retrieval
Ki-67	ab15580	Abcam	1:500	Paraffin	Sodium Citrate Buffer 12 min
Cleaved caspase 3	9661	Cell Signaling Technologies	1:500	Paraffin	Sodium Citrate Buffer 12 min
Phospho Histone γH2AX	JBW301	Millipore	1:500	Paraffin	Sodium Citrate Buffer 12 min
4-HNE	Ab46545	Abcam	1:500	Paraffin	Sodium Citrate Buffer 12 min
8-oxodG	4354-MC	Trevigen	1:2000	Paraffin	No antigen retrieval

Sodium Citrate Buffer: 10mM Sodium Citrate (2.94g Tris-sodium citrate (dihydrate) in 100 mL distilled water with 0.05% Tween20. pH adjusted to 6.0 with 1N HCl).

Bibliography

1. Bosch, A., Eroles, P., Zaragoza, R., Viña, J. R. & Lluch, A. Triple-negative breast cancer: Molecular features, pathogenesis, treatment and current lines of research. *Cancer Treatment Reviews* **36**, 206–215 (2010).
2. Stingl, J., Raouf, A., Eirew, P. & Eaves, C. J. Deciphering the Mammary Epithelial Cell Hierarchy. *Cell Cycle* **5**, 1519–1522 (2006).
3. Anderson, T. J., Ferguson, D. J. & Raab, G. M. Cell turnover in the 'resting' human breast: influence of parity, contraceptive pill, age and laterality. *Br J Cancer* **46**, 376–382 (1982).
4. Stingl, J., Raouf, A., Emerman, J. T. & Eaves, C. J. Epithelial Progenitors in the Normal Human Mammary Gland. *J Mammary Gland Biol Neoplasia* **10**, 49–59 (2005).
5. Ali, S. & Coombes, R. C. Endocrine-responsive breast cancer and strategies for combating resistance. *Nature Reviews Cancer* **2**, 101–112 (2002).
6. Prat, A. & Perou, C. M. Mammary development meets cancer genomics. *Nature Medicine* **15**, nm0809-842–842 (2009).
7. Stingl, J., Eaves, C. J., Zandieh, I. & Emerman, J. T. Characterization of bipotent mammary epithelial progenitor cells in normal adult human breast tissue. *Breast Cancer Res Treat* **67**, 93–109 (2001).
8. Gudjonsson, T., Adriance, M. C., Sternlicht, M. D., Petersen, O. W. & Bissell, M. J. Myoepithelial Cells: Their Origin and Function in Breast Morphogenesis and Neoplasia. *J Mammary Gland Biol Neoplasia* **10**, 261–272 (2005).
9. Geyer, F. C., Marchiò, C. & Reis-Filho, J. S. The role of molecular analysis in breast cancer. *Pathology* **41**, 77–88 (2009).
10. Bertos, N. R. & Park, M. Breast cancer — one term, many entities? *J Clin Invest* **121**, 3789–3796 (2011).

11. Dai, X. *et al.* Breast cancer intrinsic subtype classification, clinical use and future trends. *Am J Cancer Res* **5**, 2929–2943 (2015).

12. Sørlie, T. *et al.* Gene expression patterns of breast carcinomas distinguish tumor subclasses with clinical implications. *PNAS* **98**, 10869–10874 (2001).

13. Perou, C. M. *et al.* Molecular portraits of human breast tumours. *Nature* **406**, 35021093 (2000).

14. Goldhirsch, A. *et al.* Strategies for subtypes—dealing with the diversity of breast cancer: highlights of the St Gallen International Expert Consensus on the Primary Therapy of Early Breast Cancer 2011. *Ann Oncol* **22**, 1736–1747 (2011).

15. Longo, R., Torino, F. & Gasparini, G. Targeted Therapy of Breast Cancer. *Current Pharmaceutical Design* **13**, 497–517 (2007).

16. Li, X. *et al.* Triple-negative breast cancer has worse overall survival and cause-specific survival than non-triple-negative breast cancer. *Breast Cancer Res Treat* **161**, 279–287 (2017).

17. Lim, E. *et al.* Aberrant luminal progenitors as the candidate target population for basal tumor development in *BRCA1* mutation carriers. *Nature Medicine* **15**, nm.2000 (2009).

18. Dias, K. *et al.* Claudin-Low Breast Cancer; Clinical & Pathological Characteristics. *PLOS ONE* **12**, e0168669 (2017).

19. Lehmann, B. D. *et al.* Identification of human triple-negative breast cancer subtypes and preclinical models for selection of targeted therapies. *J. Clin. Invest.* **121**, 2750–2767 (2011).

20. Clark, S. E. *et al.* Molecular subtyping of DCIS: heterogeneity of breast cancer reflected in pre-invasive disease. *Br J Cancer* **104**, 120–127 (2011).

21. Tamimi, R. M. *et al.* Comparison of molecular phenotypes of ductal carcinoma in situ and invasive breast cancer. *Breast Cancer Res.* **10**, R67 (2008).

22. Inic, Z. *et al.* Difference between Luminal A and Luminal B Subtypes According to Ki-67, Tumor Size, and Progesterone Receptor Negativity Providing Prognostic Information. *Clin Med Insights Oncol* **8**, 107–111 (2014).

23. Metzger-Filho, O. *et al.* Patterns of Recurrence and Outcome According to Breast Cancer Subtypes in Lymph Node–Negative Disease: Results From International Breast Cancer Study Group Trials VIII and IX. *J Clin Oncol* **31**, 3083–3090 (2013).

24. Voduc, K. D. *et al.* Breast cancer subtypes and the risk of local and regional relapse. *J. Clin. Oncol.* **28**, 1684–1691 (2010).

25. Loibl, S. & Gianni, L. HER2-positive breast cancer. *The Lancet* **389**, 2415–2429 (2017).

26. Wang, C., Christin, J. R., Oktay, M. H. & Guo, W. Lineage-Biased Stem Cells Maintain Estrogen-Receptor-Positive and -Negative Mouse Mammary Luminal Lineages. *Cell Reports* **18**, 2825–2835 (2017).

27. Rodilla, V. *et al.* Luminal Progenitors Restrict Their Lineage Potential during Mammary Gland Development. *PLoS Biol* **13**, (2015).

28. Molyneux, G. *et al.* BRCA1 Basal-like Breast Cancers Originate from Luminal Epithelial Progenitors and Not from Basal Stem Cells. *Cell Stem Cell* **7**, 403–417 (2010).

29. Lim, E. *et al.* Aberrant luminal progenitors as the candidate target population for basal tumor development in *BRCA1* mutation carriers. *Nature Medicine* **15**, 907–913 (2009).

30. Wong-Brown, M. W. *et al.* Prevalence of BRCA1 and BRCA2 germline mutations in patients with triple-negative breast cancer. *Breast Cancer Res Treat* **150**, 71–80 (2015).

31. Lips, E. H. *et al.* Triple-negative breast cancer: BRCAness and concordance of clinical features with BRCA1-mutation carriers. *Br J Cancer* **108**, 2172–2177 (2013).

32. Badve, S. *et al.* Basal-like and triple-negative breast cancers: a critical review with an emphasis on the implications for pathologists and oncologists. *Modern Pathology* **24**, modpathol2010200 (2010).

33. Prat, A. & Perou, C. M. Deconstructing the molecular portraits of breast cancer. *Molecular Oncology* **5**, 5–23 (2011).

34. Dent, R. *et al.* Triple-Negative Breast Cancer: Clinical Features and Patterns of Recurrence. *Clin Cancer Res* **13**, 4429–4434 (2007).

35. Penault-Llorca, F. & Viale, G. Pathological and molecular diagnosis of triple-negative breast cancer: a clinical perspective. *Ann Oncol* **23**, vi19–vi22 (2012).

36. Oakman, C., Viale, G. & Di Leo, A. Management of triple negative breast cancer. *The Breast* **19**, 312–321 (2010).

37. Connolly, J. L. *et al.* Role of the Surgical Pathologist in the Diagnosis and Management of the Cancer Patient. (2003).

38. Goldhirsch, A. *et al.* Thresholds for therapies: highlights of the St Gallen International Expert Consensus on the Primary Therapy of Early Breast Cancer 2009. *Ann Oncol* **20**, 1319–1329 (2009).

39. Anders, C. K. & Carey, L. A. Biology, Metastatic Patterns, and Treatment of Patients with Triple-Negative Breast Cancer. *Clin Breast Cancer* **9**, S73–S81 (2009).

40. Carey, L. A. *et al.* Race, Breast Cancer Subtypes, and Survival in the Carolina Breast Cancer Study. *JAMA* **295**, 2492–2502 (2006).

41. Pareja, F. *et al.* Triple-negative breast cancer: the importance of molecular and histologic subtyping, and recognition of low-grade variants. *NPJ Breast Cancer* **2**, 16036 (2016).

42. Kandoth, C. *et al.* Mutational landscape and significance across 12 major cancer types. *Nature* **502**, 333 (2013).

43. Synnott, N. c. *et al.* Mutant p53: a novel target for the treatment of patients with triple-negative breast cancer? *Int. J. Cancer* **140**, 234–246 (2017).

44. Shah, S. P. *et al.* The clonal and mutational evolution spectrum of primary triple negative breast cancers. *Nature* **486**, (2012).

45. Fountzilas, G. *et al.* TP53 mutations and protein immunopositivity may predict for poor outcome but also for trastuzumab benefit in patients with early breast cancer treated in the adjuvant setting. *Oncotarget* **7**, 32731–32753 (2016).

46. Jordan, J. J. *et al.* Altered-function p53 missense mutations identified in breast cancers can have subtle effects on transactivation. *Mol Cancer Res* **8**, 701–716 (2010).

47. Végran, F. *et al.* Only missense mutations affecting the DNA binding domain of p53 influence outcomes in patients with breast carcinoma. *PLoS ONE* **8**, e55103 (2013).

48. Walerych, D., Napoli, M., Collavin, L. & Del Sal, G. The rebel angel: mutant p53 as the driving oncogene in breast cancer. *Carcinogenesis* **33**, 2007–2017 (2012).

49. Comprehensive molecular portraits of human breast tumors. *Nature* **490**, 61–70 (2012).

50. Lane, D. P. p53, guardian of the genome. *Nature* **358**, 15 (1992).

51. Rivlin, N., Brosh, R., Oren, M. & Rotter, V. Mutations in the p53 Tumor Suppressor Gene. *Genes Cancer* **2**, 466–474 (2011).

52. Molchadsky, A., Rivlin, N., Brosh, R., Rotter, V. & Sarig, R. p53 is balancing development, differentiation and de-differentiation to assure cancer prevention. *Carcinogenesis* **31**, 1501–1508 (2010).

53. Meletis, K. *et al.* p53 suppresses the self-renewal of adult neural stem cells. *Development* **133**, 363–369 (2006).

54. Lin, T. *et al.* p53 induces differentiation of mouse embryonic stem cells by suppressing Nanog expression. *Nat. Cell Biol.* **7**, 165–171 (2005).

55. Zhao, Z. *et al.* p53 loss promotes acute myeloid leukemia by enabling aberrant self-renewal. *Genes Dev.* **24**, 1389–1402 (2010).

56. Verma, C. S., Lane, D. P. & Khoo, K. H. Drugging the p53 pathway: understanding the route to clinical efficacy. *Nature Reviews Drug Discovery* **13**, 217 (2014).

57. Peto, J. *et al.* Prevalence of BRCA1 and BRCA2 gene mutations in patients with early-onset breast cancer. *J. Natl. Cancer Inst.* **91**, 943–949 (1999).

58. Lakhani, S. R. *et al.* The pathology of familial breast cancer: predictive value of immunohistochemical markers estrogen receptor, progesterone receptor, HER-2, and p53 in patients with mutations in BRCA1 and BRCA2. *J. Clin. Oncol.* **20**, 2310–2318 (2002).

59. Gonzalez-Angulo, A. M. *et al.* Incidence and outcome of BRCA mutations in unselected patients with triple receptor-negative breast cancer. *Clin. Cancer Res.* **17**, 1082–1089 (2011).

60. Nathanson, K. L., Wooster, R., Weber, B. L. & Nathanson, K. N. Breast cancer genetics: what we know and what we need. *Nat. Med.* **7**, 552–556 (2001).

61. Dite, G. S. *et al.* Familial risks, early-onset breast cancer, and BRCA1 and BRCA2 germline mutations. *J. Natl. Cancer Inst.* **95**, 448–457 (2003).

62. Greenup, R. *et al.* Prevalence of BRCA mutations among women with triple-negative breast cancer (TNBC) in a genetic counseling cohort. *Ann. Surg. Oncol.* **20**, 3254–3258 (2013).

63. Chun, J., Roy, R. & Powell, S. N. BRCA1 and BRCA2: different roles in a common pathway of genome protection. *Nature Reviews Cancer* **12**, 68 (2012).

64. Scully, R. *et al.* Genetic analysis of BRCA1 function in a defined tumor cell line. *Mol. Cell* **4**, 1093–1099 (1999).

65. Ye, Y. & Rape, M. Building ubiquitin chains: E2 enzymes at work. *Nat. Rev. Mol. Cell Biol.* **10**, 755–764 (2009).

66. Huynh, A. M. *et al.* BRCA1 tumour suppression occurs via heterochromatin-mediated silencing. *Nature* **477**, 179 (2011).

67. You, Z. & Bailis, J. M. DNA damage and decisions: CtIP coordinates DNA repair and cell cycle checkpoints. *Trends Cell Biol.* **20**, 402–409 (2010).

68. Heine, G. F. & Parvin, J. D. BRCA1 control of steroid receptor ubiquitination. *Sci. STKE* **2007**, pe34 (2007).

69. Foster, E. R. & Downs, J. A. Histone H2A phosphorylation in DNA double-strand break repair. *FEBS J.* **272**, 3231–3240 (2005).

70. Makharashvili, N. & Paull, T. T. CtIP: A DNA damage response protein at the intersection of DNA metabolism. *DNA Repair (Amst.)* **32**, 75–81 (2015).

71. Atipairin, A., Canyuk, B. & Ratanaphan, A. The RING heterodimer BRCA1-BARD1 is a ubiquitin ligase inactivated by the platinum-based anticancer drugs. *Breast Cancer Res. Treat.* **126**, 203–209 (2011).

72. Deng, C. X. & Brodie, S. G. Roles of BRCA1 and its interacting proteins. *Bioessays* **22**, 728–737 (2000).

73. Le, S., Moore, J. K., Haber, J. E. & Greider, C. W. RAD50 and RAD51 define two pathways that collaborate to maintain telomeres in the absence of telomerase. *Genetics* **152**, 143–152 (1999).

74. Shammas, M. A. *et al.* Dysfunctional homologous recombination mediates genomic instability and progression in myeloma. *Blood* **113**, 2290–2297 (2009).

75. Agoston, A. T., Argani, P., De Marzo, A. M., Hicks, J. L. & Nelson, W. G. Retinoblastoma Pathway Dysregulation Causes DNA Methyltransferase 1 Overexpression in Cancer via MAD2-Mediated Inhibition of the Anaphase-Promoting Complex. *Am J Pathol* **170**, 1585–1593 (2007).

76. de Souza, A. A. *et al.* Dysregulation of the Rb pathway in recurrent pleomorphic adenoma of the salivary glands. *Virchows Arch.* **467**, 295–301 (2015).

77. Zhang, H., Kajino, K., Greene, M. I. & Wang, Q. BRCA1 binds c-Myc and inhibits its transcriptional and transforming activity in cells. *Oncogene* **17**, 1939 (1998).

78. Chen, C.-F. *et al.* The Nuclear Localization Sequences of the BRCA1 Protein Interact with the Importin-α Subunit of the Nuclear Transport Signal Receptor. *J. Biol. Chem.* **271**, 32863–32868 (1996).

79. Wu, Q., Jubb, H. & Blundell, T. L. Phosphopeptide interactions with BRCA1 BRCT domains: More than just a motif. *Prog Biophys Mol Biol* **117**, 143–148 (2015).

80. Wang, B. *et al.* Abraxas and RAP80 form a BRCA1 protein complex required for the DNA damage response. *Science* **316**, 1194–1198 (2007).

81. Kettenbach, A. N. *et al.* Quantitative phosphoproteomics identifies substrates and functional modules of Aurora and Polo-like kinase activities in mitotic cells. *Sci Signal* **4**, rs5 (2011).

82. Clark, S. L., Rodriguez, A. M., Snyder, R. R., Hankins, G. D. V. & Boehning, D. Structure-Function of the Tumor Suppressor BRCA1. *Comput Struct Biotechnol J* **1**, (2012).

83. Yamane, K., Katayama, E. & Tsuruo, T. The BRCT regions of tumor suppressor BRCA1 and of XRCC1 show DNA end binding activity with a multimerizing feature. *Biochem. Biophys. Res. Commun.* **279**, 678–684 (2000).

84. Shahid, T. *et al.* Structure and Mechanism of Action of the BRCA2 Breast Cancer Tumor Suppressor. *Nat Struct Mol Biol* **21**, 962–968 (2014).

85. Venkitaraman, A. R. Cancer susceptibility and the functions of BRCA1 and BRCA2. *Cell* **108**, 171–182 (2002).

86. Ashworth, A. & Lord, C. J. RAD51, BRCA2 and DNA repair: a partial resolution. *Nature Structural and Molecular Biology* **14**, 461 (2007).

87. Lomonosov, M., Anand, S., Sangrithi, M., Davies, R. & Venkitaraman, A. R. Stabilization of stalled DNA replication forks by the BRCA2 breast cancer susceptibility protein. *Genes Dev.* **17**, 3017–3022 (2003).

88. Moynahan, M. E., Pierce, A. J. & Jasin, M. BRCA2 is required for homology-directed repair of chromosomal breaks. *Mol. Cell* **7**, 263–272 (2001).

89. Mimitou, E. P. & Symington, L. S. Nucleases and helicases take center stage in homologous recombination. *Trends in Biochemical Sciences* **34**, 264–272 (2009).

90. Stracker, T. H., Theunissen, J.-W. F., Morales, M. & Petrini, J. H. J. The Mre11 complex and the metabolism of chromosome breaks: the importance of communicating and holding things together. *DNA Repair (Amst.)* **3**, 845–854 (2004).

91. Krogh, B. O. & Symington, L. S. Recombination proteins in yeast. *Annu. Rev. Genet.* **38**, 233–271 (2004).

92. Moynahan, M. E., Chiu, J. W., Koller, B. H. & Jasin, M. Brca1 controls homology-directed DNA repair. *Mol. Cell* **4**, 511–518 (1999).

93. Kuo, L. J. & Yang, L.-X. γ-H2AX - A Novel Biomarker for DNA Double-strand Breaks. *In Vivo* **22**, 305–309 (2008).

94. Jasin, M. & Rothstein, R. Repair of Strand Breaks by Homologous Recombination. *Cold Spring Harb Perspect Biol* **5**, (2013).

95. Kass, E. M. & Jasin, M. Collaboration and competition between DNA double-strand break repair pathways. *FEBS Lett* **584**, 3703–3708 (2010).

96. Sung, P. & Klein, H. Mechanism of homologous recombination: mediators and helicases take on regulatory functions. *Nat. Rev. Mol. Cell Biol.* **7**, 739–750 (2006).

97. Ohta, T., Sato, K. & Wu, W. The BRCA1 ubiquitin ligase and homologous recombination repair. *FEBS Letters* **585**, 2836–2844 (2011).

98. Aylon, Y., Liefshitz, B. & Kupiec, M. The CDK regulates repair of double-strand breaks by homologous recombination during the cell cycle. *EMBO J.* **23**, 4868–4875 (2004).

99. Daley, J. M., Palmbos, P. L., Wu, D. & Wilson, T. E. Nonhomologous end joining in yeast. *Annu. Rev. Genet.* **39**, 431–451 (2005).

100. Ceccaldi, R., Rondinelli, B. & D'Andrea, A. D. Repair Pathway Choices and Consequences at the Double-Strand Break. *Trends in Cell Biology* **26**, 52–64 (2016).

101. Venkitaraman, A. R. Functions of BRCA1 and BRCA2 in the biological response to DNA damage. *Journal of Cell Science* **114**, 3591–3598 (2001).

102. Lisby, M., Barlow, J. H., Burgess, R. C. & Rothstein, R. Choreography of the DNA damage response: spatiotemporal relationships among checkpoint and repair proteins. *Cell* **118**, 699–713 (2004).

103. Stephens, P. J. *et al.* The landscape of cancer genes and mutational processes in breast cancer. *Nature* **486**, 400–404 (2012).

104. Frederick, A. M. *et al.* Sequence analysis of mutations and translocations across breast cancer subtypes. *Nature* **486**, 405 (2012).

105. Liedtke, C. *et al.* Response to Neoadjuvant Therapy and Long-Term Survival in Patients With Triple-Negative Breast Cancer. *JCO* **26**, 1275–1281 (2008).

106. Costa, R. L. B. & Gradishar, W. J. Triple-Negative Breast Cancer: Current Practice and Future Directions. *JOP* **13**, 301–303 (2017).

107. Clifton, K. *et al.* Adjuvant or neoadjuvant chemotherapy in early stage triple negative breast cancer (TNBC) comparison of outcomes in both BRCA positive and BRCA negative patients. *JCO* **35**, 576–576 (2017).

108. Kennedy, C. R., Gao, F. & Margenthaler, J. A. Neoadjuvant versus adjuvant chemotherapy for triple negative breast cancer. *J. Surg. Res.* **163**, 52–57 (2010).

109. Clifton, K. *et al.* Adjuvant versus neoadjuvant chemotherapy in triple-negative breast cancer patients with BRCA mutations. *Breast Cancer Res. Treat.* (2018). doi:10.1007/s10549-018-4727-9

110. Amro, A. & Newman, L. A. Surgical Management of Triple-Negative Breast Cancer. in *Triple-Negative Breast Cancer* 55–69 (Springer, Cham, 2018). doi:10.1007/978-3-319-69980-6_5

111. Isakoff, S. J. Triple Negative Breast Cancer: Role of Specific Chemotherapy Agents. *Cancer J* **16**, 53–61 (2010).

112. Lippman, M. E. *et al.* The Relation between Estrogen Receptors and Response Rate to Cytotoxic Chemotherapy in Metastatic Breast Cancer. *New England Journal of Medicine* **298**, 1223–1228 (1978).

113. Kiang, D. T., Frenning, D. H., Goldman, A. I., Ascensao, V. F. & Kennedy, B. J. Estrogen Receptors and Responses to Chemotherapy and Hormonal Therapy in Advanced Breast Cancer. *New England Journal of Medicine* **299**, 1330–1334 (1978).

114. Early Breast Cancer Trialists' Collaborative Group (EBCTCG) *et al.* Adjuvant chemotherapy in oestrogen-receptor-poor breast cancer: patient-level meta-analysis of randomised trials. *Lancet* **371**, 29–40 (2008).

115. Citron, M. L. *et al.* Randomized Trial of Dose-Dense Versus Conventionally Scheduled and Sequential Versus Concurrent Combination Chemotherapy as Postoperative Adjuvant Treatment of Node-Positive Primary Breast Cancer: First Report of Intergroup Trial C9741/Cancer and Leukemia Group B Trial 9741. *JCO* **21**, 1431–1439 (2003).

116. Gluz, O. *et al.* Triple-negative high-risk breast cancer derives particular benefit from dose intensification of adjuvant chemotherapy: results of WSG AM-01 trial. *Ann Oncol* **19**, 861–870 (2008).

117. Yang, F., Teves, S. S., Kemp, C. J. & Henikoff, S. Doxorubicin, DNA torsion, and chromatin dynamics. *Biochim Biophys Acta* **1845**, 84–89 (2014).

118. Pang, B. *et al.* Drug-induced histone eviction from open chromatin contributes to the chemotherapeutic effects of doxorubicin. *Nature Communications* **4**, 1908 (2013).

119. Doroshow, J. H. Role of hydrogen peroxide and hydroxyl radical formation in the killing of Ehrlich tumor cells by anticancer quinones. *Proc. Natl. Acad. Sci. U.S.A.* **83**, 4514–4518 (1986).

120. Ichikawa, Y. *et al.* Cardiotoxicity of doxorubicin is mediated through mitochondrial iron accumulation. *J Clin Invest* **124**, 617–630 (2014).

121. Wang, S. *et al.* Doxorubicin Induces Apoptosis in Normal and Tumor Cells via Distinctly Different Mechanisms INTERMEDIACY OF H2O2- AND p53-DEPENDENT PATHWAYS. *J. Biol. Chem.* **279**, 25535–25543 (2004).

122. Herceg, Z. & Wang, Z.-Q. Functions of poly(ADP-ribose) polymerase (PARP) in DNA repair, genomic integrity and cell death. *Mutation Research/Fundamental and Molecular Mechanisms of Mutagenesis* **477**, 97–110 (2001).

123. Altmeyer, M., Messner, S., Hassa, P. O., Fey, M. & Hottiger, M. O. Molecular mechanism of poly(ADP-ribosyl)ation by PARP1 and identification of lysine residues as ADP-ribose acceptor sites. *Nucleic Acids Res* **37**, 3723–3738 (2009).

124. DaRosa, P. A., Ovchinnikov, S., Xu, W. & Klevit, R. E. Structural insights into SAM domain-mediated tankyrase oligomerization. *Protein Sci* **25**, 1744–1752 (2016).

125. Liu, C., Vyas, A., Kassab, M. A., Singh, A. K. & Yu, X. The role of poly ADP-ribosylation in the first wave of DNA damage response. *Nucleic Acids Res* **45**, 8129–8141 (2017).

126. Eustermann, S. *et al.* The DNA-Binding Domain of Human PARP-1 Interacts with DNA Single-Strand Breaks as a Monomer through Its Second Zinc Finger. *J Mol Biol* **407**, 149–170 (2011).

127. Langelier, M.-F., Servent, K. M., Rogers, E. E. & Pascal, J. M. A third zinc-binding domain of human poly(ADP-ribose) polymerase-1 coordinates DNA-dependent enzyme activation. *J. Biol. Chem.* **283**, 4105–4114 (2008).

128. Beernink, P. T. *et al.* Specificity of Protein Interactions Mediated by BRCT Domains of the XRCC1 DNA Repair Protein. *J. Biol. Chem.* **280**, 30206–30213 (2005).

129. Till, S., Diamantara, K. & Ladurner, A. G. PARP: a transferase by any other name. *Nature Structural & Molecular Biology* **15**, 1243–1244 (2008).

130. Li, X. *et al.* Binding to WGR Domain by Salidroside Activates PARP1 and Protects Hematopoietic Stem Cells from Oxidative Stress. *Antioxid Redox Signal* **20**, 1853–1865 (2014).

131. Lord, C. J. & Ashworth, A. PARP inhibitors: Synthetic lethality in the clinic. *Science* **355**, 1152–1158 (2017).

132. Satoh, M. S. & Lindahl, T. Role of poly(ADP-ribose) formation in DNA repair. *Nature* **356**, 356 (1992).

133. Eustermann, S. *et al.* Structural Basis of Detection and Signaling of DNA Single-Strand Breaks by Human PARP-1. *Mol Cell* **60**, 742–754 (2015).

134. Dianov, G. L., Sleeth, K. M., Dianova, I. I. & Allinson, S. L. Repair of abasic sites in DNA. *Mutation Research/Fundamental and Molecular Mechanisms of Mutagenesis* **531**, 157–163 (2003).

135. Garber, J. & Polyak, K. Targeting the missing links for cancer therapy. *Nature Medicine* **17**, 283 (2011).

136. Jr, W. G. K. The Concept of Synthetic Lethality in the Context of Anticancer Therapy. *Nature Reviews Cancer* **5**, 689 (2005).

137. Szabó, C. & Jagtap, P. Poly(ADP-ribose) polymerase and the therapeutic effects of its inhibitors. *Nature Reviews Drug Discovery* **4**, 421 (2005).

138. Wei, H. & Yu, X. Functions of PARylation in DNA Damage Repair Pathways. *Genomics Proteomics Bioinformatics* **14**, 131–139 (2016).

139. Robertson, A. B., Klungland, A., Rognes, T. & Leiros, I. DNA repair in mammalian cells: Base excision repair: the long and short of it. *Cell. Mol. Life Sci.* **66**, 981–993 (2009).

140. David, S. S., O'Shea, V. L. & Kundu, S. Base-excision repair of oxidative DNA damage. *Nature* **447**, 941–950 (2007).

141. Dianov, G. L. & Hübscher, U. Mammalian base excision repair: the forgotten archangel. *Nucleic Acids Res.* **41**, 3483–3490 (2013).

142. Noren Hooten, N., Kompaniez, K., Barnes, J., Lohani, A. & Evans, M. K. Poly(ADP-ribose) Polymerase 1 (PARP-1) Binds to 8-Oxoguanine-DNA Glycosylase (OGG1). *J Biol Chem* **286**, 44679–44690 (2011).

143. Kim, M. Y., Zhang, T. & Kraus, W. L. Poly(ADP-ribosyl)ation by PARP-1: 'PAR-laying' NAD+ into a nuclear signal. *Genes Dev.* **19**, 1951–1967 (2005).

144. Caldecott, K. W. Single-strand break repair and genetic disease. *Nature Reviews Genetics* **9**, 619 (2008).

145. Durkacz, B. W., Gray, D. A., Omidiji, O. & Shall, S. (ADP-ribose)n participates in DNA excision repair. *Nature* **283**, 593 (1980).

146. Dawicki-McKenna, J. M. *et al.* PARP-1 activation requires local unfolding of an autoinhibitory domain. *Mol Cell* **60**, 755–768 (2015).

147. Krishnakumar, R. *et al.* Reciprocal binding of PARP-1 and histone H1 at promoters specifies transcriptional outcomes. *Science* **319**, 819–821 (2008).

148. Rouleau, M., Aubin, R. A. & Poirier, G. G. Poly(ADP-ribosyl)ated chromatin domains: access granted. *J. Cell. Sci.* **117**, 815–825 (2004).

149. Okano, S., Lan, L., Caldecott, K. W., Mori, T. & Yasui, A. Spatial and Temporal Cellular Responses to Single-Strand Breaks in Human Cells. *Mol. Cell. Biol.* **23**, 3974–3981 (2003).

150. Masson, M. *et al.* XRCC1 Is Specifically Associated with Poly(ADP-Ribose) Polymerase and Negatively Regulates Its Activity following DNA Damage. *Mol Cell Biol* **18**, 3563–3571 (1998).

151. Caldecott, K. W., Tucker, J. D., Stanker, L. H. & Thompson, L. H. Characterization of the XRCC1-DNA ligase III complex in vitro and its absence from mutant hamster cells. *Nucleic Acids Res* **23**, 4836–4843 (1995).

152. Kubota, Y. *et al.* Reconstitution of DNA base excision-repair with purified human proteins: interaction between DNA polymerase beta and the XRCC1 protein. *EMBO J.* **15**, 6662–6670 (1996).

153. Dunstan, M. S. *et al.* Structure and mechanism of a canonical poly(ADP-ribose) glycohydrolase. *Nat Commun* **3**, 878 (2012).

154. Ruscetti, T. *et al.* Stimulation of the DNA-dependent protein kinase by poly(ADP-ribose) polymerase. *J. Biol. Chem.* **273**, 14461–14467 (1998).

155. Chiruvella, K. K., Liang, Z. & Wilson, T. E. Repair of Double-Strand Breaks by End Joining. *Cold Spring Harb Perspect Biol* **5**, (2013).

156. Iliakis, G. Backup pathways of NHEJ in cells of higher eukaryotes: cell cycle dependence. *Radiother Oncol* **92**, 310–315 (2009).

157. Li, M., Lu, L.-Y., Yang, C.-Y., Wang, S. & Yu, X. The FHA and BRCT domains recognize ADP-ribosylation during DNA damage response. *Genes Dev.* **27**, 1752–1768 (2013).

158. Patel, A. G., Sarkaria, J. N. & Kaufmann, S. H. Nonhomologous end joining drives poly(ADP-ribose) polymerase (PARP) inhibitor lethality in homologous recombination-deficient cells. *Proc Natl Acad Sci U S A* **108**, 3406–3411 (2011).

159. Schultz, N., Lopez, E., Saleh-Gohari, N. & Helleday, T. Poly(ADP-ribose) polymerase (PARP-1) has a controlling role in homologous recombination. *Nucleic Acids Res* **31**, 4959–4964 (2003).

160. Zhang, F., Shi, J., Bian, C. & Yu, X. Poly(ADP-Ribose) Mediates the BRCA2-Dependent Early DNA Damage Response. *Cell Rep* **13**, 678–689 (2015).

161. Haince, J.-F. *et al.* PARP1-dependent kinetics of recruitment of MRE11 and NBS1 proteins to multiple DNA damage sites. *J. Biol. Chem.* **283**, 1197–1208 (2008).

162. Helleday, T., Bryant, H. E. & Schultz, N. Poly(ADP-ribose) Polymerase (PARP-1) in Homologous Recombination and as a Target for Cancer Therapy. *Cell Cycle* **4**, 1176–1178 (2005).

163. Boehler, C. *et al.* Phenotypic characterization of Parp-1 and Parp-2 deficient mice and cells. *Methods Mol. Biol.* **780**, 313–336 (2011).

164. Murai, J. *et al.* Stereospecific PARP trapping by BMN 673 and comparison with olaparib and rucaparib. *Mol. Cancer Ther.* **13**, 433–443 (2014).

165. Murai, J. *et al.* Trapping of PARP1 and PARP2 by Clinical PARP Inhibitors. *Cancer Res.* **72**, 5588–5599 (2012).

166. Pacek, M. & Walter, J. C. A requirement for MCM7 and Cdc45 in chromosome unwinding during eukaryotic DNA replication. *EMBO J.* **23**, 3667–3676 (2004).

167. Geenen, J. J. J., Linn, S. C., Beijnen, J. H. & Schellens, J. H. M. PARP Inhibitors in the Treatment of Triple-Negative Breast Cancer. *Clin Pharmacokinet* 1–11 (2017). doi:10.1007/s40262-017-0587-4

168. Fong, P. C. *et al.* Inhibition of Poly(ADP-Ribose) Polymerase in Tumors from BRCA Mutation Carriers. *New England Journal of Medicine* **361**, 123–134 (2009).

169. Marques, M. *et al.* Chemotherapy reduces PARP1 in cancers of the ovary: implications for future clinical trials involving PARP inhibitors. *BMC Medicine* **13**, 217 (2015).

170. Gelmon, K. A. *et al.* Olaparib in patients with recurrent high-grade serous or poorly differentiated ovarian carcinoma or triple-negative breast cancer: a phase 2, multicentre, open-label, non-randomised study. *The Lancet Oncology* **12**, 852–861 (2011).

171. Robson, M. *et al.* Olaparib for Metastatic Breast Cancer in Patients with a Germline BRCA Mutation. *New England Journal of Medicine* **377**, 523–533 (2017).

172. Puhalla, S. *et al.* Final results of a phase 1 study of single-agent veliparib (V) in patients (pts) with either BRCA1/2-mutated cancer (BRCA+), platinum-refractory ovarian, or basal-like breast cancer (BRCA-wt). *JCO* **32**, 2570–2570 (2014).

173. Veliparib Falls Short in Phase III NSCLC, TNBC Trials. *OncLive* Available at: http://www.onclive.com/web-exclusives/veliparib-falls-short-in-phase-iii-nsclc-tnbc-trials. (Accessed: 2nd December 2017)

174. Sandhu, S. K. *et al.* The poly(ADP-ribose) polymerase inhibitor niraparib (MK4827) in BRCA mutation carriers and patients with sporadic cancer: a phase 1 dose-escalation trial. *The Lancet Oncology* **14**, 882–892 (2013).

175. A Phase III Trial of Niraparib Versus Physician's Choice in HER2 Negative, Germline BRCA Mutation-positive Breast Cancer Patients - Full Text View - ClinicalTrials.gov. Available at: https://clinicaltrials.gov/ct2/show/NCT01905592. (Accessed: 3rd December 2017)

176. Peshkin, B. N., Alabek, M. L. & Isaacs, C. BRCA1/2 MUTATIONS AND TRIPLE NEGATIVE BREAST CANCERS. *Breast Dis* **32**, (2010).

177. Brown, J. S., Kaye, S. B. & Yap, T. A. PARP inhibitors: the race is on. *British Journal of Cancer* **114**, 713 (2016).

178. Migliaccio, E. *et al.* Opposite effects of the p52shc/p46shc and p66shc splicing isoforms on the EGF receptor-MAP kinase-fos signalling pathway. *EMBO J.* **16**, 706–716 (1997).

179. Ursini-Siegel, J. & Muller, W. J. The ShcA adaptor protein is a critical regulator of breast cancer progression. *Cell Cycle* **7**, 1936–1943 (2008).

180. Lai, K. M. & Pawson, T. The ShcA phosphotyrosine docking protein sensitizes cardiovascular signaling in the mouse embryo. *Genes Dev.* **14**, 1132–1145 (2000).

181. Migliaccio, E. *et al.* The $p66^{shc}$ adaptor protein controls oxidative stress response and life span in mammals. *Nature* **402**, 309 (1999).

182. Arany, I., Faisal, A., Nagamine, Y. & Safirstein, R. L. p66shc Inhibits Pro-survival Epidermal Growth Factor Receptor/ERK Signaling during Severe Oxidative Stress in Mouse Renal Proximal Tubule Cells. *J. Biol. Chem.* **283**, 6110–6117 (2008).

183. Pacini, S. *et al.* p66SHC promotes apoptosis and antagonizes mitogenic signaling in T cells. *Mol. Cell. Biol.* **24**, 1747–1757 (2004).

184. Natalicchio, A. *et al.* Role of the p66Shc isoform in insulin-like growth factor I receptor signaling through MEK/Erk and regulation of actin cytoskeleton in rat myoblasts. *J. Biol. Chem.* **279**, 43900–43909 (2004).

185. Sakaguchi, K. *et al.* Shc phosphotyrosine-binding domain dominantly interacts with epidermal growth factor receptors and mediates Ras activation in intact cells. *Mol. Endocrinol.* **12**, 536–543 (1998).

186. Giorgio, M. *et al.* Electron transfer between cytochrome c and p66Shc generates reactive oxygen species that trigger mitochondrial apoptosis. *Cell* **122**, 221–233 (2005).

187. Okada, S. *et al.* The 66-kDa Shc isoform is a negative regulator of the epidermal growth factor-stimulated mitogen-activated protein kinase pathway. *J. Biol. Chem.* **272**, 28042–28049 (1997).

188. SHC1 (SHC (Src homology 2 domain containing) transforming protein 1). Available at: http://atlasgeneticsoncology.org/Genes/SHC1ID42287ch1q21.html. (Accessed: 17th November 2018)

189. Pelicci, G. *et al.* A novel transforming protein (SHC) with an SH2 domain is implicated in mitogenic signal transduction. *Cell* **70**, 93–104 (1992).

190. Ventura, A., Luzi, L., Pacini, S., Baldari, C. T. & Pelicci, P. G. The p66Shc Longevity Gene Is Silenced through Epigenetic Modifications of an Alternative Promoter. *J. Biol. Chem.* **277**, 22370–22376 (2002).

191. Stevenson, L. E. & Frackelton, A. R. Constitutively tyrosine phosphorylated p52 Shc in breast cancer cells: correlation with ErbB2 and p66 Shc expression. *Breast Cancer Res. Treat.* **49**, 119–128 (1998).

192. Jackson, J. G., Yoneda, T., Clark, G. M. & Yee, D. Elevated Levels of p66 Shc Are Found in Breast Cancer Cell Lines and Primary Tumors with High Metastatic Potential. *Clin Cancer Res* **6**, 1135–1139 (2000).

193. Khanday, F. A. *et al.* Rac1 Leads to Phosphorylation-dependent Increase in Stability of the p66shc Adaptor Protein: Role in Rac1-induced Oxidative Stress. *Mol Biol Cell* **17**, 122–129 (2006).

194. Orsini, F. *et al.* The Life Span Determinant p66Shc Localizes to Mitochondria Where It Associates with Mitochondrial Heat Shock Protein 70 and Regulates Trans-membrane Potential. *J. Biol. Chem.* **279**, 25689–25695 (2004).

195. Yang, C. P. & Horwitz, S. B. Taxol mediates serine phosphorylation of the 66-kDa Shc isoform. *Cancer Res.* **60**, 5171–5178 (2000).

196. Yannoni, Y. M., Gaestel, M. & Lin, L.-L. P66(ShcA) interacts with MAPKAP kinase 2 and regulates its activity. *FEBS Lett.* **564**, 205–211 (2004).

197. Khalid, S. *et al.* cJun N-terminal kinase (JNK) phosphorylation of serine 36 is critical for p66Shc activation. *Scientific Reports* **6**, 20930 (2016).

198. Haller, M. *et al.* Novel Insights into the PKCβ-dependent Regulation of the Oxidoreductase p66Shc. *J. Biol. Chem.* jbc.M116.752766 (2016). doi:10.1074/jbc.M116.752766

199. Galimov, E. R. The Role of p66shc in Oxidative Stress and Apoptosis. *Acta Naturae* **2**, 44–51 (2010).

200. Zhen, Y., Hoganson, C. W., Babcock, G. T. & Ferguson-Miller, S. Definition of the interaction domain for cytochrome c on cytochrome c oxidase. I. Biochemical, spectral, and kinetic characterization of surface mutants in subunit ii of Rhodobacter sphaeroides cytochrome aa(3). *J. Biol. Chem.* **274**, 38032–38041 (1999).

201. Nemoto, S. & Finkel, T. Redox Regulation of Forkhead Proteins Through a p66shc-Dependent Signaling Pathway. *Science* **295**, 2450–2452 (2002).

202. Khanday, F. A. *et al.* Sos-mediated activation of rac1 by p66shc. *J Cell Biol* **172**, 817–822 (2006).

203. Trinei, M. *et al.* A p53-p66Shc signalling pathway controls intracellular redox status, levels of oxidation-damaged DNA and oxidative stress-induced apoptosis. *Oncogene* **21**, 3872–3878 (2002).

204. Xiao, D. & Singh, S. V. p66shc Is Indispensable for Phenethyl Isothiocyanate-induced Apoptosis in Human Prostate Cancer Cells. *Cancer Res* **70**, 3150–3158 (2010).

205. Finkel, T. Signal transduction by mitochondrial oxidants. *J. Biol. Chem.* **287**, 4434–4440 (2012).

206. Han, D., Williams, E. & Cadenas, E. Mitochondrial respiratory chain-dependent generation of superoxide anion and its release into the intermembrane space. *Biochem J* **353**, 411–416 (2001).

207. Al-Dalaen, S. M. & Al-Qtaitat, A. I. Review Article: Oxidative Stress Versus Antioxidants. *American Journal of Bioscience and Bioengineering* **2**, 60 (2014).

208. Brand, M. D. The sites and topology of mitochondrial superoxide production. *Exp Gerontol* **45**, 466–472 (2010).

209. Kawamata, H. & Manfredi, G. Import, Maturation, and Function of SOD1 and Its Copper Chaperone CCS in the Mitochondrial Intermembrane Space. *Antioxid Redox Signal* **13**, 1375–1384 (2010).

210. Gogvadze, V., Orrenius, S. & Zhivotovsky, B. Multiple pathways of cytochrome c release from mitochondria in apoptosis. *Biochimica et Biophysica Acta (BBA) - Bioenergetics* **1757**, 639–647 (2006).

211. Fenton, H. J. H. LXXIII.—Oxidation of tartaric acid in presence of iron. *J. Chem. Soc., Trans.* **65**, 899–910 (1894).

212. Kehrer, J. P. The Haber–Weiss reaction and mechanisms of toxicity. *Toxicology* **149**, 43–50 (2000).

213. Shen, H. & Anastasio, C. A Comparison of Hydroxyl Radical and Hydrogen Peroxide Generation in Ambient Particle Extracts and Laboratory Metal Solutions. *Atmos Environ* **46**, 665–668 (2012).

214. Pantopoulos, K. & Schipper, H. M. *Principles of free radical biomedicine*. (Nova Science Publ., 2012).

215. Dalle-Donne, I. *et al.* Protein carbonylation, cellular dysfunction, and disease progression. *J. Cell. Mol. Med.* **10**, 389–406 (2006).

216. Martínez, A., Portero-Otin, M., Pamplona, R. & Ferrer, I. Protein targets of oxidative damage in human neurodegenerative diseases with abnormal protein aggregates. *Brain Pathol.* **20**, 281–297 (2010).

217. Castro, J. P., Jung, T., Grune, T. & Almeida, H. Actin carbonylation: from cell dysfunction to organism disorder. *J Proteomics* **92**, 171–180 (2013).

218. Butterfield, D. A. & Dalle-Donne, I. Redox proteomics: from protein modifications to cellular dysfunction and disease. *Mass Spec Rev* **33**, 1–6 (2014).

219. Grune, T., Jung, T., Merker, K. & Davies, K. J. A. Decreased proteolysis caused by protein aggregates, inclusion bodies, plaques, lipofuscin, ceroid, and 'aggresomes' during oxidative stress, aging, and disease. *Int. J. Biochem. Cell Biol.* **36**, 2519–2530 (2004).

220. Kanvah, S. *et al.* Oxidation of DNA: Damage to Nucleobases. *Acc. Chem. Res.* **43**, 280–287 (2010).

221. Bentle, M. S., Reinicke, K. E., Bey, E. A., Spitz, D. R. & Boothman, D. A. Calcium-dependent Modulation of Poly(ADP-ribose) Polymerase-1 Alters Cellular Metabolism and DNA Repair. *J. Biol. Chem.* **281**, 33684–33696 (2006).

222. Yin, H., Xu, L. & Porter, N. A. Free radical lipid peroxidation: mechanisms and analysis. *Chem. Rev.* **111**, 5944–5972 (2011).

223. Esterbauer, H., Eckl, P. & Ortner, A. Possible mutagens derived from lipids and lipid precursors. *Mutat. Res.* **238**, 223–233 (1990).

224. Schaur, R. J. Basic aspects of the biochemical reactivity of 4-hydroxynonenal. *Mol. Aspects Med.* **24**, 149–159 (2003).

225. Choe, M., Jackson, C. & Yu, B. P. Lipid peroxidation contributes to age-related membrane rigidity. *Free Radic. Biol. Med.* **18**, 977–984 (1995).

226. Hudson, J. *et al.* p66ShcA Promotes Breast Cancer Plasticity by Inducing an Epithelial-to-Mesenchymal Transition. *Mol Cell Biol* **34**, 3689–3701 (2014).

227. Ahn, R. *et al.* The ShcA PTB Domain Functions as a Biological Sensor of Phosphotyrosine Signaling during Breast Cancer Progression. *Cancer Res* **73**, 4521–4532 (2013).

228. Balakrishnan, S. K., Witcher, M., Berggren, T. W. & Emerson, B. M. Functional and Molecular Characterization of the Role of CTCF in Human Embryonic Stem Cell Biology. *PLoS One* **7**, (2012).

229. Peña-Hernández, R. *et al.* Genome-wide targeting of the epigenetic regulatory protein CTCF to gene promoters by the transcription factor TFII-I. *Proc. Natl. Acad. Sci. U.S.A.* **112**, E677-686 (2015).

230. Pommier, Y., O'Connor, M. J. & Bono, J. de. Laying a trap to kill cancer cells: PARP inhibitors and their mechanisms of action. *Science Translational Medicine* **8**, 362ps17-362ps17 (2016).

231. Ashworth, A. & Lord, C. J. BRCAness revisited. *Nature Reviews Cancer* **16**, 110 (2016).

232. McCabe, N. *et al.* Deficiency in the Repair of DNA Damage by Homologous Recombination and Sensitivity to Poly(ADP-Ribose) Polymerase Inhibition. *Cancer Res* **66**, 8109–8115 (2006).

233. Tong, A. H. *et al.* Systematic genetic analysis with ordered arrays of yeast deletion mutants. *Science* **294**, 2364–2368 (2001).

234. DiPaola, R. S. To Arrest or Not To G2-M Cell-Cycle Arrest : Commentary re: A. K. Tyagi et al., Silibinin Strongly Synergizes Human Prostate Carcinoma DU145 Cells to Doxorubicin-induced Growth Inhibition, G2-M Arrest, and Apoptosis. Clin. Cancer Res., 8: 3512–3519, 2002. *Clin Cancer Res* **8**, 3311–3314 (2002).

235. Pulliam, N. *et al.* An Effective Epigenetic-PARP Inhibitor Combination Therapy for Breast and Ovarian Cancers Independent of BRCA Mutations. *Clin Cancer Res* **24**, 3163–3175 (2018).

236. Hou, D. *et al.* Increased oxidative stress mediates the antitumor effect of PARP inhibition in ovarian cancer. *Redox Biology* **17**, 99–111 (2018).

237. Liu, Q. *et al.* PARP-1 inhibition with or without ionizing radiation confers reactive oxygen species-mediated cytotoxicity preferentially to cancer cells with mutant TP53. *Oncogene* **37**, 2793–2805 (2018).

238. Alli, E., Sharma, V. B., Sunderesakumar, P. & Ford, J. M. Defective Repair of Oxidative DNA Damage in Triple-negative Breast Cancer Confers Sensitivity to Inhibition of Poly(ADP-ribose) Polymerase. *Cancer Res* **69**, 3589–3596 (2009).

239. Yin, Z.-X. *et al.* PARP-1 inhibitors sensitize HNSCC cells to APR-246 by inactivation of thioredoxin reductase 1 (TrxR1) and promotion of ROS accumulation. *Oncotarget* **9**, 1885–1897 (2017).

240. Hou, D. *et al.* Increased oxidative stress mediates the antitumor effect of PARP inhibition in ovarian cancer. *Redox Biology* **17**, 99–111 (2018).

241. Nile, D. L., Rae, C., Hyndman, I. J., Gaze, M. N. & Mairs, R. J. An evaluation in vitro of PARP-1 inhibitors, rucaparib and olaparib, as radiosensitisers for the treatment of neuroblastoma. *BMC Cancer* **16**, 621 (2016).

242. Liu, Q. *et al.* PARP-1 inhibition with or without ionizing radiation confers reactive oxygen species-mediated cytotoxicity preferentially to cancer cells with mutant TP53. *Oncogene* **37**, 2793–2805 (2018).

243. Muñoz-Gámez, J. A. *et al.* PARP inhibition sensitizes p53-deficient breast cancer cells to doxorubicin-induced apoptosis. *Biochemical Journal* **386**, 119–125 (2005).

244. Turrens, J. F. Mitochondrial formation of reactive oxygen species. *The Journal of Physiology* **552**, 335–344 (2003).

245. Matulonis, U. A. & Monk, B. J. PARP inhibitor and chemotherapy combination trials for the treatment of advanced malignancies: does a development pathway forward exist? *Annals of Oncology* mdw697 (2017). doi:10.1093/annonc/mdw697

246. Murai, J. *et al.* Rationale for Poly(ADP-ribose) Polymerase (PARP) Inhibitors in Combination Therapy with Camptothecins or Temozolomide Based on PARP Trapping versus Catalytic Inhibition. *Journal of Pharmacology and Experimental Therapeutics* **349**, 408–416 (2014).

247. Patel, A. G. *et al.* Enhanced Killing of Cancer Cells by Poly(ADP-ribose) Polymerase Inhibitors and Topoisomerase I Inhibitors Reflects Poisoning of Both Enzymes. *Journal of Biological Chemistry* **287**, 4198–4210 (2012).

248. Kaye, S. B. *et al.* Phase II, Open-Label, Randomized, Multicenter Study Comparing the Efficacy and Safety of Olaparib, a Poly (ADP-Ribose) Polymerase Inhibitor, and Pegylated Liposomal Doxorubicin in Patients With *BRCA1* or *BRCA2* Mutations and Recurrent Ovarian Cancer. *Journal of Clinical Oncology* **30**, 372–379 (2012).

249. Del Conte, G. *et al.* Phase I study of olaparib in combination with liposomal doxorubicin in patients with advanced solid tumours. *British Journal of Cancer* **111**, 651–659 (2014).

250. Dasari, S. & Bernard Tchounwou, P. Cisplatin in cancer therapy: Molecular mechanisms of action. *European Journal of Pharmacology* **740**, 364–378 (2014).

251. Marullo, R. *et al.* Cisplatin Induces a Mitochondrial-ROS Response That Contributes to Cytotoxicity Depending on Mitochondrial Redox Status and Bioenergetic Functions. *PLoS ONE* **8**, e81162 (2013).

252. Korkmaz-Icöz, S. *et al.* Olaparib protects cardiomyocytes against oxidative stress and improves graft contractility during the early phase after heart transplantation in rats:

Protection by olaparib against cardiac injury. *British Journal of Pharmacology* **175**, 246–261 (2018).

253. INHIBITION OF POLY(ADP-RIBOSE) POLYMERASE REDUCES CARDIOMYOC... : Shock. Available at: https://journals.lww.com/shockjournal/fulltext/2006/02000/INHIBITION_OF_POLY_ADP_RIBOSE__POLYMERASE_REDUCES.11.aspx. (Accessed: 20th November 2018)

254. Qin, W. *et al.* cardiomyocytes from inflammation and apoptosis in diabetic. 14

255. Szatrowski, T. P. & Nathan, C. F. Production of Large Amounts of Hydrogen Peroxide by Human Tumor Cells. *Cancer Res* **51**, 794–798 (1991).

256. Toyokuni, S., Okamoto, K., Yodoi, J. & Hiai, H. Persistent oxidative stress in cancer. *FEBS Letters* **358**, 1–3 (1995).

257. Kawanishi, S., Hiraku, Y., Pinlaor, S. & Ma, N. Oxidative and nitrative DNA damage in animals and patients with inflammatory diseases in relation to inflammation-related carcinogenesis. *Biological Chemistry* **387**, 365–372 (2006).

258. Wang, X.-J. *et al.* Nrf2 enhances resistance of cancer cells to chemotherapeutic drugs, the dark side of Nrf2. *Carcinogenesis* **29**, 1235–1243 (2008).

259. Miran, T., Vogg, A. T. J., Drude, N., Mottaghy, F. M. & Morgenroth, A. Modulation of glutathione promotes apoptosis in triple-negative breast cancer cells. *The FASEB Journal* **32**, 2803–2813 (2018).

260. Daemen, A. *et al.* Pan-Cancer Metabolic Signature Predicts Co-Dependency on Glutaminase and De Novo Glutathione Synthesis Linked to a High-Mesenchymal Cell State. *Cell Metabolism* **28**, 383-399.e9 (2018).

261. Trachootham, D., Alexandre, J. & Huang, P. Targeting cancer cells by ROS-mediated mechanisms: a radical therapeutic approach? *Nature Reviews Drug Discovery* **8**, 579–591 (2009).

262. Postovit, L., Widmann, C., Huang, P. & Gibson, S. B. Harnessing Oxidative Stress as an Innovative Target for Cancer Therapy. *Oxid Med Cell Longev* **2018**, (2018).

263. Pulliam, N. *et al.* An Effective Epigenetic-PARP Inhibitor Combination Therapy for Breast and Ovarian Cancers Independent of BRCA Mutations. *Clinical Cancer Research* **24**, 3163–3175 (2018).